SANDIA NATIONAL LABORATORIES
WASTE ISOLATION PILOT PLANT

ANALYSIS REPORT FOR CULEBRA FLOW AND TRANSPORT IN THE REPLACEMENT PANELS PLANNED CHANGE REQUEST (RPPCR)

REVISION 0

Author:	James Bethune	Signature on File	11/7/2023
	Print	Signature	Date
Technical Reviewer:	Kristopher Kuhlman	Signature on File	11/7/2023
	Print	Signature	Date
Technical Reviewer:	Clifford Hansen	Signature on File	11/7/2023
	Print	Signature	Date
QA Reviewer:	Shelly R. Nielsen	Shelly R. Nielsen	11-7-2023
	Print	Signature	Date
Management Reviewer:	Steve Wagner		11/7/2023
	Print	Signature	Date

ERMS #579725

NOVEMBER 2023

WIPP:4.4.1.2.1:PA:QA-L:578831

Information Only

This page intentionally left blank.

Information Only

Executive Summary

As currently permitted, the Waste Isolation Pilot Plant (WIPP) includes ten panels for waste emplacement. For operational reasons, less than the total volume of the ten panels will be used for waste disposal. The U.S. Department of Energy (DOE) plans to excavate two new panels, termed replacement panels, to provide an equivalent disposal capacity, and may consider excavating up to seven panels beyond the two replacement panels, defined here as additional panels. A Performance Assessment (PA) has been executed by Sandia National Laboratories (SNL) to quantify the long-term performance of the repository with the replacement and additional panels, named the Replacement Panels Planned Change Request (RPPCR) PA.

This analysis report describes the parameters, models, and results of the Culebra flow and transport components of the RPPCR PA. Results from the RPPCR are compared to those obtained in the 2019 Compliance Recertification Application (CRA-2019) to assess repository performance in terms of the most recent regulatory submittal. The CRA-2019 used Culebra transport simulation results from the 2009 Compliance Recertification Application (CRA-2009) Performance Assessment Baseline Calculation (PABC09). Results are also compared to the Replacement Panels Performance Assessment (RPPA), which included some but not all the updates in the RPPCR.

Changes incorporated into the RPPCR include inventory updates, changes related to the replacement and additional panels, updates due to new information and model revisions since the CRA-2019 PA, and updates to the PA codes and computing platform. Specific changes that have significant impact on the Culebra flow and transport models include simulation of actinide transport from the replacement and additional panels, updated realizations of Culebra transmissivity fields, and updates to the actinide oxidation state model.

The primary output of interest in the Culebra flow and transport simulations is the cumulative solute mass crossing the WIPP Land Withdrawal Boundary (LWB) over the 10,000-year regulatory period. Calculations are performed for a suite of discrete sources (release points) located in the Culebra over the waste panel area and two flow fields scenarios modified with potash mining, either outside the LWB (partial mining) or throughout the domain (full mining). Results show relatively higher mass transported to the LWB in full mining simulations with mass released above the westernmost additional panels than in the other flow or release location simulations. Particle tracking simulations illustrate flow over the westernmost panels in the full mining scenario is oriented towards the western edge of the LWB. Transport in partial mining simulations continues to have relatively low radionuclide mass breakthrough to the LWB for all simulated isotopes and release points.

Information Only

This page intentionally left blank.

Information Only

TABLE OF CONTENTS

EXECUTIVE SUMMARY ..... **III**

1.0 INTRODUCTION **1**

1.1 Changes Since the CRA19 2
1.1.1 Updated Culebra Transport Procedure 2
1.1.2 Updated Oxidation State Model 3
1.1.3 Updated T-fields 4
1.1.4 Hardware and Computational Code Updates 4
1.2 Changes Incorporated in the RPPA 5

2.0 CONCEPTUAL APPROACH OVERVIEW **7**

2.1 Domain and Discretization 8
2.2 Boundary and Initial Conditions 9
2.3 Uncertainty 10
2.3.1 Subjective Uncertainty 10
2.3.2 Stochastic Uncertainty 10

3.0 CULEBRA MODEL METHODOLOGY **12**

3.1 Mining Modification 13
3.2 Groundwater Flow Simulations 14
3.3 Particle Tracking 14
3.4 Radionuclide Transport 15
3.5 Sensitivity Analysis 17
3.6 Code Execution and Run Control 18
3.6.1 Flow 18
3.6.2 Transport 20

4.0 RESULTS **22**

4.1 Flow 23
4.2 Particle Tracking 27
4.3 Radionuclide Transport 36
4.4 Sensitivity Analysis 67

Information Only

5.0 SUMMARY 73

6.0 REFERENCES 75

7.0 APPENDIX A MININGMOD 79

7.1 Utility enlarge_mining_areas.py 79
7.1.1 Execution and Syntax 79
7.1.2 Input and Output Files 80
7.1.3 Validation Test 0 81
7.1.4 RPPCR Execution 81
7.2 Utility mining_mod.py 82
7.2.1 Execution and Syntax 82
7.2.2 Input and Output Files 83
7.2.3 Validation Test 1 83
7.2.4 RPPCR Execution 85
7.3 Utility 100x100_to_50x50.py 85
7.3.1 Execution and Syntax 86
7.3.2 Input and Output Files 87
7.3.3 Validation Test 2 87
7.3.4 RPPCR Execution 89
7.4 References 89

8.0 APPENDIX B SUMMARIZE DTRKMF 90

8.1 Execution 90
8.2 Input and Output Files 90
8.3 Validation Test 91
8.4 RPPCR Implementation 91
8.5 References 92

9.0 APPENDIX C CBC2BUD 93

9.1 Build Information 93
9.2 Execution and Syntax 93
9.3 Functionality 94
9.4 Validation 94
9.5 RPPCR Implementation 96
9.6 References 97

Information Only

10.0 APPENDIX D BUD2TXT 99

Information Only

LIST OF TABLES

Table 1 – Culebra release point coordinates 3
Table 2 – Culebra model domain coordinates 8
Table 3 – Culebra flow uncertain parameter distributions 14
Table 4 – Deterministic physical parameter values 15
Table 5 – Uncertain physical parameter distributions 16
Table 6 – Deterministic physical parameter values 16
Table 7 – Uncertain chemical parameters distributions 17
Table 8 – Mean particle travel time to LWB 34
Table 9 – Median particle travel time to LWB 34
Table 10 – Minimum particle travel time to LWB 35
Table 11 – Maximum particle travel time to LWB 35
Table 12 – Mean cumulative mass [kg] to LWB over 10,000 years 63
Table 13 – Median cumulative mass [kg] to LWB over 10,000 years 64
Table 14 – Maximum cumulative mass [kg] to LWB over 10,000 years 65
Table 15 – Cumulative 10,000-yr mass to LWB [count > 10^{-9} kg] 66
Table 16 – Rank correlation Am-241 70
Table 17 – Rank correlation Pu-239 70
Table 18 – Rank correlation Th-23A 71
Table 19 – Rank correlation U-234 71

Information Only

LIST OF FIGURES

Figure 1 – Culebra release point locations 3
Figure 2 – Schematic of dual-porosity model 7
Figure 3 – Culebra modeling domain 9
Figure 4 – Mining scenarios and mass release points 11
Figure 5 – Culebra flow model run control diagram 19
Figure 6 – Culebra transport model run control diagram 21
Figure 7 – Ensemble mean RPPCR flow rate 24
Figure 8 – Ensemble mean CRA19 flow rate 24
Figure 9 – Ensemble standard deviation RPPCR flow rate 25
Figure 10 – Ensemble standard deviation CRA19 flow rate 25
Figure 11 – Ensemble standard deviation RPPCR flow direction 26
Figure 12 – Ensemble standard deviation CRA19 flow direction 26
Figure 13 – DTRKMF particle travel time to LWB scatter plots 28
Figure 14 – DTRKMF particle tracks, full mining scenario 29
Figure 15 – DTRKMF particle tracks, partial mining scenario 30
Figure 16 – Particle travel time to LWB exceedance probabilities, Replicate 1 31
Figure 17 – Particle travel time to LWB exceedance probabilities, Replicate 2 32
Figure 18 – Particle travel time to LWB exceedance probabilities, Replicate 3 33
Figure 19 – Mass breakthrough at 10,000-yr: RPPCR CRP1 versus CRA19 42
Figure 20 – Mass breakthrough of Am-241 43
Figure 21 – Exceedance probability of Am-241 mass to LWB in 10,000 years, Replicate 1 44
Figure 22 – Exceedance probability of Am-241 mass to LWB in 10,000 years, Replicate 2 45
Figure 23 – Exceedance probability of Am-241 mass to LWB in 10,000 years, Replicate 3 46
Figure 24 – Mass breakthrough of Pu-239 47
Figure 25 – Exceedance probability of Pu-239 mass to the LWB in 10,000 years, Replicate 1 ... 48
Figure 26 – Exceedance probability of Pu-239 mass to the LWB in 10,000 years, Replicate 2 ... 49
Figure 27 – Exceedance probability of Pu-239 mass to the LWB in 10,000 years, Replicate 3 ... 50
Figure 28 – Mass breakthrough of Th-230A 51
Figure 29 – Exceedance probability of Th-23A mass to LWB in 10,000 years, Replicate 1 52
Figure 30 – Exceedance probability of Th-23A mass to LWB in 10,000 years, Replicate 2 53
Figure 31 – Exceedance probability of Th-23A mass to LWB in 10,000 years, Replicate 3 54

Information Only

Figure 32 – Mass breakthrough of U-234 55
Figure 33 – Exceedance probability of U-234 mass to LWB in 10,000 years, Replicate 1 56
Figure 34 – Exceedance probability of U-234 mass to LWB in 10,000 years, Replicate 2 57
Figure 35 – Exceedance probability of U-234 mass to LWB in 10,000 years, Replicate 3 58
Figure 36 – Mass breakthrough of Th-230 59
Figure 37 – Exceedance probability of Th-230 mass to LWB in 10,000 years, Replicate 1 60
Figure 38 – Exceedance probability of Th-230 mass to LWB in 10,000 years, Replicate 2 61
Figure 39 – Exceedance probability of Th-230 mass to LWB in 10,000 years, Replicate 3 62
Figure 40 – Transport results sensitivity, full mining, CRP1 68
Figure 41 – Transport results sensitivity, full mining, CRP4 69
Figure 42 – DTRKMF particle travel time to LWB [years] versus mining factor [MINPFAC] ... 72
Figure 43 – Mining impacts stencil 79
Figure 44 – enlarge_mining_areas.in contents 81
Figure 45 – Test 1 mining_mod.in contents 84
Figure 46 – Calibrated and mining modified T-fields 84
Figure 47 – Test 2 *100x100_to_50x50.in* contents 87
Figure 48 - 100-m input and 50-m output T-field array 88
Figure 49. Subset 100-m input and 50-m output boundary conditions 88
Figure 50. Python script *compare_txt.py* 96

Information Only

1.0 INTRODUCTION

The Waste Isolation Pilot Plant (WIPP), located in southeastern New Mexico, has been developed by the U.S. Department of Energy (DOE) for the geologic (deep underground) disposal of transuranic (TRU) waste. Containment of TRU waste at the WIPP is regulated by the U.S. Environmental Protection Agency (EPA) according to the regulations set forth in Title 40 of the Code of Federal Regulations (CFR), Part 191.

The DOE demonstrates compliance with the containment requirements according to the Certification Criteria in Title 40 CFR Part 194 by means of performance assessment (PA) calculations performed by Sandia National Laboratories (SNL). WIPP PA calculations estimate the probability and consequence of potential radionuclide releases from the repository to the accessible environment for a regulatory period of 10,000 years after facility closure. The models used in PA are maintained and updated with new information as part of an ongoing process. Improved information regarding important WIPP features, events, and processes typically results in refinements and modifications to PA models and the parameters used in them. Planned changes to the repository or the components therein also result in updates to WIPP PA models. WIPP PA models are used to support the repository recertification process that occurs at five-year intervals following the receipt of the first waste shipment at the site in 1999.

PA calculations were included in the 1996 Compliance Certification Application (CCA) (U.S. DOE, 1996), and in a subsequent Performance Assessment Verification Test (PAVT) (MacKinnon and Freeze, 1997a; 1997b; 1997c). Based in part on the CCA and PAVT PA calculations, the EPA certified that the WIPP met the regulatory containment criteria. The facility was approved for disposal of transuranic waste in May 1998 (EPA, 1998). Subsequent CRA PA submittals including the CRA-2004, CRA-2009, CRA-2014, and CRA-2019 have included PA calculations. EPA requested additional PA calculations, termed Performance Assessment Baseline Calculations (PABC) for the CRA-2004 and CRA-2009 submittals before recertification. The EPA conducted a separate analysis, termed CRA19-COMB, based on the CRA-2019 PA with several different assumptions and models (Section 4.6; EPA 2022).

As currently permitted, the WIPP includes ten panels for waste emplacement. For operational reasons, less than the total volume of the ten excavated panels will be used for waste disposal. The DOE plans to submit a Planned Change Request (PCR) to excavate two panels, termed replacement panels, to provide an equivalent disposal capability. Additionally, the DOE may consider excavating up to seven panels beyond the two replacement panels, defined here as replacement panels. SNL executed the Replacement Panels Planned Change Request (RPPCR) PA to quantify the long-term performance of the repository with the replacement and additional panels in support of the DOE's submittal of the PCR. The PA executed in support of the RPPCR is detailed in AP-204 (Hansen et al. 2023).

This analysis report documents the Culebra flow and radionuclide transport components of the RPPCR PA. The Culebra flow and transport analysis begins with Latin Hypercube Sampling (LHS) of uncertain parameters (Zeitler, 2023) and calibrated fields of Culebra transmissivity, anisotropy, storativity, and recharge (Bowman et al., 2023). The resulting radionuclide transport to the LWB is used by the WIPP PA software CCDFGF to calculate potential radionuclide releases through the Culebra to the accessible environment (Brunell and Zeitler, 2023).

Information Only

The RPPCR results are compared to those in the 2019 Compliance Recertification Application PA (CRA19) to assess repository performance in terms of the most recent regulatory submittal (Zeitler et al., 2019). The CRA19 used Culebra flow and transport results from the PABC09 (Kuhlman, 2010). Results are also compared to the Replacement Panels Performance Assessment (RPPA), a PA based on the CRA19 that considered many but not all changes implemented for the RPPCR (Hansen, 2022).

1.1 Changes Since the CRA19

Changes incorporated into the RPPCR PA since the CRA19 include inventory updates, changes related to the replacement and additional panels, routine updates due to new information, and updates to PA computing software and platform (Hansen et al., 2023). Changes relevant to the Culebra flow and transport models include:

- Updated procedure for calculating releases through the Culebra
- Revised actinide oxidation state model
- Updated transmissivity fields in the Culebra
- Hardware and computational software updates

Inventory parameters are not incorporated into the Culebra flow or transport models.

Two other changes were made to the PA calculations that do not affect the Culebra transport output. First, the particle tracking release point location over the currently permitted 10-waste panel region was moved approximately 15 meters to the south to coincide with the corresponding mass transport release point location. The particle tracks are used in a sensitivity analysis to create a ranked index of the flow fields, but do not impact the Culebra mass release calculations or WIPP PA results. Second, the binary flow field files are imported directly by the transport preprocessing software, PRESECOTP2D, rather than being preprocessed by the VTRAN utility (Gilkey, 2013).

1.1.1 Updated Culebra Transport Procedure

In each simulation, the Culebra transport models include mass release into the Culebra at a discreet location above the waste panels. The CRA19 considered only a single mass release point at the center of the currently permitted 10-panel repository. The two replacement waste panels (numbered 11 and 12) and seven additional panels (numbered 13 through 19) considered in this analysis extend to the west of the current repository footprint away from the CRA19 release point (Figure 1, modified from Sjomeling, 2019). The RPPCR includes the CRA19 Culebra release point (hereafter, referred to as CRP1 when discussing the RPPCR results and CRA19 when discussing the CRA19 results), plus three additional Culebra release points (CRP2 through CRP4) to characterize transport through the Culebra over the additional panels region (Bethune and Brunell, 2022). The UTM NAD27 Zone 13N coordinates of the release points are listed in Table 1.

Information Only

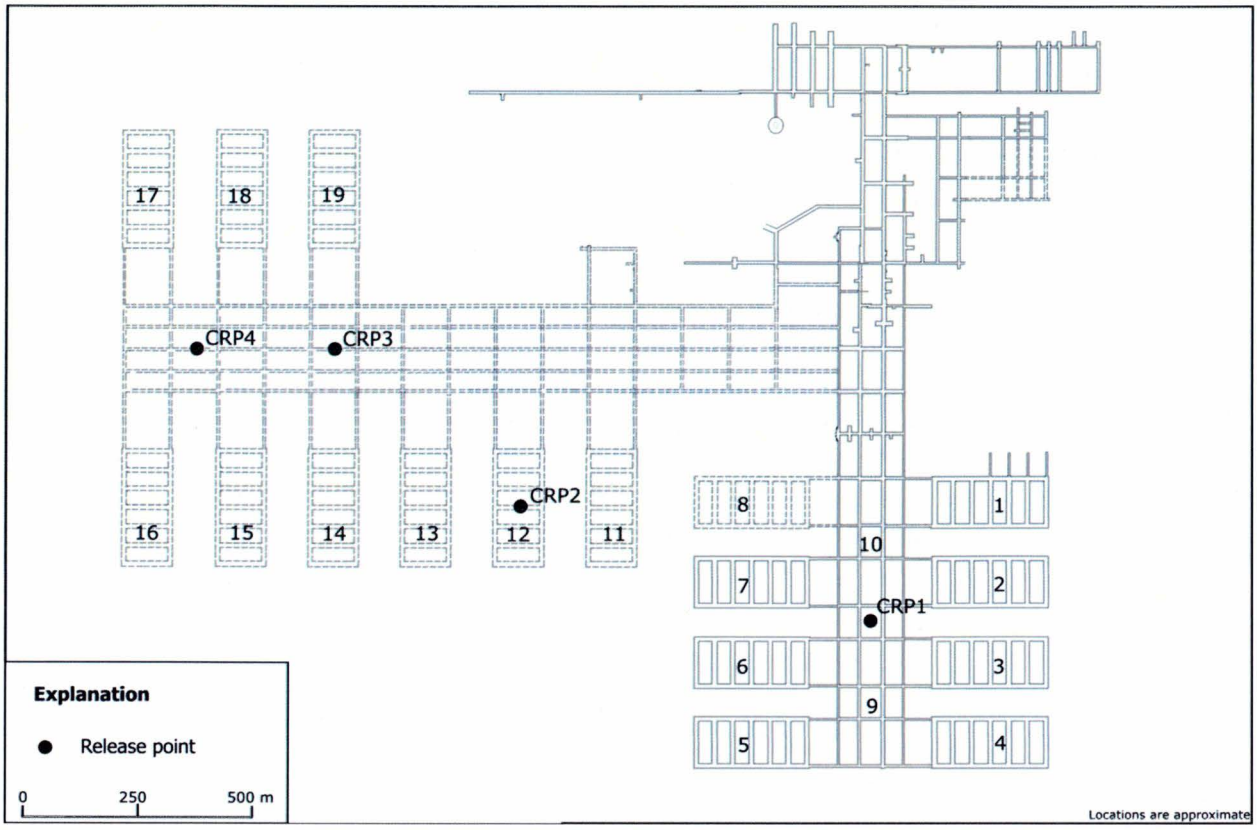


Figure 1 – Culebra release point locations

Table 1 – Culebra release point coordinates

Culebra Release Point	X-Coordinate [m]	Y-Coordinate [m]	Description
CRP1	613597.5	3581385.2	CRA19 release point, centroid of panels 1 through 10
CRP2	612828.3	3581621.4	New release point, centroid of panels 11 through 13
CRP3	612424.1	3581961.0	New release point, centroid of panels 14 and 19
CRP4	612120.2	3581957.6	New release point, centroid of panels 15 through 18

1.1.2 Updated Oxidation State Model

Actinides Pu and U are simulated with either high or low oxidation states in the Culebra transport simulations. In the CRA19, high or low oxidation states of both U and Pu were equally likely, and were determined by a single oxidation state parameter, preventing mixed oxidation states. In the RPPCR, the oxidation state model was extended with actinide-specific oxidation state threshold parameters to allow for a mix of oxidation states (Lucchini and Swanson, 2023). The RCCPR

Information Only

oxidation state threshold for Pu results in a 25:75 ratio of Pu(III) to Pu(IV) simulations. The oxidation cutoff for U continues to result in a 50:50 distribution of U(IV) to U(VI) simulations.

1.1.3 Updated T-fields

The Culebra flow model incorporates spatially variable, calibrated fields of transmissivity, storativity, anisotropy, and recharge (collectively referred to as T-fields). A geostatistical model produces an ensemble of 1000 uncalibrated parameter fields from quantitative and qualitative observations of hypothesized hydrogeologic controls (Hart et al., 2008). The CRA19 T-fields were calibrated with the Parameter ESTimation (PEST) calibration software and MODFLOW-2000 groundwater flow simulator (Hart et al., 2009). For the RPPCR, the ensemble set of 1,000 base T-fields were recalibrated with updated steady-state and transient targets and updated model boundary conditions using the PEST++ Iterative Ensemble Solver (PEST++ IES) algorithm and the MODFLOW 6 groundwater flow simulator (Bowman et al., 2023). The calibrations were evaluated based on their ability to recreate observed head data, and the best 100 calibrations were selected as the final calibrated set (Bowman et al., 2023).

1.1.4 Hardware and Computational Code Updates

The run control for both the flow and transport models was updated to accommodate particle tracking and mass release simulations at the new release points. There were additional significant software and run control updates to the Culebra flow model, including:

- Incorporation of the Culebra flow model into the formal WIPP run control system (Long, 2023).
- Migration of the Culebra flow model from MODFLOW-2000 to MODFLOW 6, the sixth core version of the U.S. Geological Survey software suite MODFLOW (Langevin, 2017).
- Modification of the Culebra flow utility scripts to work with the MODFLOW 6 file formats (Appendix A; Appendix B).
- The utility CBC2BUD was developed to convert the MODFLOW 6 binary cell-by-cell file output to MODFLOW-2000 format compatible with the particle tracking software DTRKMF. The CBCBUD was qualified under NP 9-1 (Appendix C).

There were additional minor updates to the Culebra transport computational code execution. The SECOTP2D boundary conditions were changed from type 'Automatic' to type 'Dirichlet' boundaries of zero value. Automatic boundary conditions had been previously identified to cause mass balance errors where mass reached lateral edges with mixed boundary conditions (Loukota, 1997). The impact of the automatic boundary conditions in the CRA19 Culebra results was minor, both because most simulated mass exits the domain on the southern boundary instead of the lateral boundaries and because the few simulations that did develop mass boundary errors were identified in the WIPP run control system and rerun with alternative numerical controls (Bethune, 2022).

Calculations for the CRA19 were performed on the WIPP PA Solaris Cluster, which consisted of Intel hardware running the Solaris operating system (Long, 2019). Flow and particle tracking calculations for the PABC09 were performed on the WIPP PA Pentium 4 cluster. Transport calculations for the PABC09 were performed on the WIPP PA Alpha Cluster. The RPPCR calculations were performed on the WIPP PA HPC/Linux Cluster, which consists of Dell PowerEdge C6420 hardware running CentOS7 (Long, 2020; Long and King 2022).

Information Only

1.2 Changes Incorporated in the RPPA

The RPPA included the updated Culebra transport procedure with multiple particle and mass release points described in Section 1.1.1. The RPPA did not include the updated T-fields or oxidation state model.

Information Only

This page intentionally left blank.

Information Only

2.0 CONCEPTUAL APPROACH

The Culebra flow and transport models implement the WIPP conceptual models for Culebra Hydrogeology, Transport of Dissolved Actinides in the Culebra, and Transport of Colloidal Actinides in the Culebra, which are unchanged from the CRA19 (Hansen, 2021). The Culebra Dolomite Member of the Rustler Formation has been identified as the most transmissive saturated unit above the Salado Formation and consequently it is the most likely subsurface release pathway of radionuclides to the LWB.

Radionuclide movement through the Culebra is a function of the groundwater flow-field and the transport properties of the media and radionuclide species being considered. Flow occurs through fractures, vugs and, to some extent, intergranular pores. There is a large permeability contrast between the different scales of interconnected porosity that suggests a dual porosity conceptualization consisting of advective porosity (i.e., fracture porosity) and diffusive porosity (i.e., matrix porosity; Figure 2). Tracer tests conducted in the Culebra at the WIPP site have clearly shown characteristics of both advective transport and matrix diffusion (Meigs et al., 2000).

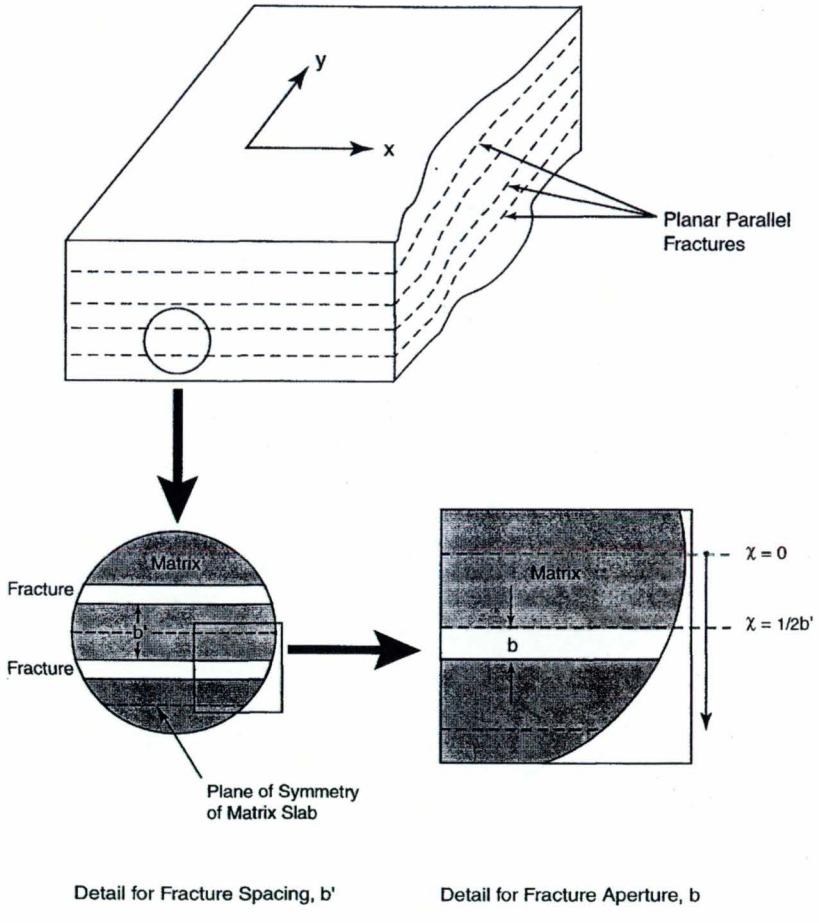


Figure 2 – Schematic of dual-porosity model

Potash mining in the WIPP area involves resource extraction below the Culebra dolomite in the McNutt Potash zone, a subsection of the Salado Formation is above the repository horizon but that

Information Only

underlies the Rustler Formation. It is hypothesized that subsidence of the Culebra due to potash mining leads to fracturing, resulting in higher Culebra transmissivities and altered groundwater flow patterns. This increase in transmissivity may significantly change the transport behavior of any nuclides entering the aquifer via human intrusion from the underlying repository.

2.1 Domain and Discretization

The Culebra flow and transport model domain extent and discretization are the same as in the CRA19 calculations (Kuhlman, 2010). The flow model domain is a two-dimensional horizontal layer that extends 28.4 kilometers in the east-west direction and 30.7 kilometers in the north-south direction (Table 2). The flow domain is aerially discretized into 100-meter square cells, yielding a model that is 284 cells wide (east-west) by 307 cells tall (north-south). The flow domain is vertically discretized into a single horizontal layer of uniform 7.75-meter thickness. The transport model domain is a 7.5-kilometer by 5.4-kilometer subregion of the flow domain that encompasses the southern extent of the LWB. The transport domain is shifted off-center in the north-south direction because the undisturbed groundwater flow direction is generally north to south. The transport domain is discretized into 50-meter grid cells that are created by bisecting the Culebra 100-m flow model cells on both the x and y axes. Although the Culebra properties vary in the vertical direction, the error introduced by modeling the Culebra in two rather than three dimensions has been determined to be negligible (Corbet, 1995).

Table 2 – Culebra model domain coordinates

Domain Corner	X Coordinate [A] [m]	Y Coordinate [A] [m]
Flow Model Domain		
Northeast	630,000	3,597,200
Northwest	601,700	3,597,200
Southwest	601,700	3,566,500
Southeast	630,000	3,566,500
WIPP Land Withdrawal Boundary		
Northeast	616,941	3,585,109
Northwest	610,495	3,585,068
Southwest	610,567	3,578,623
Southeast	617,015	3,578,681
Transport Model Domain		
Northeast	617,750	3,583,000
Northwest	610,250	3,583,000
Southwest	610,250	3,577,600
Southeast	617,750	3,577,600

[A] UTM NAD27 Zone 13

Information Only

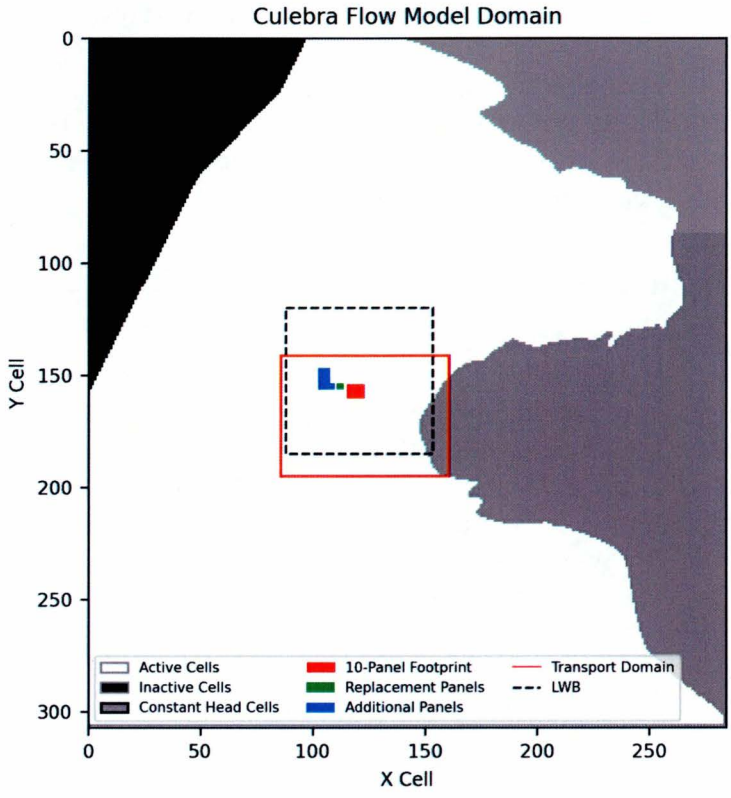


Figure 3 – Culebra modeling domain

2.2 Boundary and Initial Conditions

The constant-head region associated with the halite-sandwiched portion of the Culebra is specified head, set to the land surface elevation. The model boundary conditions along straight-line portions of the north, west, and south edges of the domain are specified head. A multi-parameter parametric surface was used to fill initial head and boundary condition values everywhere except in the constant-head zone east of the halite margin (Bowman et al., 2023). The piecewise-linear boundary in the northwest corner is a no-flow boundary parallel to the axis of the Nash Draw topographic depression, which is conceptualized as a groundwater divide.

The regional gradient across the domain is approximately:

(944.14 m – 908.88 m)/30.7 km = 0.00115

as calculated by averaging the constant heads along the non-halite-sandwiched portion of the northern boundary (columns 1 to 140, 944.14 m), subtracting the average heads along the entire southern boundary (908.88-m), and then dividing by the north-south model domain distance (30.7 km). This is approximately 9.4% steeper than the CRA19 gradient of 0.00105 (Kuhlman 2010).

Information Only

2.3 Uncertainty

There is significant uncertainty associated with characterizing the physical properties of geologic materials that influence Culebra flow and transport behavior. Properties such as permeability and porosity are usually measured indirectly and vary significantly depending upon location and scale. The uncertainty in a particular physical property value is called subjective (epistemic) uncertainty. Stochastic (aleatory) uncertainty is associated with incomplete knowledge of future events. WIPP PA addresses these types of uncertainty separately.

2.3.1 Subjective Uncertainty

Subjective uncertainty is modeled by defining and sampling from distributions that characterize uncertain parameters. Uncertain physical properties in the Culebra flow and transport models are categorized as epistemic. To reduce the number of realizations required and to ensure that low probability (and possibly high consequence) combinations are represented, Latin Hypercube Sampling (LHS) is used to create the realizations. For the WIPP PA, the LHS software is used to create 100 distinct parameter sets, or vectors, that are sampled from the full range of parameter uncertainty (WIPP PA, 2021). To ensure that the Latin Hypercube parameter sets are representative and mean releases are convergent, three replicates are created for a total of 300 separate vectors.

2.3.2 Stochastic Uncertainty

Stochastic uncertainty is addressed in the PA by generating 10,000 random sequences of future events, termed futures, using the WIPP PA software program CCDFGF. To estimate releases by Culebra transport in a random future, radionuclide transport is calculated for defined scenarios and these scenario results are used to construct the releases for all futures.

Two aspects of the Culebra flow and transport model are addressed through defined scenarios, including potash mining impacts on flow, and the location of future drilling events. Consistent with the CRA19 calculations, two mining scenarios are considered: full mining, in which mining is assumed in all economically feasible potash reserves throughout the domain, and partial mining, in which mining is assumed to occur only outside the LWB. Since the potash-mining horizon is below the Culebra, the areas in the Culebra that are disturbed by mining activities in the Salado are larger than the mined areas due to angle-of-draw effects, in which the subsidence effects are assumed to propagate up and out at 45° angles from horizontal. The areal extent of minable potash was provided by the Bureau of Land Management (Cranston, 2009). Because of the changes to the repository footprint in the RPPCR, the mining-impacted cells extend approximately 300 meters across the western edge of the footprint of the additional panels, while in the CRA19 the closest mining-impacted cells were adjacent to but not overlapping with the footprint of the southeast panels. Uncertainty in the location of future drilling events that could potentially connect the Culebra with the repository waste region is addressed by modeling mass release into the Culebra at four different release point locations, termed CRP1 through CRP4 (Figure 1, Section 1.1).

Transport is evaluated for each combination of mining scenario and release point (Figure 4).

Information Only

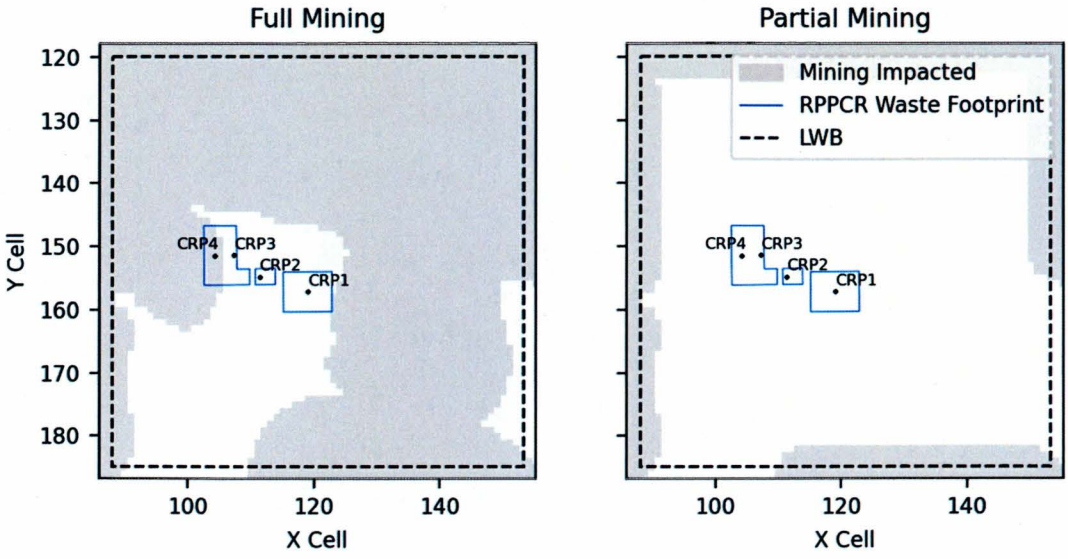


Figure 4 – Mining scenarios and mass release points

Information Only

This page intentionally left blank.

Information Only

3.0 CULEBRA MODEL METHODOLOGY

The primary result of interest in the Culebra transport calculations is the cumulative transport of radionuclides to the LWB over the 10,000-year regulatory period, conditional on sources placed in the Culebra at 50 years post-closure. There are five steps in estimating radionuclide transport through the Culebra, including:

Step 1. Construction of 1,000 base geostatistical realizations of Culebra hydraulic transmissivity (T), anisotropy, storativity, and recharge fields (collectively referred to as "T-fields");

Step 2. Calibration of the T-fields to observed head and pumping drawdowns;

Step 3. Modification of the T-fields to account for potential subsidence due to potash mining beneath the Culebra;

Step 4. Calculation of steady-state groundwater flow-fields for each mining-modified T-field using MODFLOW; and

Step 5. Calculation of radionuclide transport through the Culebra to the LWB for each simulated flow-field and release location using SECOTP2D.

The work presented in this report is limited to Step 3 through Step 5. Steps 1 and 2 produce 100 equally likely T-fields that are input to Step 3. Step 1 is documented in Hart et al. (2008). Step 2 is documented in Bowman et al. (2023). The output of Step 4 and Step 5 are used in sensitivity analyses to determine the relative importance of the input variables. The output of Step 5 is used by the WIPP software CCDFGF to calculate potential radionuclide releases through the Culebra to the accessible environment (Brunell and Zeitler, 2023).

3.1 Mining Modification

The calibrated transmissivity fields are modified into the two mining scenarios with the Python scripts *enlarge_mining_areas.py* and *mining_mod.py* (Appendix A Sections 1 and 2). The script *enlarge_mining_areas.py* enlarges the mining regions to account for the angle of draw and distinguishes the mining impacted cells within the LWB. The script *mining_mod.py* modifies the transmissivity fields of the calibrated transmissivity fields in the mining impacted regions.

WIPP PA Parameter Database (PAPDB) designations for the parameters involved in the mining modification calculation are shown in Table 3. The parameter MINP_FAC is a multiplier on the transmissivity values that controls the degree of impact of mining. The parameter TRANSIDX is used as an index to create a random pairing between calibrated T-field realizations with LHS vectors. Each vector in the RPPCR has the same LHS values as in the CRA19; however, the T-field index value is associated with a different T-field realization because the recalibration resulted in a different set of 100 best calibrations.

Information Only

Table 3 – Culebra flow uncertain parameter distributions

Model Parameter	MATERIAL: PROPERTY	Units	Distribution	Range	Median
Flow-field index	GLOBAL:TRANSIDX	-	Uniform	[0.00E+0, 1.00E+0]	0.50
Mining factor	CULEBRA:MINP_FAC	-	Uniform	[1.00E+0, 1.00E+3]	500.5

3.2 Groundwater Flow Simulations

MODFLOW simulates steady-state flow with the mining-modified transmissivity fields at two resolutions:

1) 100-m grid used in the T-field calibrations and particle tracking simulations
2) 50-m grid used in the mass transport simulations

The flow model is converted to 50×50-meter grid cells by subdividing each of the 100-meter model grid cells into four equal-sized cells with the properties of the larger cells copied directly into the smaller cells, including data fields for the boundary conditions, top and bottom elevation arrays, the starting head array, and the T-fields input anisotropy, mining modified conductivity, recharge, and storage using the script *100x100m_to_50x50m.py* (Appendix A, Section 3). The boundary condition head values are smoothed along the exterior two rows and columns of the domain.

3.3 Particle Tracking

A single particle is tracked through the simulated flow fields to the LWB for each combination of release point, transmissivity field, parameter vector, and mining scenario. The 100-m flow solutions are converted to the MODFLOW-2000 budget format so that particle tracking calculations may be performed using DTRKMF (Appendix C). A problem was found in DTRKMF that can cause a particle track to get stuck, then suddenly jump in an unrealistic way (SPR 23-001). This issue happens rarely and did not impact any results presented here.

Results are then summarized into text tables with the Python script *summarize_dtrkmf.py* (Appendix B). Consistent with the CRA19, porosity was set to 16%, and the particle travel times tabulated in the summary files have been multiplied by the factor 4.0/7.75 to adjust the values from the 7.75-meter thickness of the Culebra used in the MODFLOW flow simulations to the 4.0-meter transport thickness used in the transport simulations (Holt, 1997; Kuhlman, 2010).

Particle tracking output is used to index the flow fields by travel time to the LWB for the sensitivity analysis. It also allows for visualization and quantification of the flow characteristics from each of the Culebra release points to the LWB. The particle tracking results do not take into consideration retardation, dispersion, or molecular diffusion.

Information Only

3.4 Radionuclide Transport

Mass transport is simulated with the WIPP PA software SECOTP2D assuming parallel plate fracturing where fluid flow is restricted to the advective continuum (fractures), and mass is transferred between the advective and diffusive (matrix) continua via molecular diffusion. Retardation is implemented in the diffusive domain assuming linear equilibrium isotherms defined with a matrix distribution coefficient for each species. Radioactive decay is implemented with multiple straight decay chains. Only flow velocity is spatially distributed in the Culebra transport model; other quantities are implemented as constant values over the entire spatial extent for each simulation.

The transport preprocessing program PRESECOTP2D performs several transformations to prepare the MODFLOW 50-m cell-by-cell flow output for the transport simulations, including performing basic coordinate system transformations, windowing into the transport subdomain, converting the volumetric flow rates to the vertical thickness of 4.0 m to focus all flow through the more permeable portion of the Culebra, and multiplying the volumetric flow rates by the LHS sampled climate factor parameter.

In each transport simulation, 1 kg of each of four radionuclides is released at one of the four release points during the first 50 years after repository closure. The radionuclides transported in the Culebra are Am-241, Pu-239, Th-230, and U-234. Transport of the Th-230 daughter product of U-234 decay is calculated and tracked as a separate species. Throughout this document, Th-230 will refer to the U-234 daughter product and Th-23A will refer to the Th-230 released at the release point. The cumulative fraction of the mass that crosses the LWB is then tabulated at 50-year intervals for each radionuclide.

The PAPDB designations for the deterministic and uncertain physical transport parameters are shown in Table 4 and Table 5, respectively. These parameter values have not changed since the CCA. Advective and diffusive porosity and matrix half-block length are used in the dual-domain mass transport equations. The climate index parameter is used to scale the computed mining-modified flow velocity to account for the potential impact of climate change (Corbet and Swift, 1996). For uncertain quantities, one sampled value is used to specify a particular parameter value over its entire spatial extent in a single realization.

Table 4 – Deterministic physical parameter values

Model Parameter	MATERIAL: PROPERTY	Units	Value
Longitudinal dispersivity	CULEBRA:DISP_L	m	0
Transverse dispersivity	CULEBRA:DISPT_L	m	0
Fracture tortuosity	CULEBRA:FTORT	-	1.0
Diffusive tortuosity	CULEBRA:DTORT	-	0.11
Skin resistance	CULEBRA:SKIN_RES	-	0
Material grain density	CULEBRA:DNSGRAIN	kg/m^3	2820

Information Only

Table 5 – Uncertain physical parameter distributions

Model Parameter	MATERIAL: PROPERTY	Units	Distribution	Range	Median
Advective porosity	CULEBRA:APOROS	-	Log-uniform	[1.00E-4, 1.00E-2]	0.001
Diffusive porosity	CULEBRA:DPOROS	-	Cumulative	[1.00E-1, 2.50E-1]	0.160
Matrix half-block length	CULEBRA:HMBLKLT	m	Uniform	[5.00E-2, 5.00E-1]	0.275
Climate index	GLOBAL:CLIMTIDX	-	Cumulative	[1.00E+0, 2.25E+0]	1.170

The PAPDB designations for the deterministic and uncertain physical transport parameters are shown in Table 6 and Table 7, respectively. Actinides Pu and U may be present in high or low oxidation states, with separate matrix distribution coefficient parameter distributions and molecular diffusion values defined for each. The OXSTAT parameter is used to determine the oxidation state. New to the RPPCR, two constant parameters define actinide-specific thresholds of the OXSTAT value to determine the actinide oxidation state. The oxidation cutoff for U results in 50% likelihoods of U(IV) or U(VI), while the oxidation cutoff for Pu results in a 25% likelihood of Pu(III) and a 75% likelihood of Pu(IV). Oxidation states are correlated in that both U and Pu oxidation states are determined by the single parameter OXSTAT. In the CRA19 and RPPA, the likelihood was 50% for both Pu(III) and Pu(IV).

Table 6 – Deterministic physical parameter values

Species	Model Parameter	MATERIAL: PROPERTY	Units	Value
Am-241	Atomic Weight	AM241:ATWEIGHT	kg/mole	2.411E-01
	Half-life	AM241:HALFLIFE	s	1.364E+10
	Molecular Diffusion	AM+3:MD0	[m^2/s]	3.00E-10
Pu-239	Atomic Weight	Pu239:ATWEIGHT	kg/mole	2.391E-01
	Half-life	Pu239:HALFLIFE	s	7.594E+11
	Oxidation state threshold	PU:OXCUTOFF	-	0.25
	Molecular Diffusion	Pu+3:MD0	[m^2/s]	3.00E-10
	Molecular Diffusion	Pu+4:MD0	[m^2/s]	1.53E-10
Th-230	Atomic Weight	Th230:ATWEIGHT	kg/mole	2.300E-01
	Half-life	Th230:HALFLIFE	s	2.430E+12
	Molecular Diffusion	Th+4:MD0	[m^2/s]	1.53E-10
U-234	Atomic Weight	U234:ATWEIGHT	kg/mole	2.340E-01
	Half-life	U234:HALFLIFE	s	7.716E+12
	Oxidation state threshold	U:OXCUTOFF	-	0.50

Information Only

	Molecular Diffusion	U+4:MD0	[m²/s]	1.53E-10
	Molecular Diffusion	U+6:MD0	[m²/s]	4.26E-10

Table 7 – Uncertain chemical parameters distributions

Model Parameter	MATERIAL: PROPERTY	Units	Distribution	Range	Median
Oxidation state index	GLOBAL:OXSTAT	-	Uniform	[0.00E+0, 1.00E+0]	0.50
Matrix distribution coefficient					
Am(III)	AM+3:MKD_AM	m³/kg	Log-uniform	[5.00E-3, 4.00E-1]	4.50E-2
Pu(III)	PU+3:MKD_PU	m³/kg	Log-uniform	[5.00E-3, 4.00E-1]	4.50E-2
Pu(IV)	PU+4:MKD_PU	m³/kg	Log-uniform	[5.00E-4, 1.00E+1]	7.10E-2
Th(IV)	TH+4:MKD_TH	m³/kg	Log-uniform	[5.00E-4, 1.00E+1]	7.10E-2
U(IV)	U+4:MKD_U	m³/kg	Log-uniform	[5.00E-4, 1.00E+1]	7.10E-2
U(VI)	U+6:MKD_U	m³/kg	Log-uniform	[3.00E-5, 2.00E-2]	7.70E-4

3.5 Sensitivity Analysis

The WIPP program STEPWISE is used to determine the relative influence of the sampled parameters on the uncertainty in the output mass discharge to the LWB. STEPWISE performs a stepwise multiple regression analysis on the ranked dependent and independent variables. For the Culebra transport analysis, the cumulative mass transport to the LWB at 10,000 years post-closure is input to STEPWISE as the dependent variable. Independent variables include the following LHS sampled parameter values.

- GLOBAL:CLIMIDX
- CULEBRA:FPOROS
- CULEBRA:MPOROS
- CULEBRA:HMBKLT

Additional independent variables and the DTRKMF output travel times to the LWB, which are used to index the MODFLOW flow fields, and the matrix distribution coefficients:

- DTRK_TIME: particle travel time to the LWB as a surrogate for flow field impact.
- MKD_L: matrix distribution coefficient for each isotope *L*.

Where MKD represents the combined LHS samples for the oxidation state dependent matrix distribution coefficient, computed for Pu-239 as:

$$MKD_PU_v = \begin{cases} PU+3: MKDPU_v \; if \; GLOBAL: OXSTAT_v \leq PU: OXCUTOFF \\ PU+4: MKDPU_v \; if \; GLOBAL: OXSTAT_v > PU: OXCUTOFF \end{cases}$$

and for U-234 as: $MKD_U_v = \begin{cases} U+4: MKDU_v \; if \; GLOBAL: OXSTAT_v \leq U: OXCUTOFF \\ U+6: MKDU_v \; if \; GLOBAL: OXSTAT_v > U: OXCUTOFF \end{cases}$

Information Only

in which v indicates the LHS vector and the LHS material and properties are defined in Table 6 and Table 7.

3.6 Code Execution and Run Control

Culebra flow and transport calculations are automated by the WIPP PA Run Control System on the Sandia Carlsbad Linux computing cluster. A full description of the RPPCR run control, including names and locations of input and output files, can be found in Long (2023).

3.6.1 Flow

The run control diagram for the flow simulations is shown on Figure 5. The MODFLOW software is used in conjunction with several utility programs (GENMESH, MATSET, POSTLHS, SUMMARIZE) which variously set model parameters, material properties, sample from the probability distributions for subjectively uncertain parameters, and write output summary text files.

Several Python utilities are qualified for use in this analysis per Nuclear Waste Management Procedure NP 9-1: Analyses (Nielsen, 2020), including:

- *enlarge_mining_areas.py*, *mining_mod.py*, and *100x100_to_50x50.py* (Appendix A)
- *summarize_dtrkmf.py* (Appendix B)
- *CBC2BUD* (Appendix C)

The other software used in the analysis are qualified per Nuclear Waste Management Procedure NP 19-1: Software Requirements (Long, 2020).

Information Only

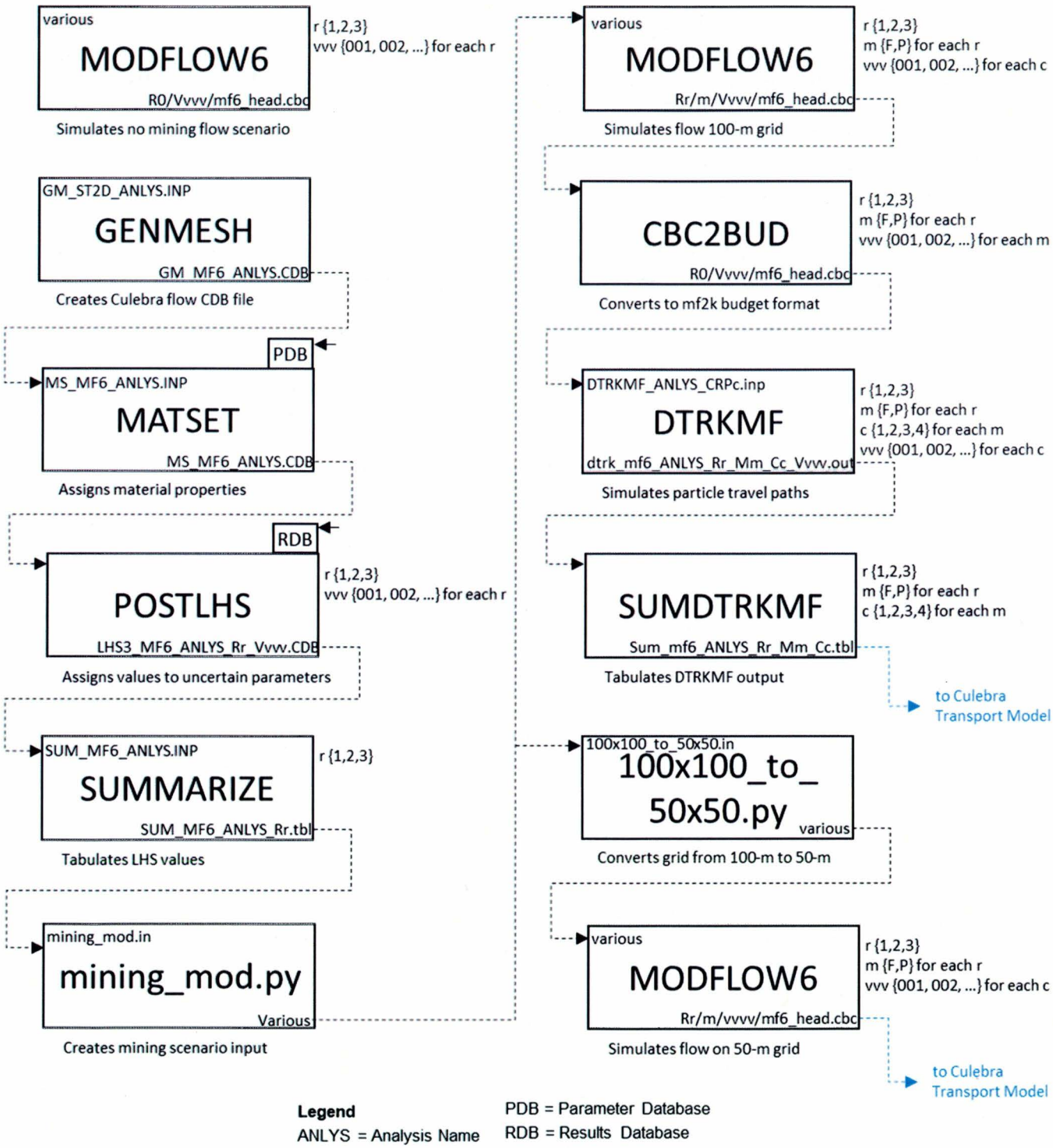


Figure 5 – Culebra flow model run control diagram

Information Only

3.6.2 Transport

The run control diagram for the transport simulations is shown on Figure 6. The Culebra transport model includes 2,400 calls to the WIPP groundwater transport software SECOTP2D (3 replicates, 2 mining scenarios, 4 mass release points, 100 vectors). The SECOTP2D mass transport simulator is used in conjunction with a preprocessor utility (PRESECOTP2D) and a postprocessor utility (POSTSECOTP2D). In addition, several utility codes are used to sample from the probability distributions for subjectively uncertain parameters, define the mesh, set material properties, and set model parameters. As a part of the Culebra transport model, the STEPWISE software is used to conduct a sensitivity analysis to determine the relative importance of the input parameters in the Culebra transport calculation. The codes used in the transport analysis are qualified per Nuclear Waste Management Procedure NP 19-1: Software Requirements (Long, 2020).

Information Only

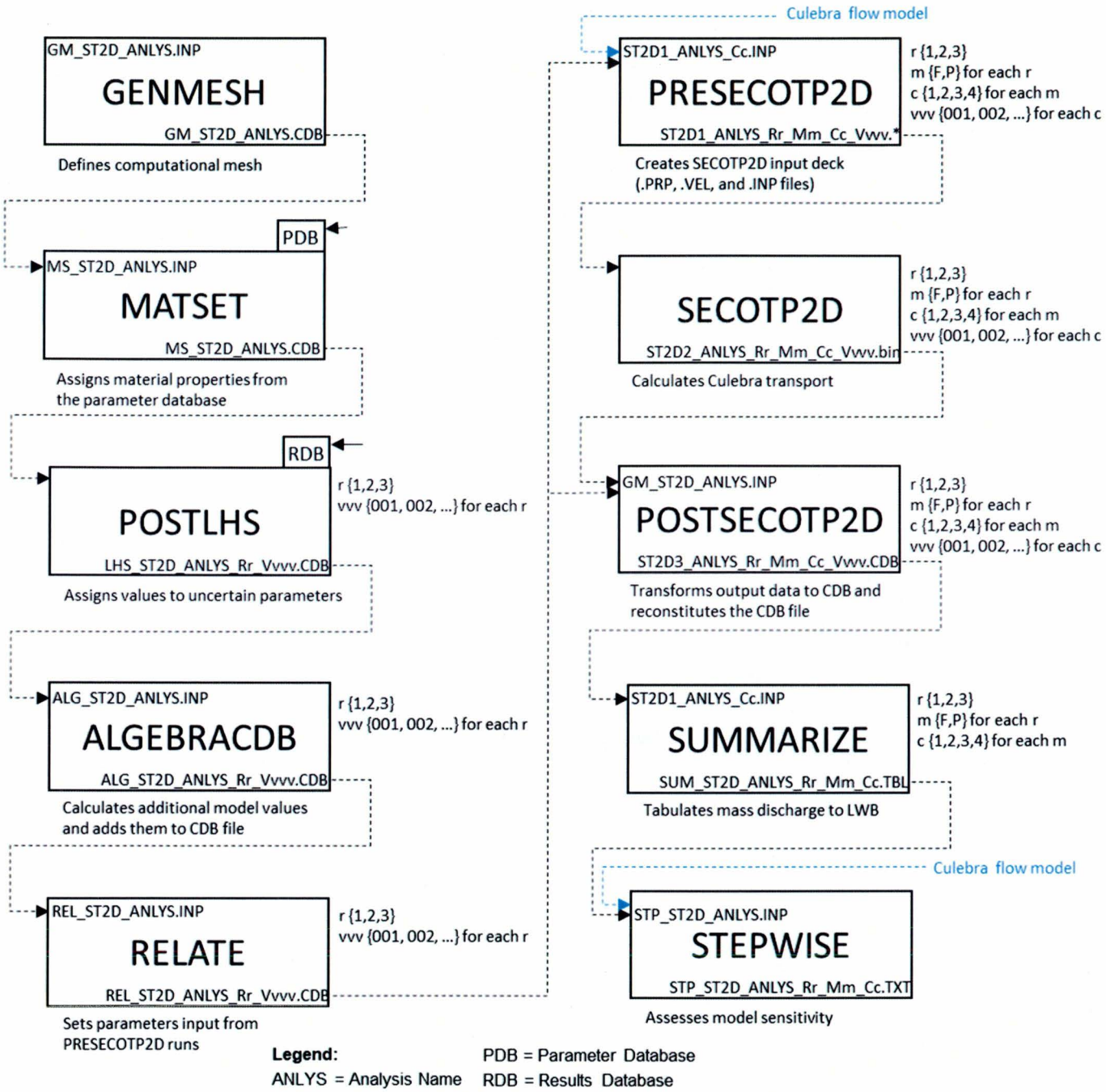


Figure 6 – Culebra transport model run control diagram

Information Only

This page intentionally left blank.

Information Only

4.0 RESULTS

This section presents results from the RPPCR flow, particle tracking, and mass transport calculations. Flow results are compared to the CRA19. Particle track and mass transport results are compared to both the CRA19 and RPPA model output where appropriate.

4.1 Flow

This section presents results from the RPPCR MODFLOW 100-m flow simulations. The output files were converted from budget format to text format with the Python script *bud2ascii.py* for display and post-processing (Appendix D). Results are compared to the CRA19 flow files fetched from the CVS repository *MiningMod* module *Outputs/R{1,2,3}/{full,part}/r{rrr}/modeled_flow.bud*, also converted to text format with the *bud2ascii.py* utility script.

The plots in Figure 7 and Figure 8 show the ensemble average of $\log_{10}$ flow rates within the LWB in the RPPCR and CRA19, respectively. The high-transmissivity pathway observed during the SNL-14 pumping test (the linear north-south feature located in the southern half of the domain approximately following column 130) is apparent in both the full and partial mining scenarios of both analyses, though more prominent in CRA19 than the RPPCR. The edges of the areas affected by potash mining are visible in both mining scenarios, in the full mining case as an irregular shaped region with lighter color extending over the LWB everywhere but the southwest quadrant, and in the partial-mining case just inside the periphery of the WIPP LWB.

The plots in Figure 9 and Figure 10 show the standard deviation of the magnitude of the $\log_{10}$ Darcy flow rates for the RPPCR and CRA19, respectively. In general, the RPPCR flow rates were less variable than the CRA19 flow rates, particularly in the northwest region of the controlled area and in a smaller region along the south of the LWB. This is consistent with the lower standard deviation observed in the updated calibrated T-fields, attributed to the greater number of calibration targets in this region (Bowman et al., 2023).

The plots in Figure 11 and Figure 12 show the flow direction variability within the LWB for the RPPCR and CRA19. The outline of the mining impacted regions is visible in both the RPPCR and CRA19, where the flow direction variability drops to close to zero. The CRA19 flow direction appears to be more variable along the southern extent of the LWB in the partial mining scenario.

Information Only

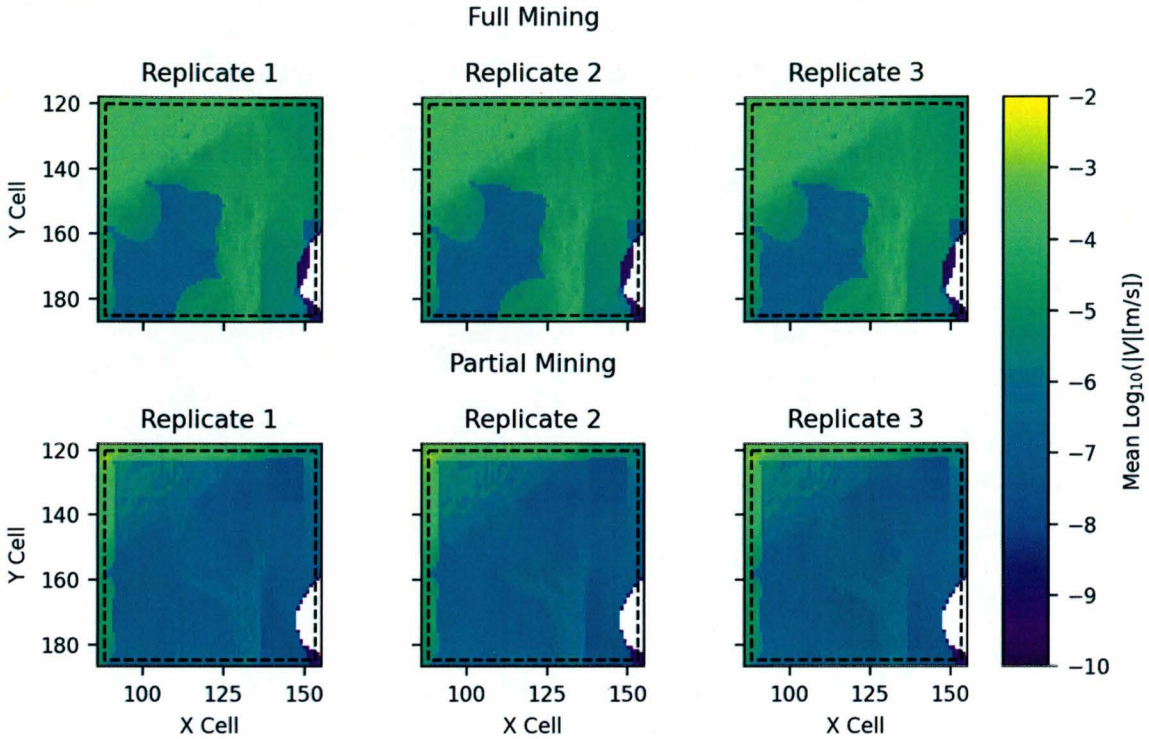


Figure 7 – Ensemble mean RPPCR flow rate

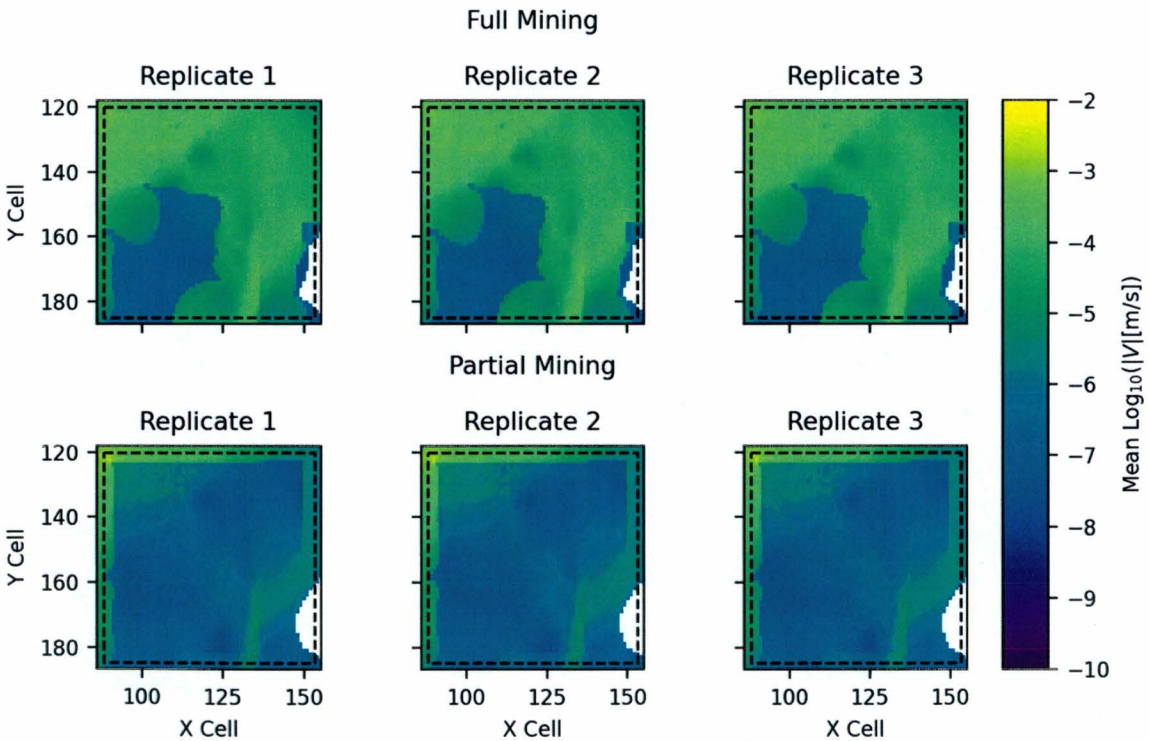


Figure 8 – Ensemble mean CRA19 flow rate

Information Only

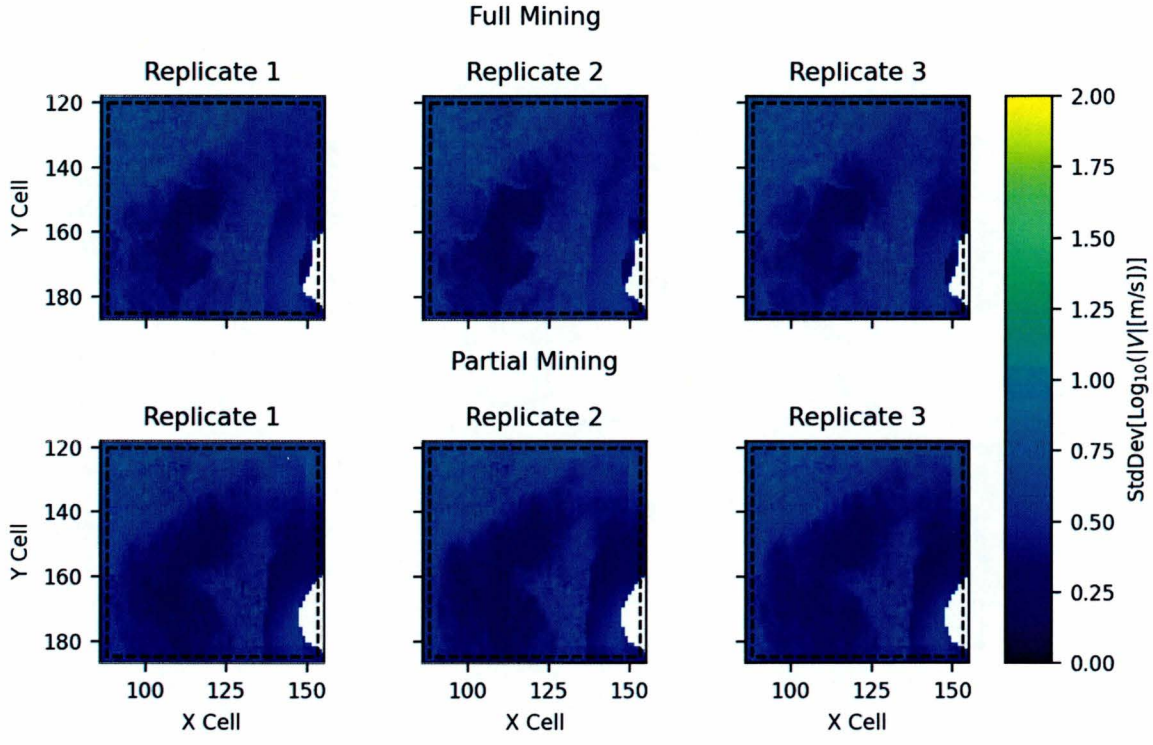


Figure 9 – Ensemble standard deviation RPPCR flow rate

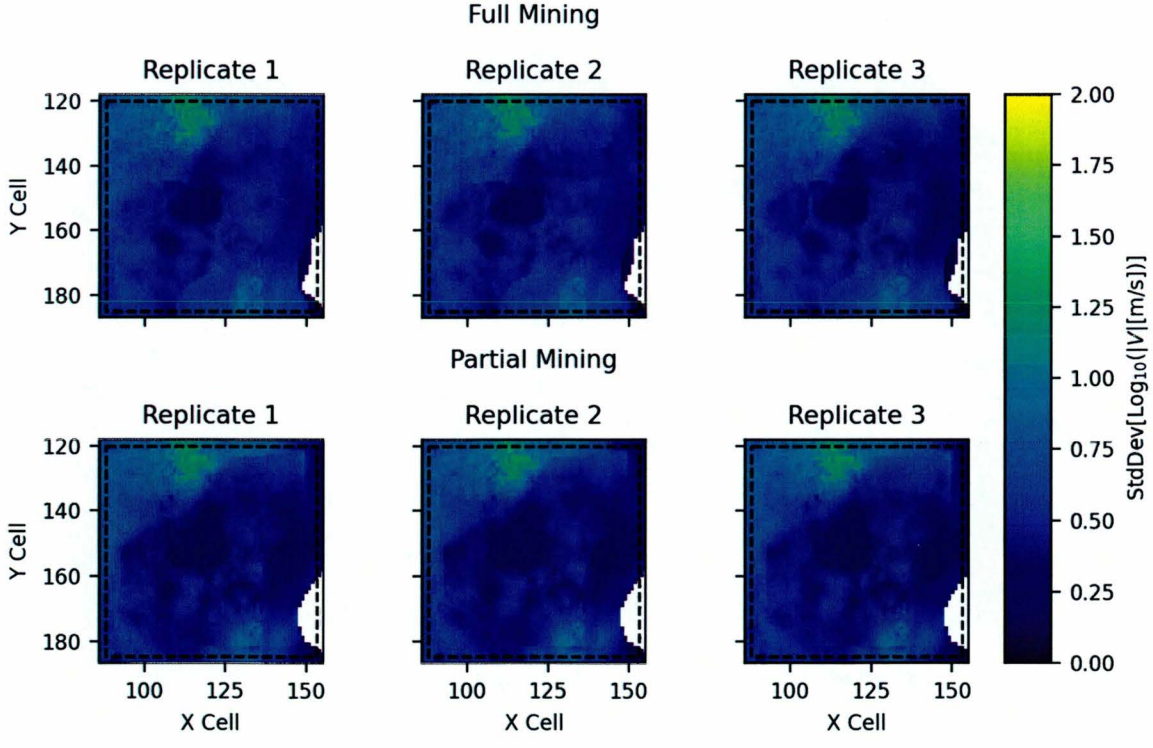


Figure 10 – Ensemble standard deviation CRA19 flow rate

Information Only

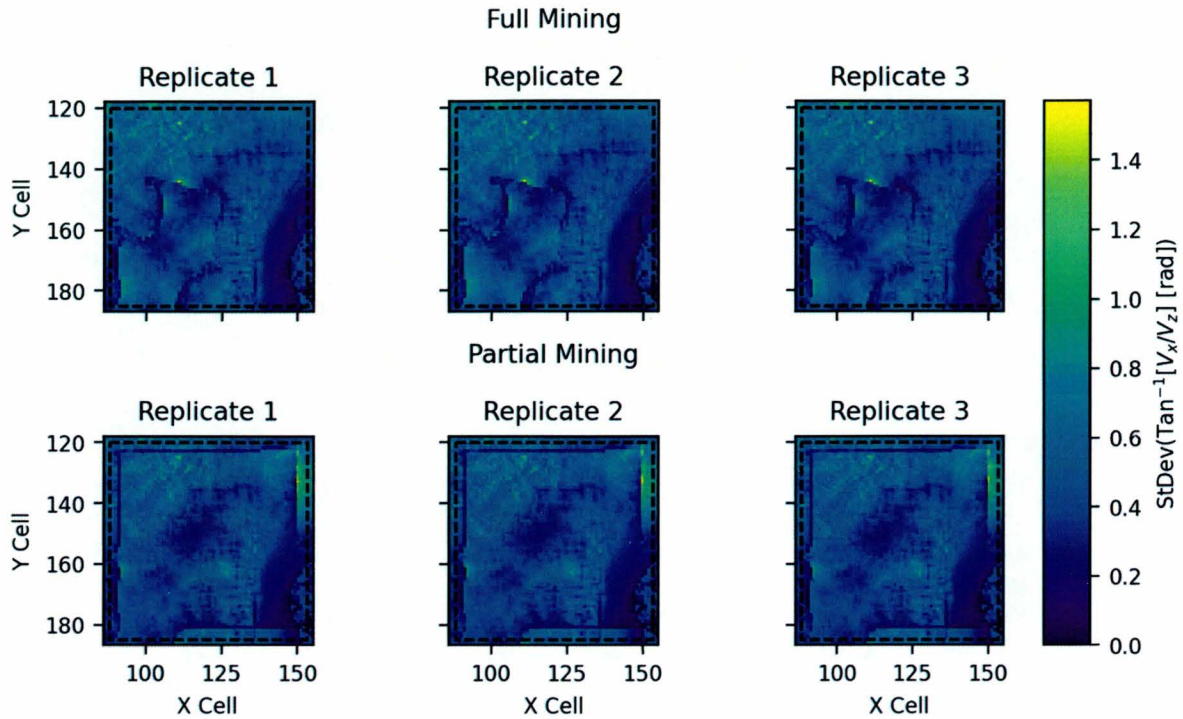


Figure 11 – Ensemble standard deviation RPPCR flow direction

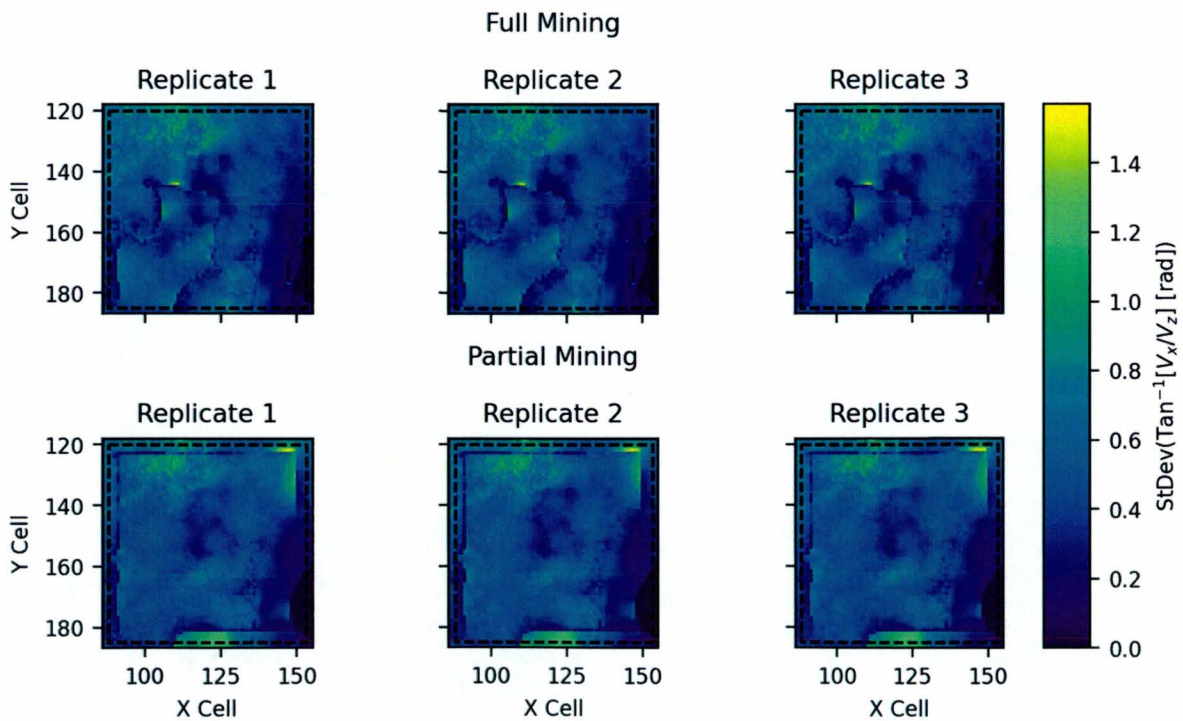


Figure 12 – Ensemble standard deviation CRA19 flow direction

Information Only

4.2 Particle Tracking

This section presents results from the DTRKMF output particle time and position (*dtrk_mf6_RPPCR_r{1,2,3}_m{f,p}_c{1,2,3,4}_v{vvv}.out*), and the associated summary table files (*sum_mf6_RPPCR_r{1,2,3}_m{f,p}_c{1,2,3,4}_v{vvv}.tbl*). Particle track results are presented for three replicates of 100 vectors each for two mining scenarios and four release points for a total of 2400 particle tracks. The CRA19 DTRKMF summary tables (*wipplwb_results_R{1,2,3}_{full,part}.out*) were obtained from the CVS repository *MiningMod* module *Outputs/Summary/*.

Results from RPPCR CRP1 are compared to the values in CRA19 in the scatter plots in Figure 13. Vectors with a faster travel time to the LWB in the RPPCR plot below the dashed 1:1 reference line. Rank correlations between analysis vectors and associated p-values were calculated with the Python stats package and are displayed directly on the figures. Correlation values show there is no association between the RPPCR and CRA19 travel times in the full mining scenario, and a positive but low correlation in the partial mining simulations. Any correlation between the analysis results can be attributed to the mining factor, which is consistent between analyses. The general lack of correlation indicates that the T-fields are a more important control than mining factor for particle travel times in the CRP1 simulations.

Map view plots are constructed showing the spatial distribution of 100 particle tracks from each release point and replicate in the full mining scenario (Figure 14) and partial mining scenario (Figure 15), with the mining-impacted area shown in gray. The particle tracks show flow downstream of release points CRP1, CRP2, and CRP3 is generally oriented toward the south. In the full mining scenario, particle tracks show the flow field is typically oriented toward the full mining impacted area to the southeast, then deflects along the mining affected region interface to the southern LWB. The partial mining particle tracks are more broadly distributed across the east-west direction (i.e., not focused by any persistent features across realizations), but are also generally directed toward the south. In contrast, the particle tracks from CRP4 vary significantly between scenarios: the full mining particle tracks continue west then turn sharply to the south near the western edge of the LWB, while the partial mining particle tracks generally lead south.

The cumulative distribution of the time taken for a particle to reach the LWB along each particle track is plotted as an exceedance probability for each replicate, mining scenario, and release point (Figure 16 though Figure 18). These plots describe the likelihood of a particle crossing the LWB within the range of observed particle travel times. Results from the RPPA and CRA19 (CRP1 only) are included for reference. Mean, median, minimum, and maximum travel times are presented in Table 9 through Table 11. The CRA19 results are shown in Figure 16 but are omitted from the tables because the RPPA CRP1 are functionally equivalent to CRA19, with the same T-fields and LHS parameters. Consistent with the RPPA, particles exit the LWB in the full mining CRP4 scenario significantly earlier than the other scenarios across all probability levels; however, the full mining scenario RPPCR particle travel times from CRP4 are longer than the RPPA particle travel times. Travel times to the LWB from the CRP2 and CRP3 release points are longer than travel times to the LWB from the CRP1 release points.

Information Only

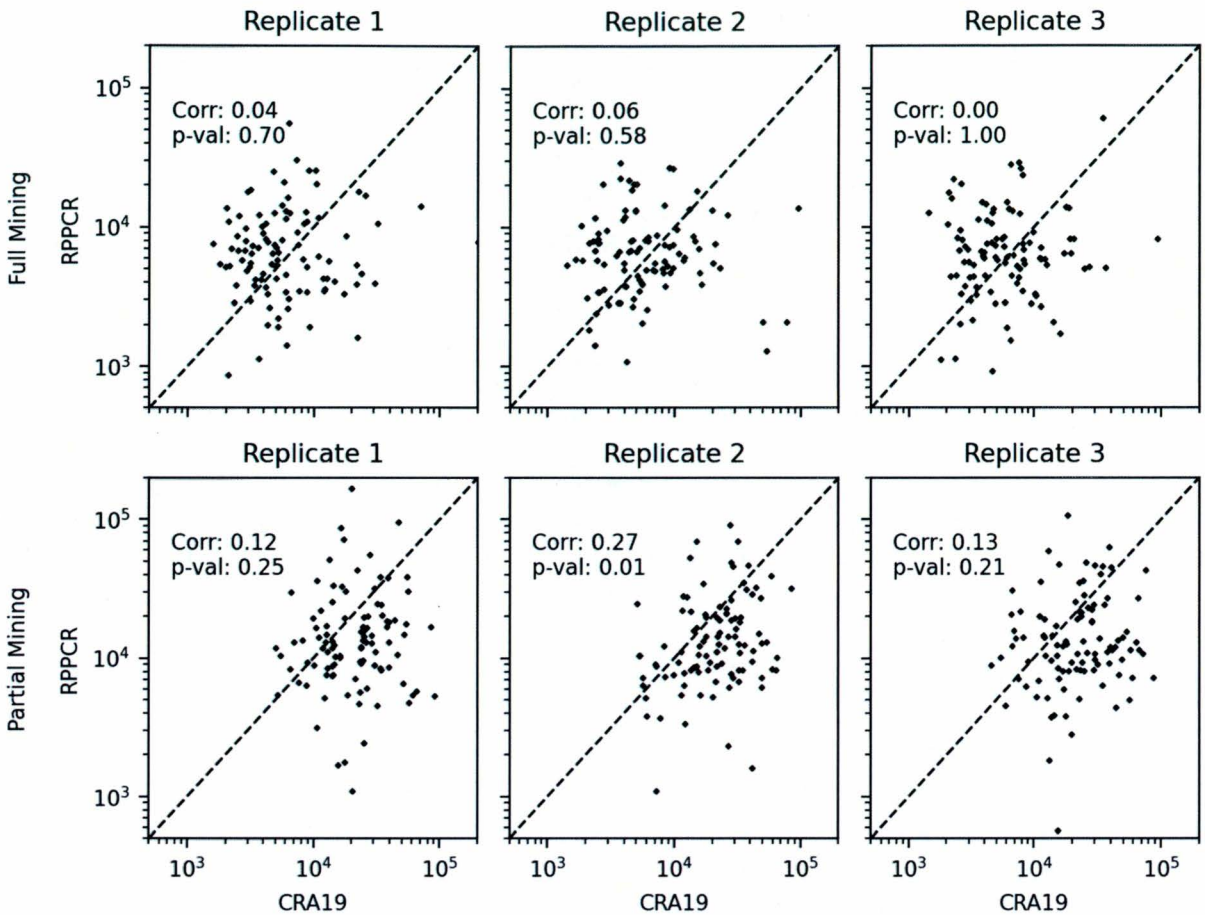


Figure 13 – DTRKMF particle travel time to LWB scatter plots

Information Only

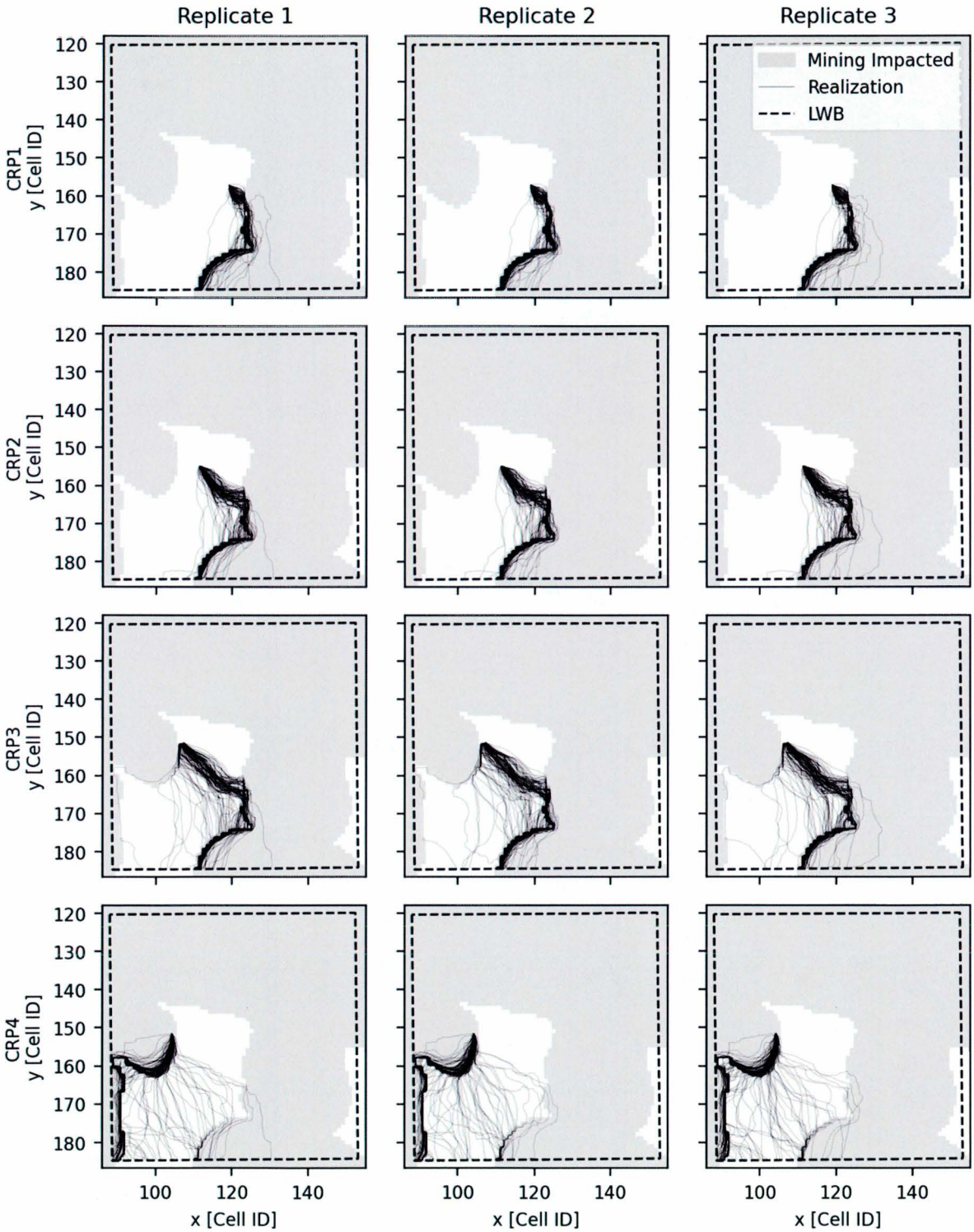


Figure 14 – DTRKMF particle tracks, full mining scenario

Information Only

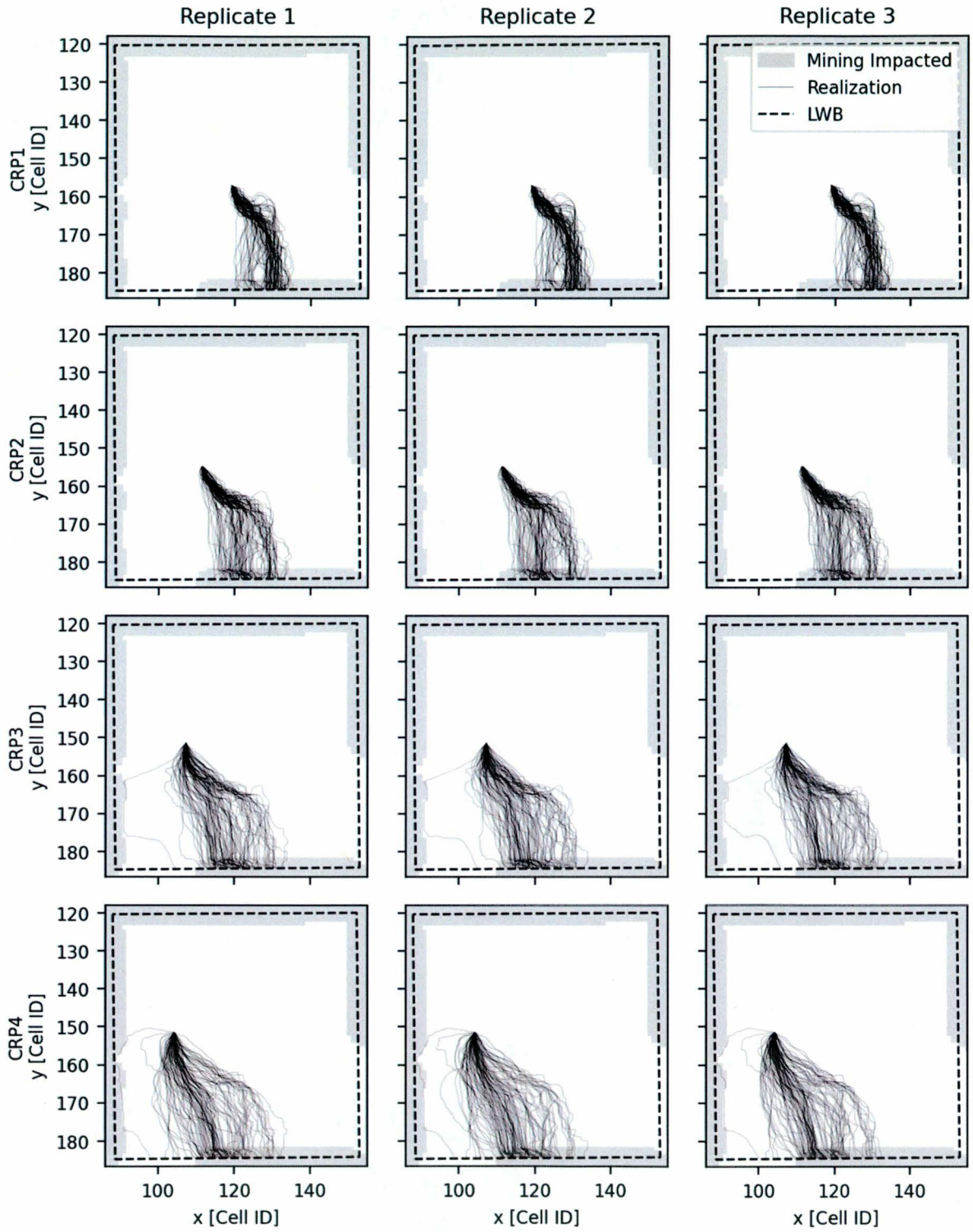


Figure 15 – DTRKMF particle tracks, partial mining scenario

Information Only

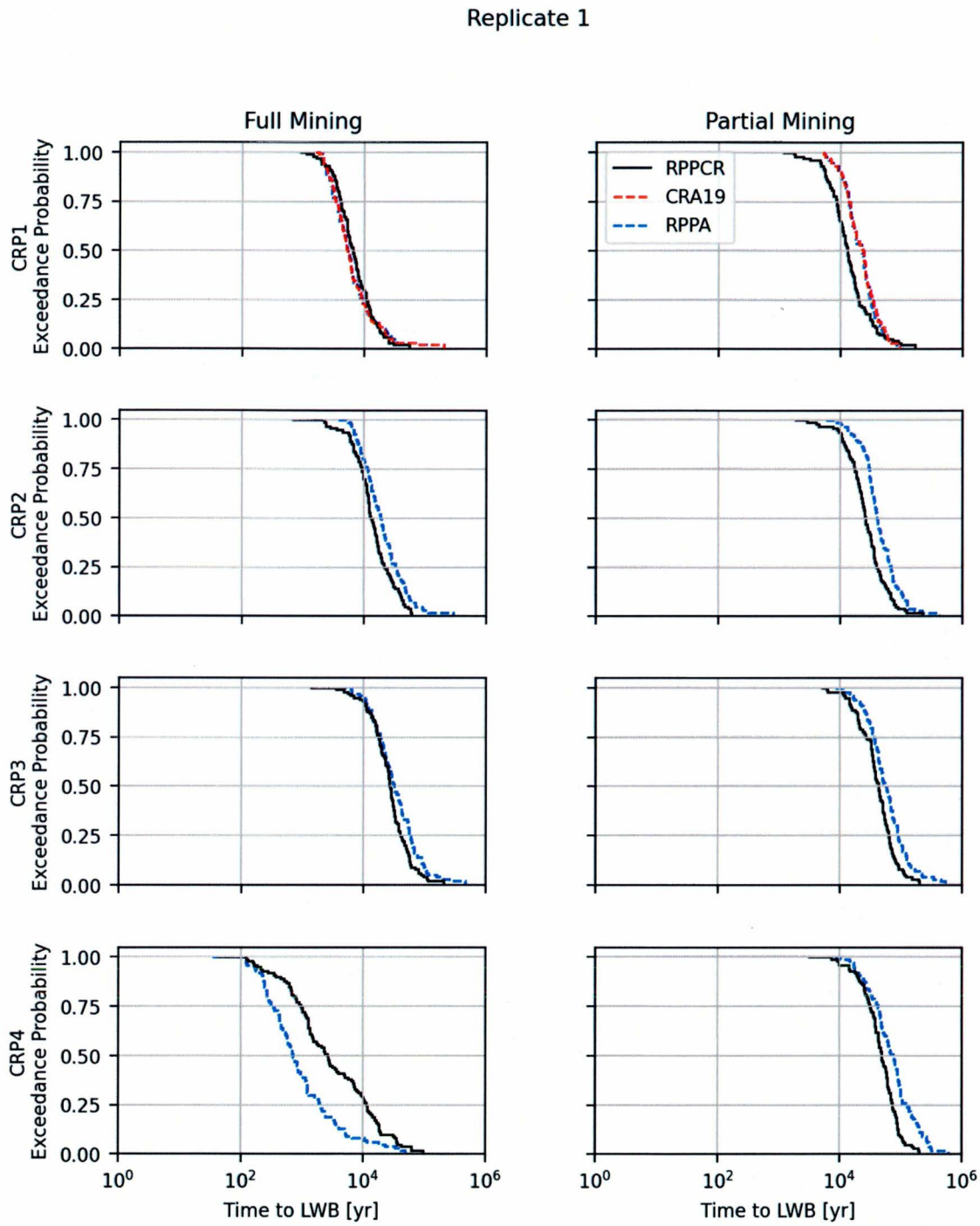


Figure 16 – Particle travel time to LWB exceedance probabilities, Replicate 1

Information Only

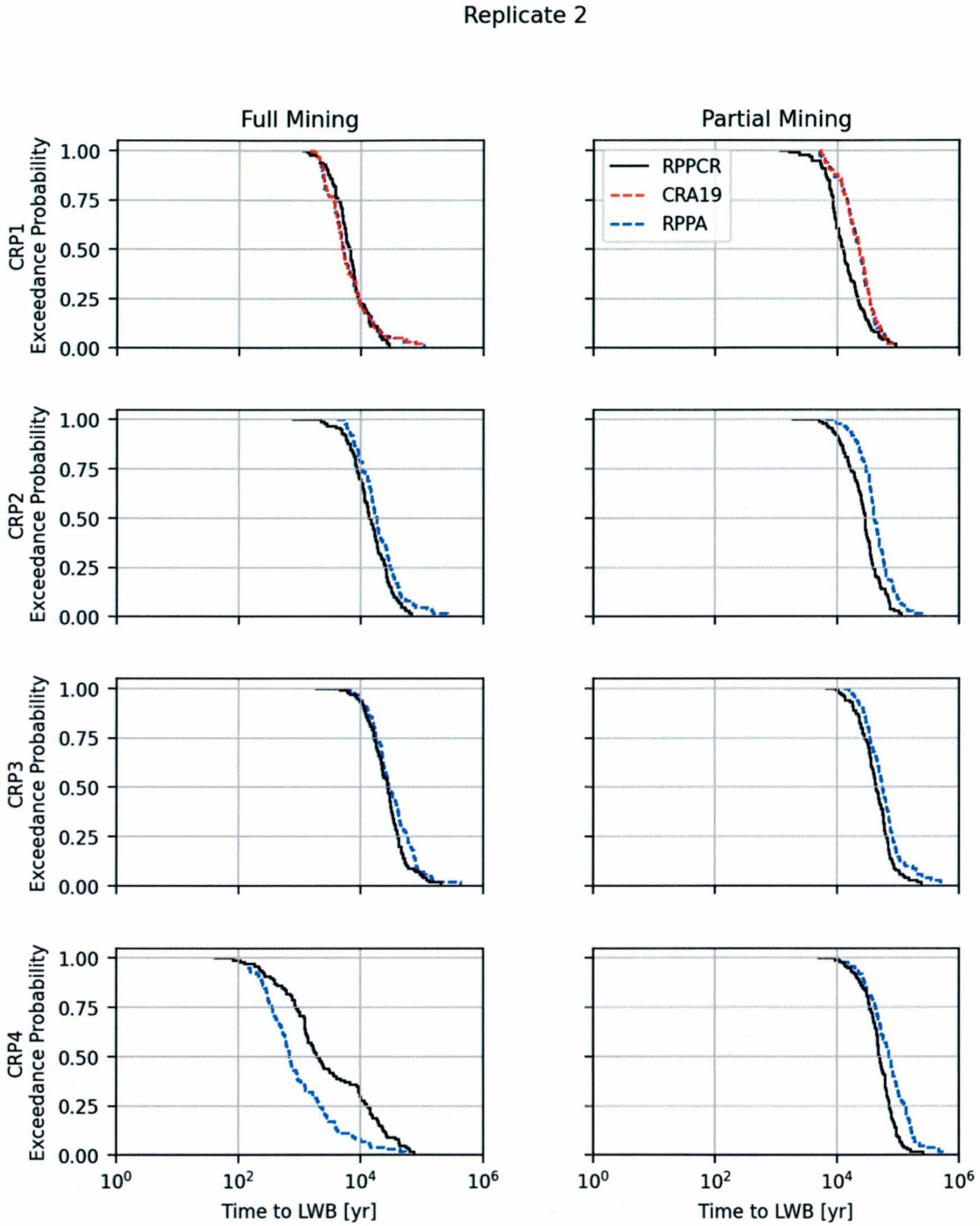


Figure 17 – Particle travel time to LWB exceedance probabilities, Replicate 2

Information Only

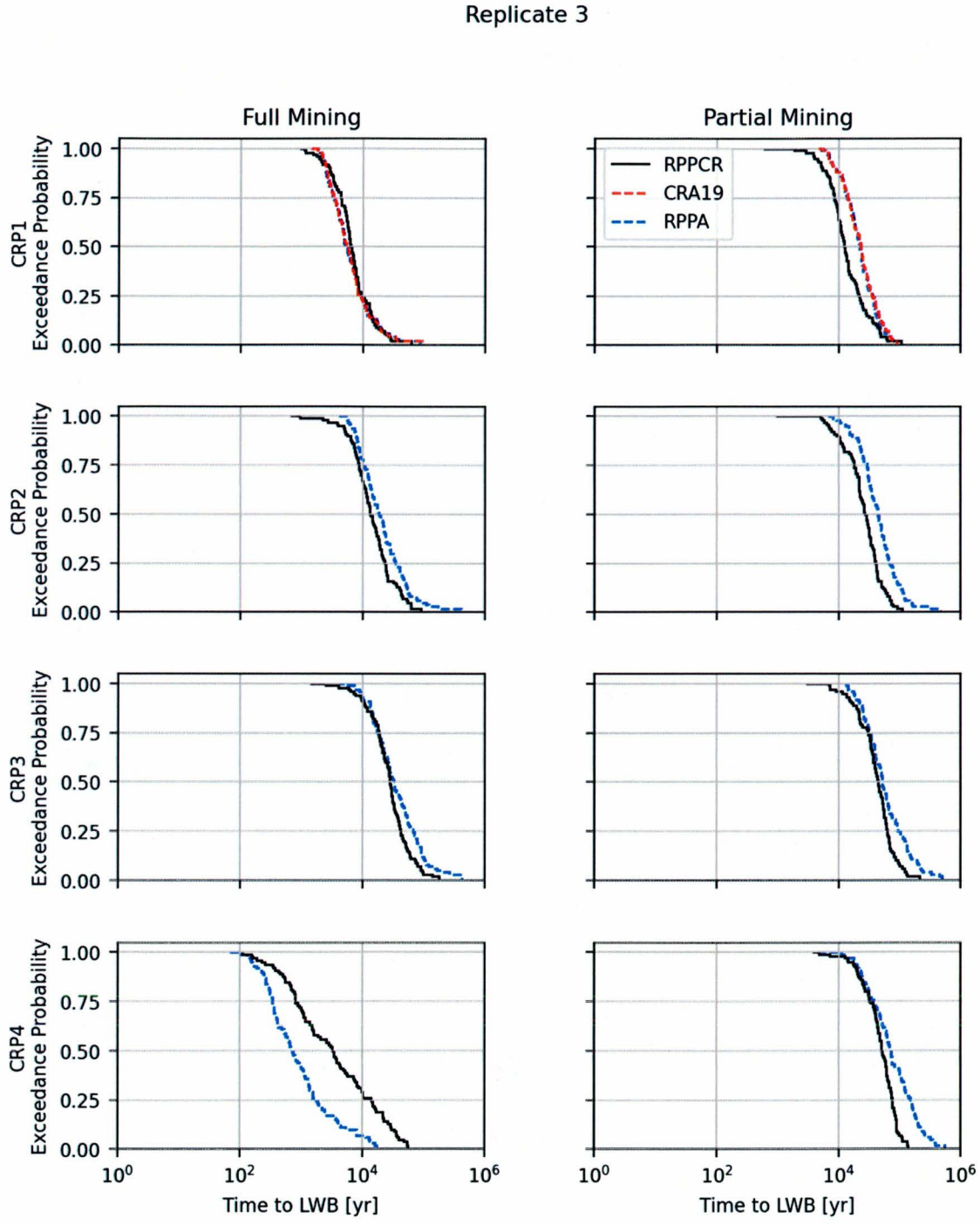


Figure 18 – Particle travel time to LWB exceedance probabilities, Replicate 3

Information Only

Table 8 – Mean particle travel time to LWB

	Full Mining				Partial Mining			
	CRP1	CRP2	CRP3	CRP4	CRP1	CRP2	CRP3	CRP4
RPPCR								
R1	8.57E+03	1.78E+04	3.40E+04	8.86E+03	1.87E+04	3.32E+04	4.86E+04	5.53E+04
R2	7.97E+03	1.79E+04	3.34E+04	9.35E+03	1.70E+04	3.14E+04	5.06E+04	5.62E+04
R3	8.38E+03	1.83E+04	3.43E+04	9.32E+03	1.73E+04	3.05E+04	4.88E+04	5.43E+04
GLOBAL	8.31E+03	1.80E+04	3.39E+04	9.18E+03	1.77E+04	3.17E+04	4.93E+04	5.53E+04
RPPA								
R1	9.10E+03	2.80E+04	4.86E+04	3.06E+03	2.47E+04	5.45E+04	7.74E+04	9.77E+04
R2	9.36E+03	2.75E+04	4.41E+04	2.97E+03	2.49E+04	5.10E+04	7.64E+04	9.45E+04
R3	8.33E+03	3.07E+04	5.36E+04	2.05E+03	2.55E+04	5.81E+04	7.93E+04	1.02E+05
GLOBAL	8.93E+03	2.88E+04	4.88E+04	2.69E+03	2.50E+04	5.45E+04	7.77E+04	9.81E+04

Table 9 – Median particle travel time to LWB

	Full Mining				Partial Mining			
	CRP1	CRP2	CRP3	CRP4	CRP1	CRP2	CRP3	CRP4
RPPCR								
R1	6.49E+03	1.28E+04	2.72E+04	2.48E+03	1.29E+04	2.54E+04	4.22E+04	4.80E+04
R2	6.39E+03	1.35E+04	2.71E+04	1.91E+03	1.20E+04	2.79E+04	4.21E+04	4.75E+04
R3	6.23E+03	1.32E+04	2.80E+04	3.31E+03	1.21E+04	2.65E+04	4.31E+04	5.03E+04
GLOBAL	6.38E+03	1.33E+04	2.75E+04	2.43E+03	1.23E+04	2.61E+04	4.24E+04	4.92E+04
RPPA								
R1	5.30E+03	1.92E+04	3.19E+04	7.05E+02	2.26E+04	3.98E+04	5.55E+04	7.11E+04
R2	5.11E+03	1.79E+04	2.86E+04	7.00E+02	2.23E+04	3.92E+04	5.48E+04	7.09E+04
R3	5.26E+03	1.79E+04	3.18E+04	7.02E+02	2.20E+04	4.36E+04	5.16E+04	6.99E+04
GLOBAL	5.23E+03	1.84E+04	3.08E+04	7.02E+02	2.23E+04	4.08E+04	5.33E+04	7.08E+04

Information Only

Table 10 – Minimum particle travel time to LWB

	Full Mining				Partial Mining			
	CRP1	CRP2	CRP3	CRP4	CRP1	CRP2	CRP3	CRP4
RPPCR								
R1	8.66E+02	6.43E+02	1.29E+03	4.09E+01	1.09E+03	1.76E+03	4.79E+03	2.97E+03
R2	1.09E+03	7.49E+02	1.77E+03	3.99E+01	1.09E+03	1.76E+03	6.26E+03	4.70E+03
R3	9.23E+02	6.43E+02	1.41E+03	1.05E+02	5.70E+02	9.23E+02	2.83E+03	3.60E+03
GLOBAL	8.66E+02	6.43E+02	1.29E+03	3.99E+01	5.70E+02	9.23E+02	2.83E+03	2.97E+03
RPPA								
R1	1.58E+03	3.84E+03	3.84E+03	3.49E+01	5.11E+03	5.90E+03	8.53E+03	8.40E+03
R2	1.41E+03	4.12E+03	3.43E+03	8.02E+01	5.07E+03	6.20E+03	1.25E+04	8.53E+03
R3	1.41E+03	4.06E+03	3.65E+03	6.97E+01	4.47E+03	6.65E+03	1.33E+04	4.40E+03
GLOBAL	1.41E+03	3.84E+03	3.43E+03	3.49E+01	4.47E+03	5.90E+03	8.53E+03	4.40E+03

Table 11 – Maximum particle travel time to LWB

	Full Mining				Partial Mining			
	CRP1	CRP2	CRP3	CRP4	CRP1	CRP2	CRP3	CRP4
RPPCR								
R1	5.55E+04	6.15E+04	2.09E+05	9.90E+04	1.67E+05	2.17E+05	1.98E+05	2.02E+05
R2	2.91E+04	6.70E+04	2.03E+05	7.51E+04	9.12E+04	1.13E+05	2.45E+05	2.55E+05
R3	6.03E+04	8.95E+04	1.77E+05	5.61E+04	1.07E+05	1.09E+05	2.11E+05	1.38E+05
GLOBAL	6.03E+04	8.95E+04	2.09E+05	9.90E+04	1.67E+05	2.17E+05	2.45E+05	2.55E+05
RPPA								
R1	1.06E+05	3.01E+05	4.69E+05	5.06E+04	9.13E+04	4.08E+05	5.36E+05	5.94E+05
R2	1.07E+05	2.61E+05	4.33E+05	5.38E+04	8.53E+04	2.77E+05	5.10E+05	5.58E+05
R3	8.68E+04	4.19E+05	4.29E+05	1.74E+04	8.86E+04	4.70E+05	4.95E+05	5.53E+05
GLOBAL	1.07E+05	4.19E+05	4.69E+05	5.38E+04	9.13E+04	4.70E+05	5.36E+05	9.00E+00

Information Only

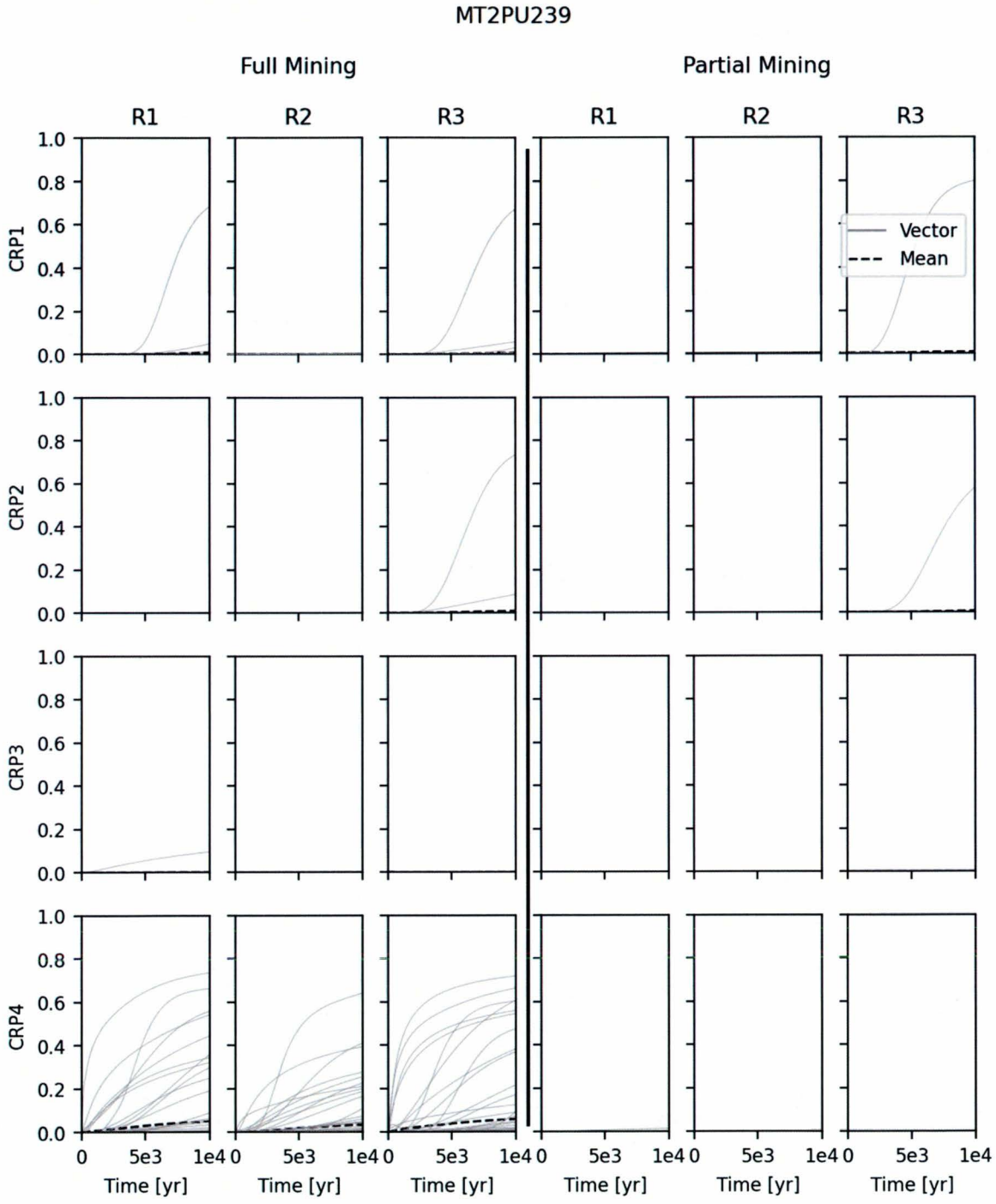
4.3 Radionuclide Transport

This section presents results from the SECOTP2D transport simulation summary output tables (*sum_st2d_RPPCR_r{1,2,3}_m{f,p}_c{1,2,3,4}.tbl*). Results are shown on the following types of figures:

- Scatter plots of mass breakthrough at 10,000 years for the RPPCR CRP1 versus CRA19 (Figure 19)

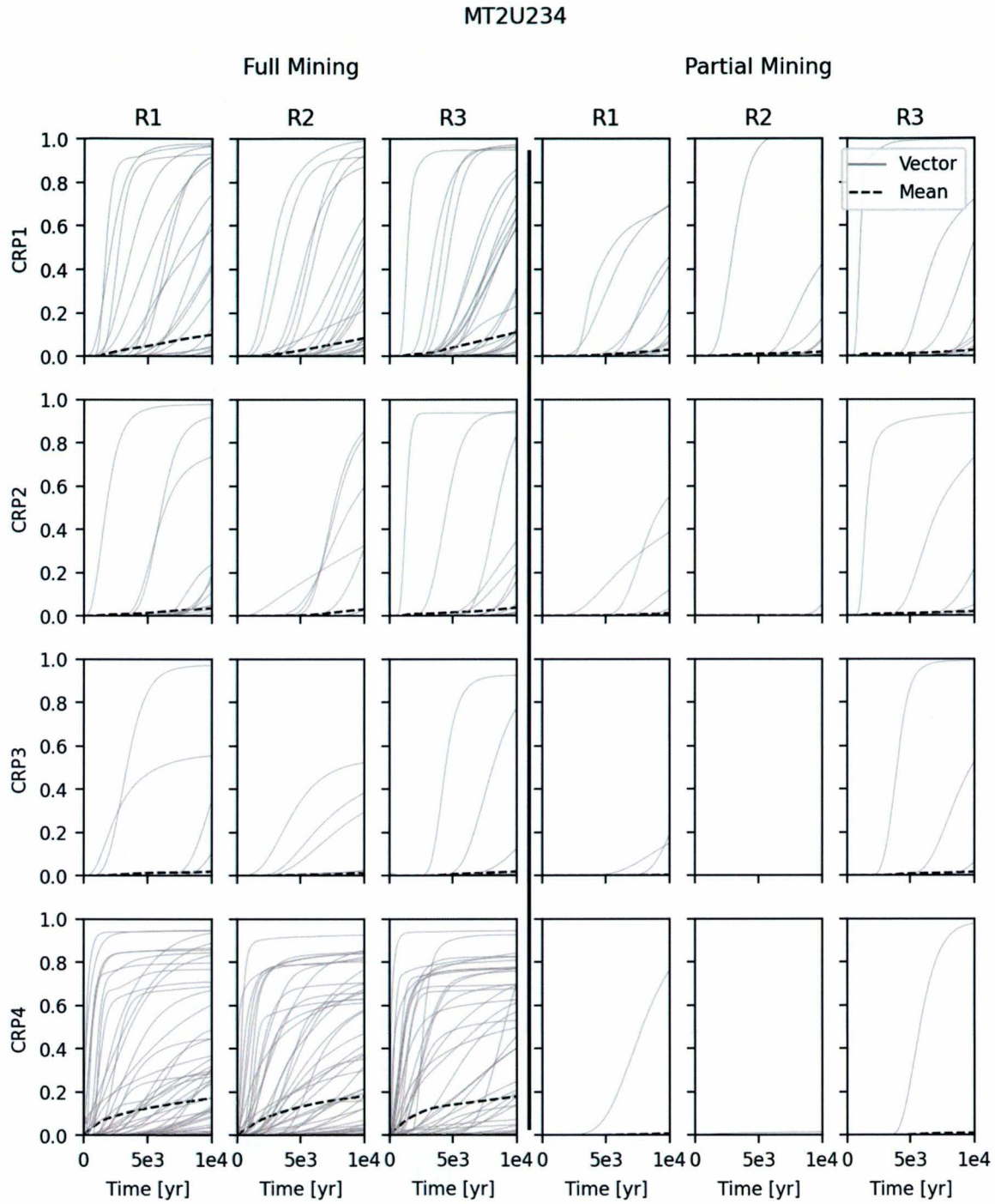
Information Only

Breakthrough curves of mass discharge to the LWB over time showing both individual vector and replicate means (Figure 20



Information Only

Figure 24 Figure 28



- Figure 32, and). The breakthrough curves are shown on a linear ordinate from 0 to 1 kg for all scenarios and isotopes. One replicate of 100 simulations is included in each subplot, though in most subplots many vectors plot very close to the x-axis over the entire simulation period.
- Exceedance probability curves of cumulative mass reaching the LWB by t=10,000 years model time (Figure 21 through Figure 23, Figure 25 through Figure 27, Figure 29 through

Information Only

Figure 31, Figure 33 through Figure 35, and Figure 37 through Figure 39). The histograms are shown on a logarithmic abscissa from 10^{-10} to 1 kg, again for all isotopes and scenarios. The 10^{-9} kg significance threshold was chosen for consistency with the PABC09 report (Kuhlman, 2010). Results below the plotting limits are not shown on the figures, and as a result some subplots display few or even no results due to the low predictions of mass to the LWB by SECOTP2D. CRA19 values are shown in red on the CRP1 exceedance subplots.

Summary statistics are presented in Table 12 through Table 15 including the mean, median, maximum cumulative release, and vector count with mass transported to the LWB greater than 10^{-9} kg. Values below 10^{-24} kg are tabulated as zero.

The CRA19 and RPPCR CRP1 mass transport results on Figure 19 show that the new flow fields are causing the results to scatter widely away from the 1:1 line. The other input difference between these analyses is the updated Pu-239 oxidation state model, which shifts 25% percent of the simulations from Pu(III) to Pu(IV), likely contributing to additional scattering in Pu mass transport results.

Several features are apparent in the plotted data for the new release points. Releases from the full mining scenario are larger than the releases from the partial mining scenarios for all isotopes and release points, particularly for CRP4. The breakthrough curves for all isotopes show earlier, more complete, and more frequent breakthrough from CPR4 in full-mining conditions, than in any other scenario, while the exceedance probability curves demonstrate that the cumulative releases at 10,000 years are highest in full-mining, CRP4 simulations across all displayed probability ranges. For all isotopes, the CRP2 release is lower than the CRP3 release, which in turn is lower than the CRP1 and PABC09 results. Most of the breakthrough curves from partial-mining scenario calculations are below the plotting limits for all isotopes and release points. The cumulative mass transported to the LWB from all release points and mining scenarios from Am-241 are lowest and U-234 are the highest, with the Th-23A and Pu-239 values in-between. The U-234 decay product Th-230 breakthrough curves are not visible above the x-axis for all

Information Only

simulations in all subplots (

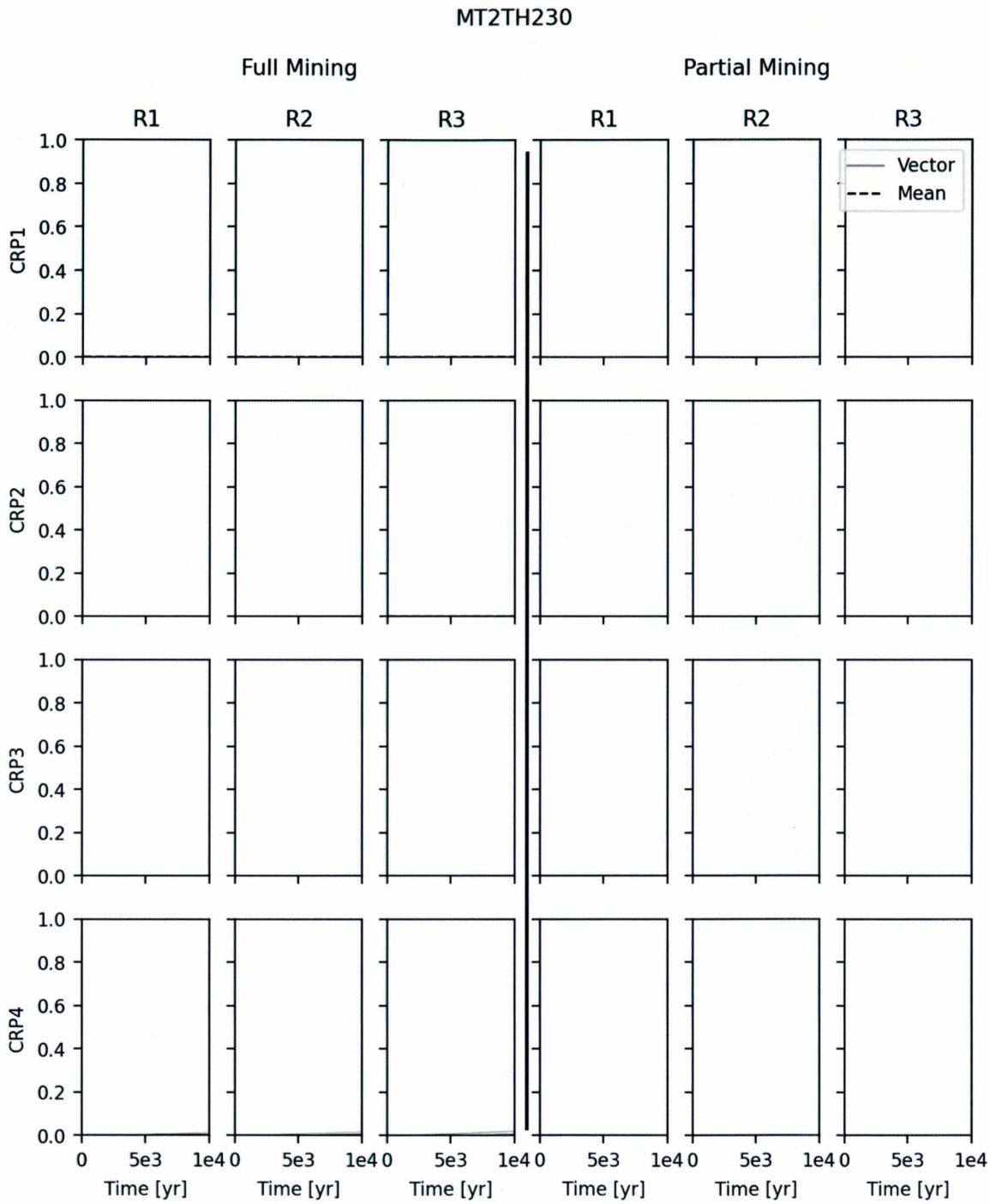


Figure 36).

Table 12 shows the mean cumulative mass transported to the LWB by 10,000 years. Under full mining conditions, the mean transported mass is highest for all isotopes in CRP4 simulations. In the full-mining, CRP4 scenario the mean cumulative mass transported to the LWB values are

Information Only

1.76×10^{-1} kg U-234, 4.83×10^{-2} kg Th-23A, 4.70×10^{-2} kg Pu-239, and 1.92×10^{-3} kg Am-241. Under partial mining conditions, mean mass transported to the LWB is highest in CRP1 for Pu-239, Th-23A, U-234, and Th-230, and in CRP4 for Am-241.

Table 13 shows the median cumulative mass transported to the LWB by 10,000 years. Median mass is highest for all isotopes in the full mining, CRP4 simulations. Within the full mining, CRP4 results, U-234 has the highest median value of 4.90×10^{-4} kg. Full mining results from CRP2 are below the reporting threshold criterion 10^{-24} kg. Median mass values in all partial mining simulations are also below the reporting criterion.

Table 14 shows the maximum mass transported to the LWB at 10,000 years. The results show that U-234 has near complete breakthrough from all release points in the full mining scenario. Due to rounding, the maximum cumulative U-234 mass slightly exceeds 1.00 kg in CRA19 Replicate 3. CRP4 simulations result in the highest maximum mass breakthrough for the other isotopes, including 0.74 kg of Pu-239, 0.87 kg of Th-23A, 0.24 kg of Am-241, and 0.02 kg of Th-230. The highest partial mining maximum values were obtained in the CRP1 simulations. The partial mining values are substantially lower than the full mining values, except for the U-234 values, which are more similar.

Table 15 shows the number of vectors exceeding the 10^{-9} kg cumulative transport at 10,000 years threshold criterion. The results show greater numbers of vectors exceeding the threshold for all isotopes in the full-mining/CRP4 scenario than in the other scenarios. In the partial mining scenario, the greatest number of vectors exceeding the threshold occurred at CRP1 for all isotopes, except for Am-241, which had the most exceedances in CRP4 simulations, though relatively few exceedances are observed across all scenarios.

Information Only

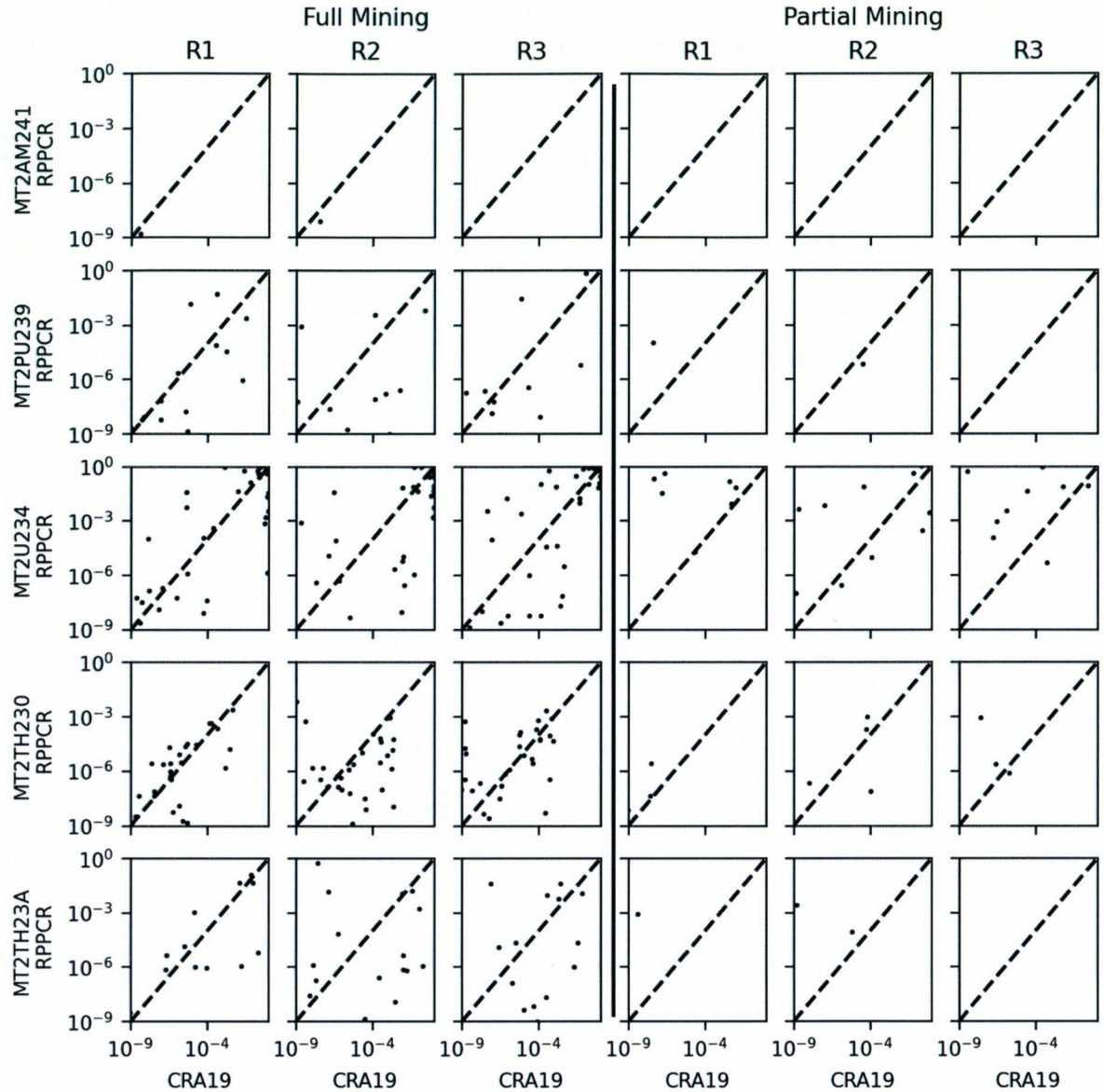


Figure 19 – Mass breakthrough at 10,000-yr: RPPCR CRP1 versus CRA19

Information Only

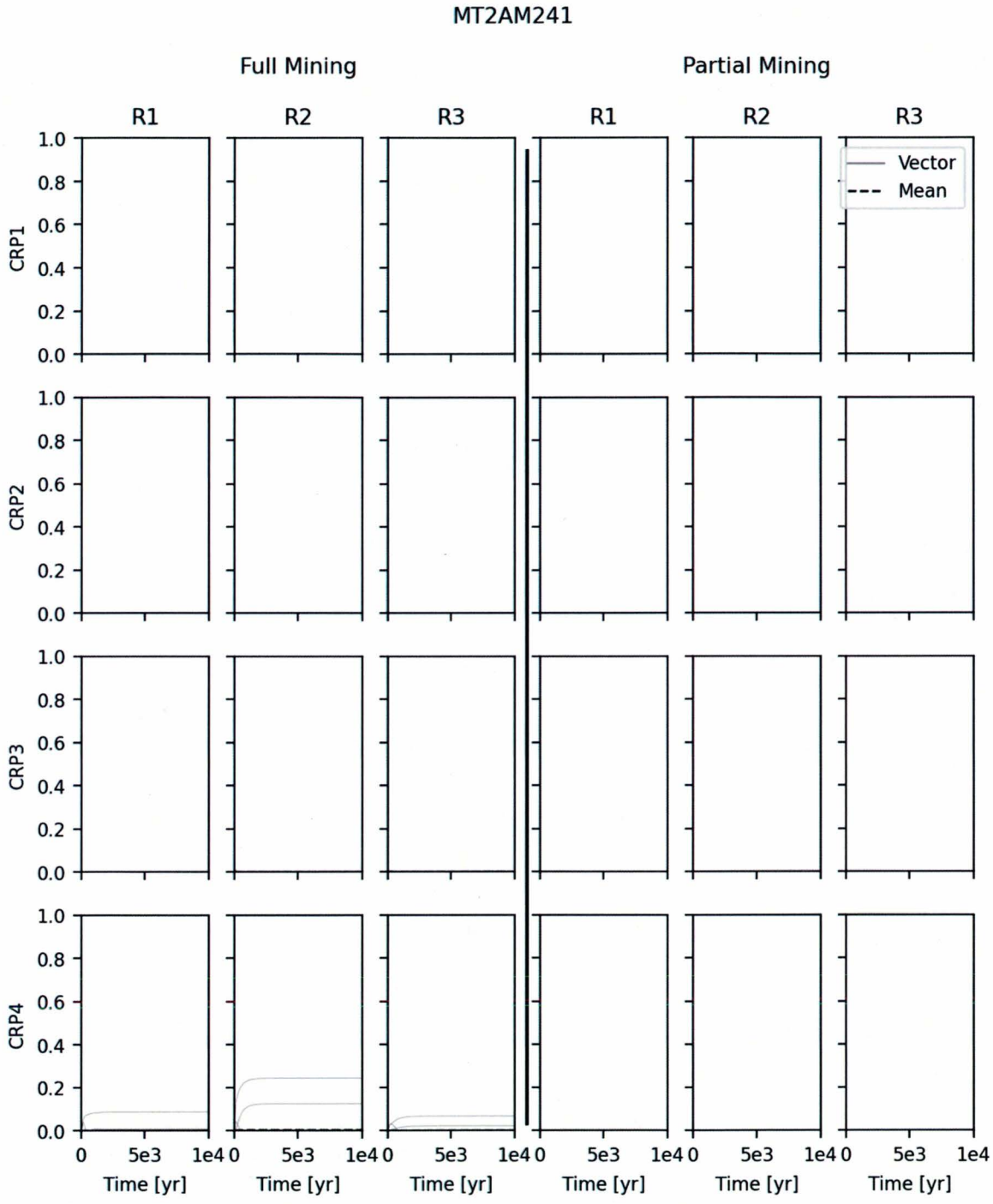


Figure 20 – Mass breakthrough of Am-241

Information Only

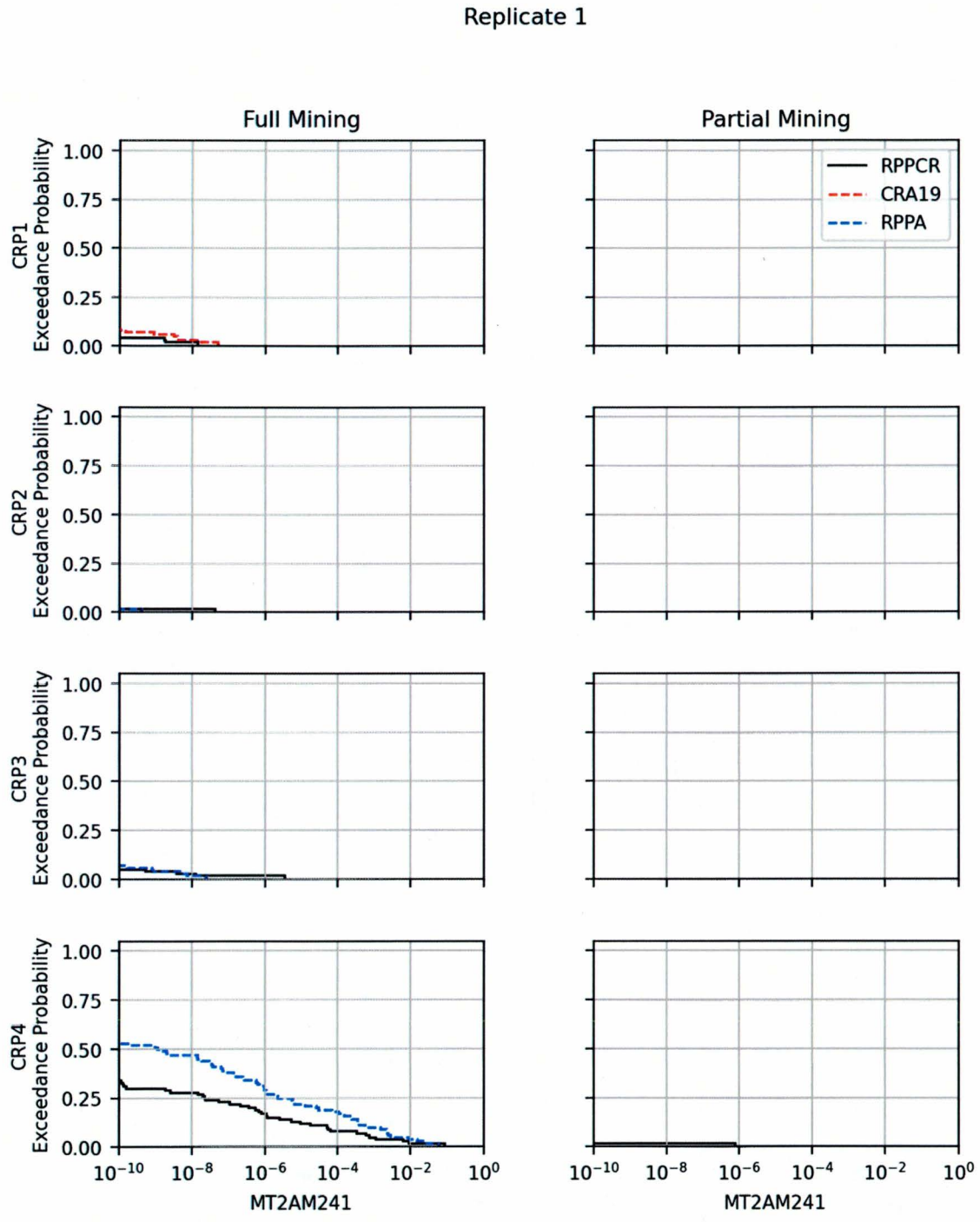


Figure 21 – Exceedance probability of Am-241 mass to LWB in 10,000 years, Replicate 1

Information Only

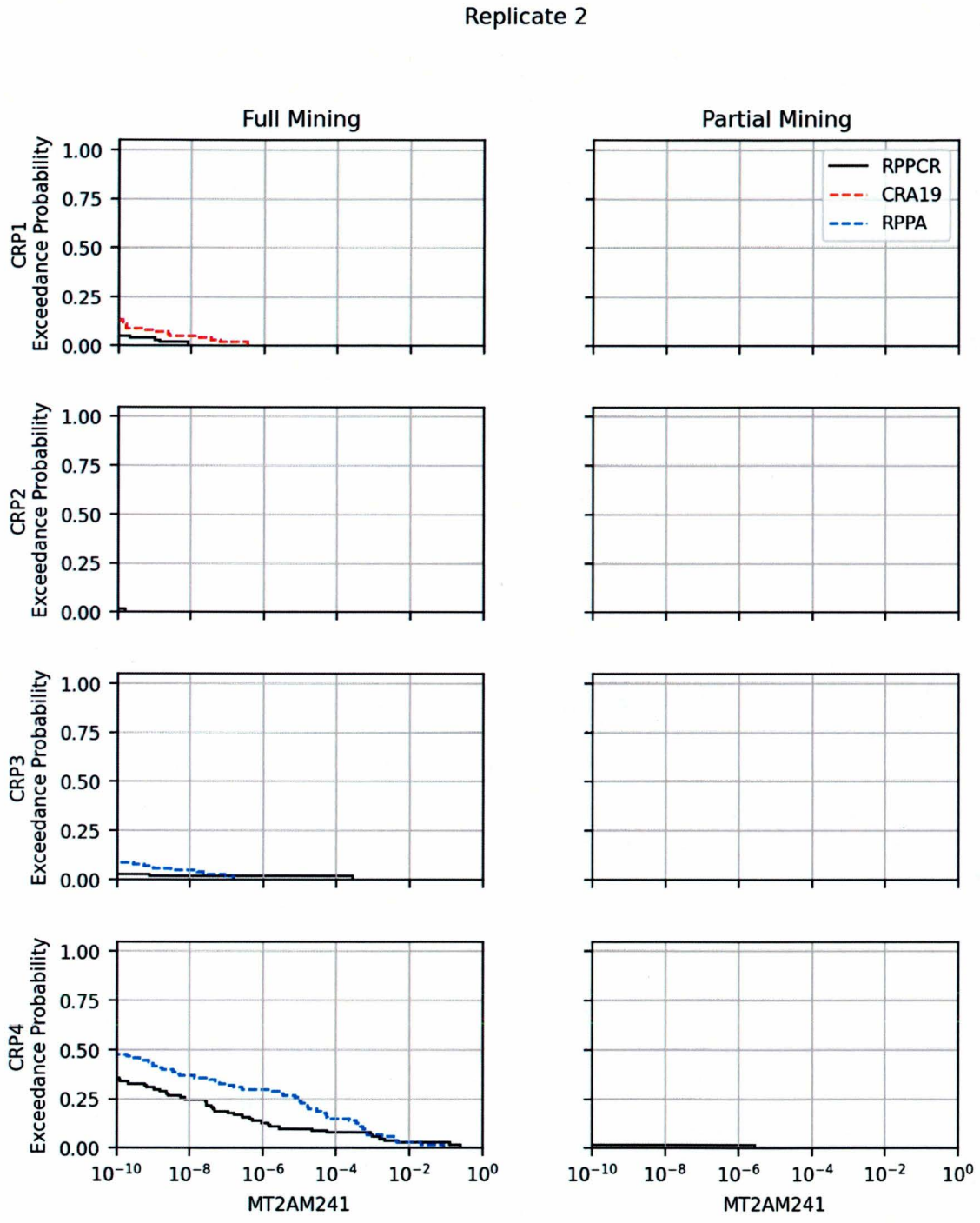


Figure 22 – Exceedance probability of Am-241 mass to LWB in 10,000 years, Replicate 2

Information Only

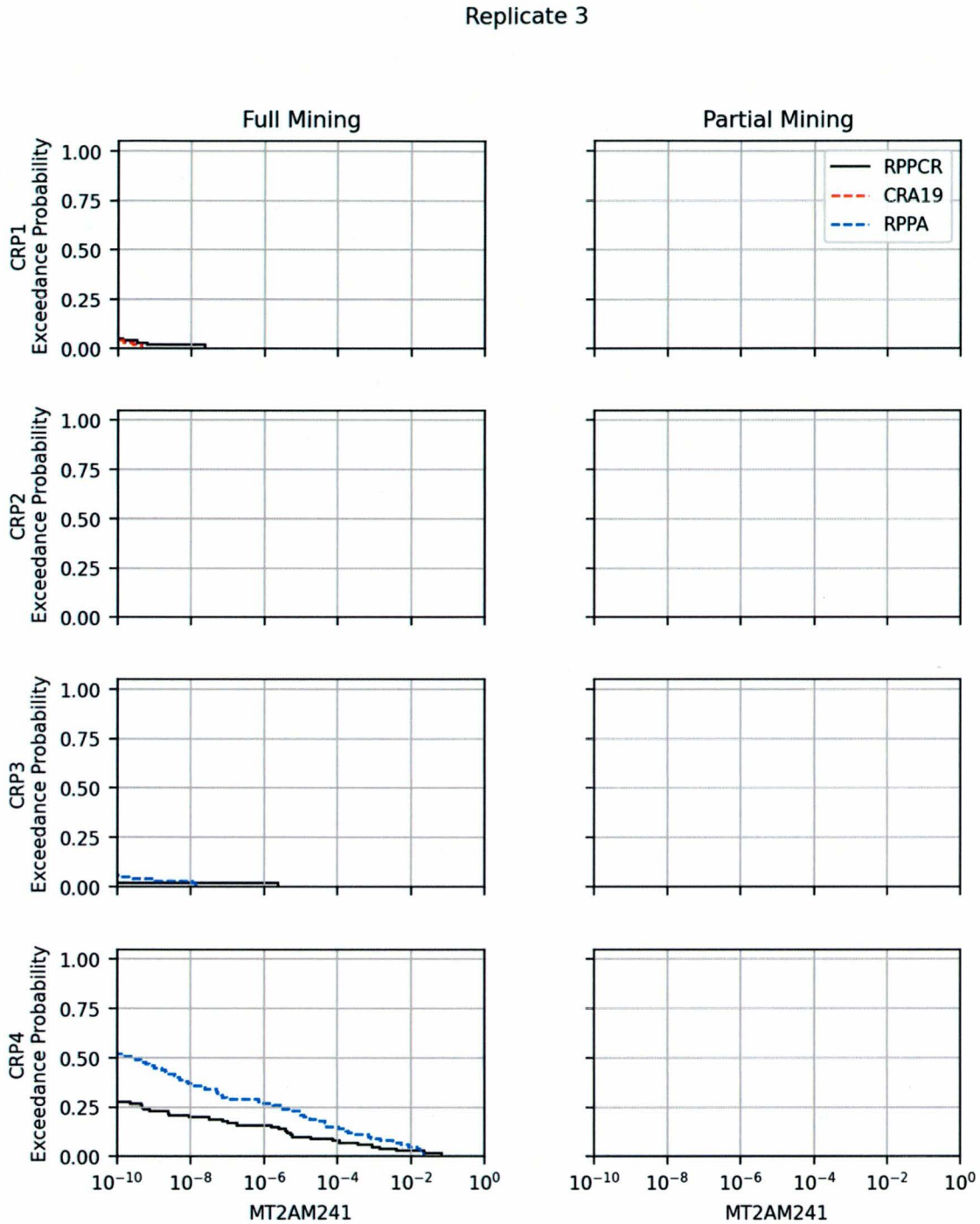


Figure 23 – Exceedance probability of Am-241 mass to LWB in 10,000 years, Replicate 3

Information Only

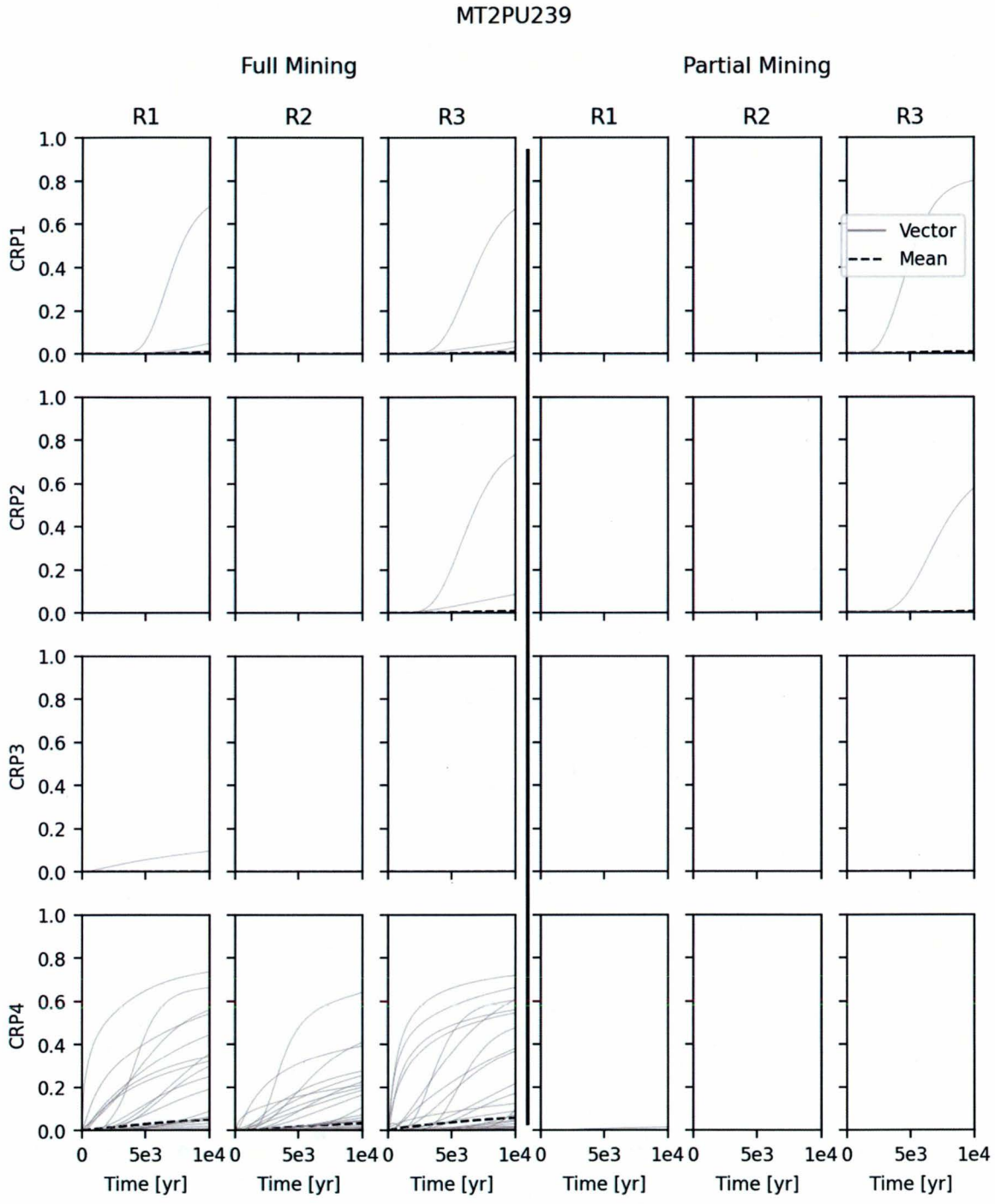


Figure 24 – Mass breakthrough of Pu-239

Information Only

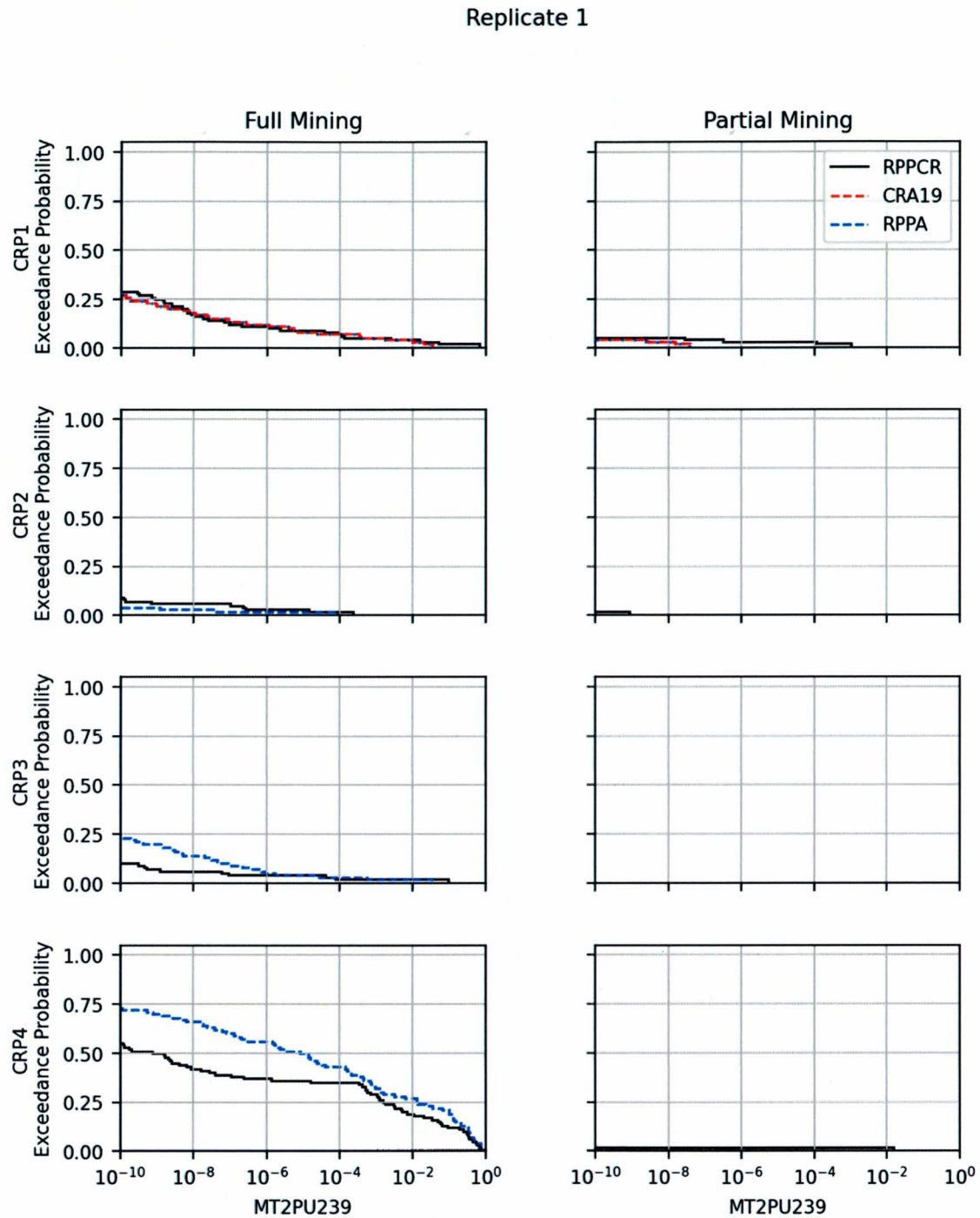


Figure 25 – Exceedance probability of Pu-239 mass to the LWB in 10,000 years, Replicate 1

Information Only

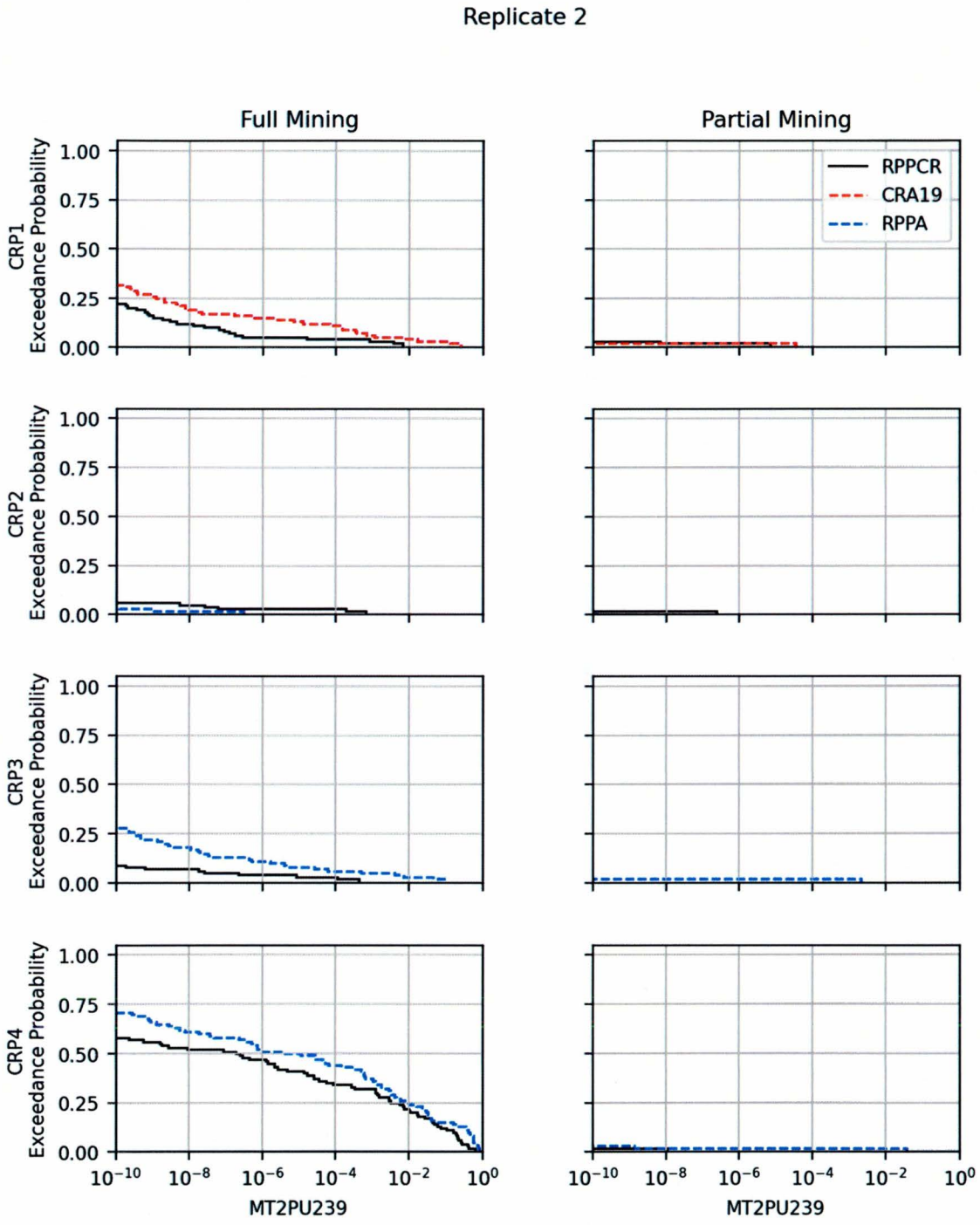


Figure 26 – Exceedance probability of Pu-239 mass to the LWB in 10,000 years, Replicate 2

Information Only

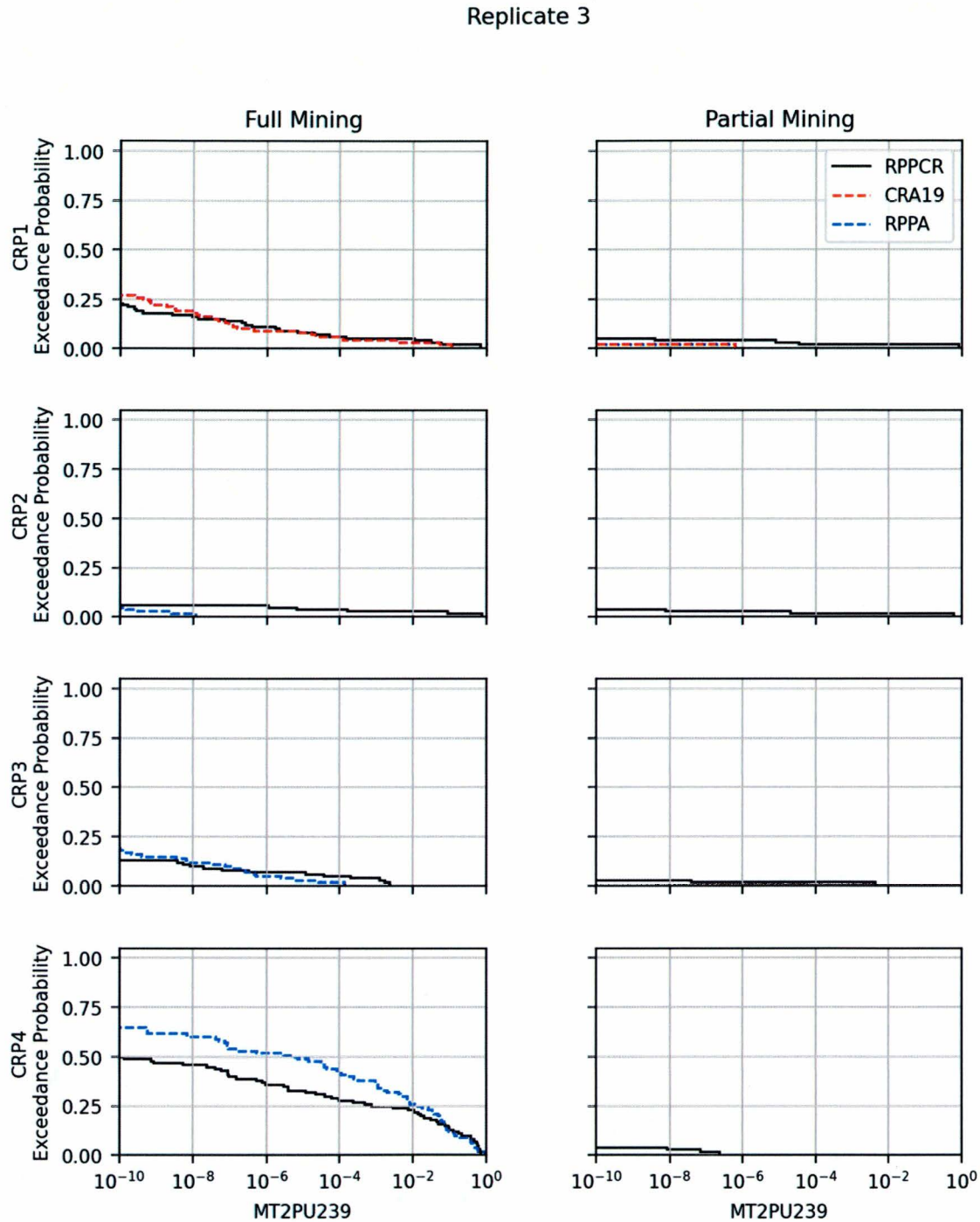


Figure 27 – Exceedance probability of Pu-239 mass to the LWB in 10,000 years, Replicate 3

Information Only

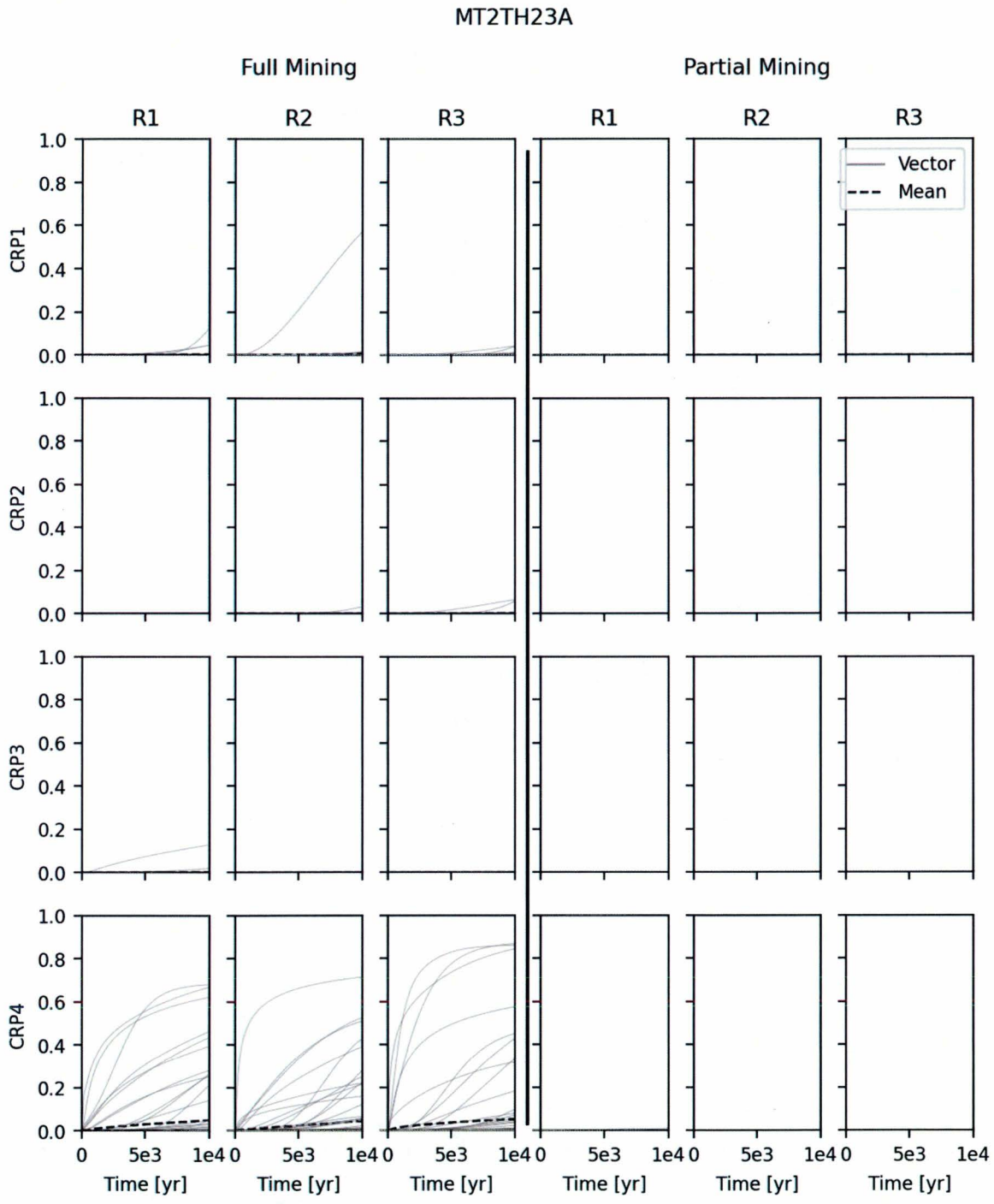


Figure 28 – Mass breakthrough of Th-230A

Information Only

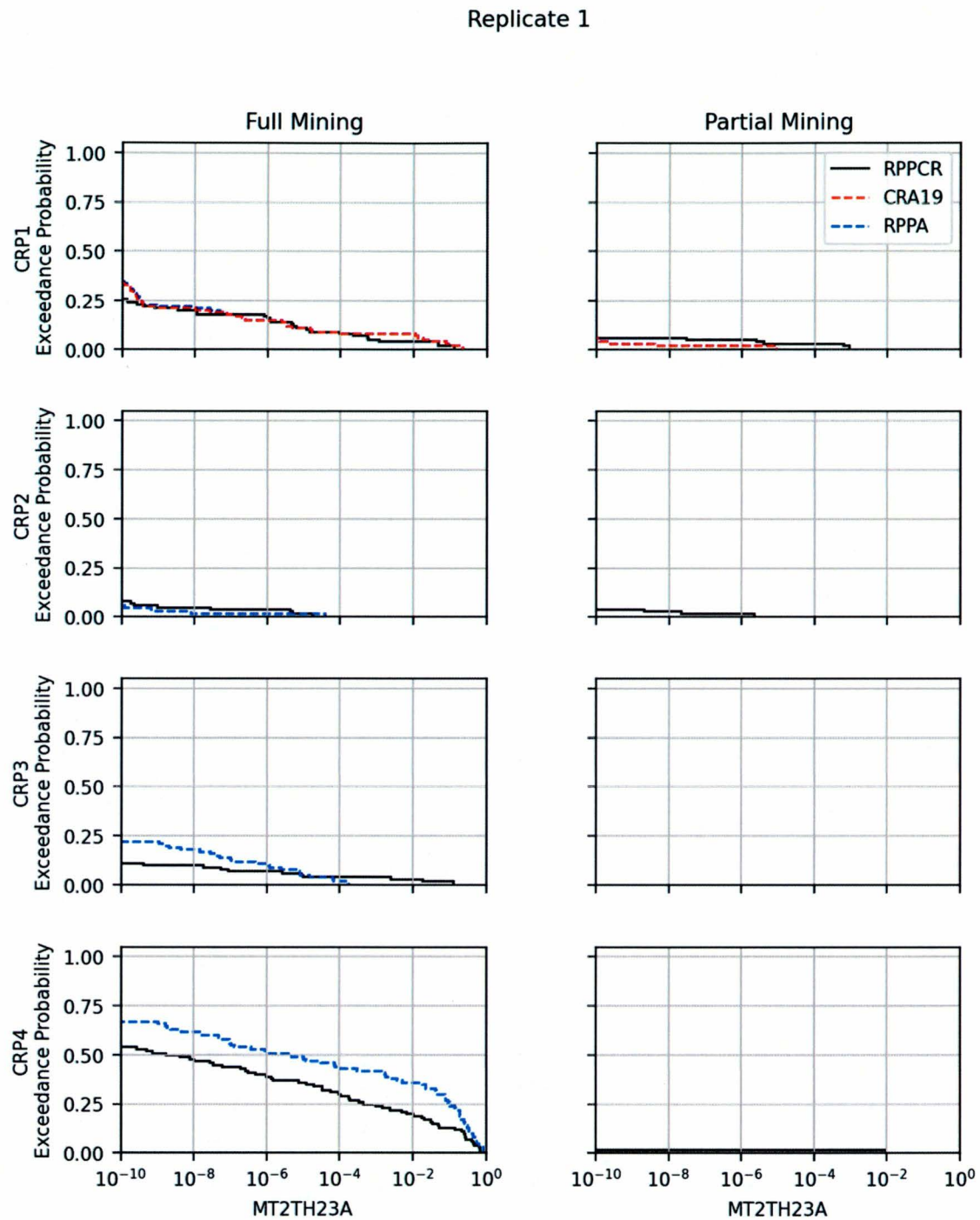


Figure 29 – Exceedance probability of Th-23A mass to LWB in 10,000 years, Replicate 1

Information Only

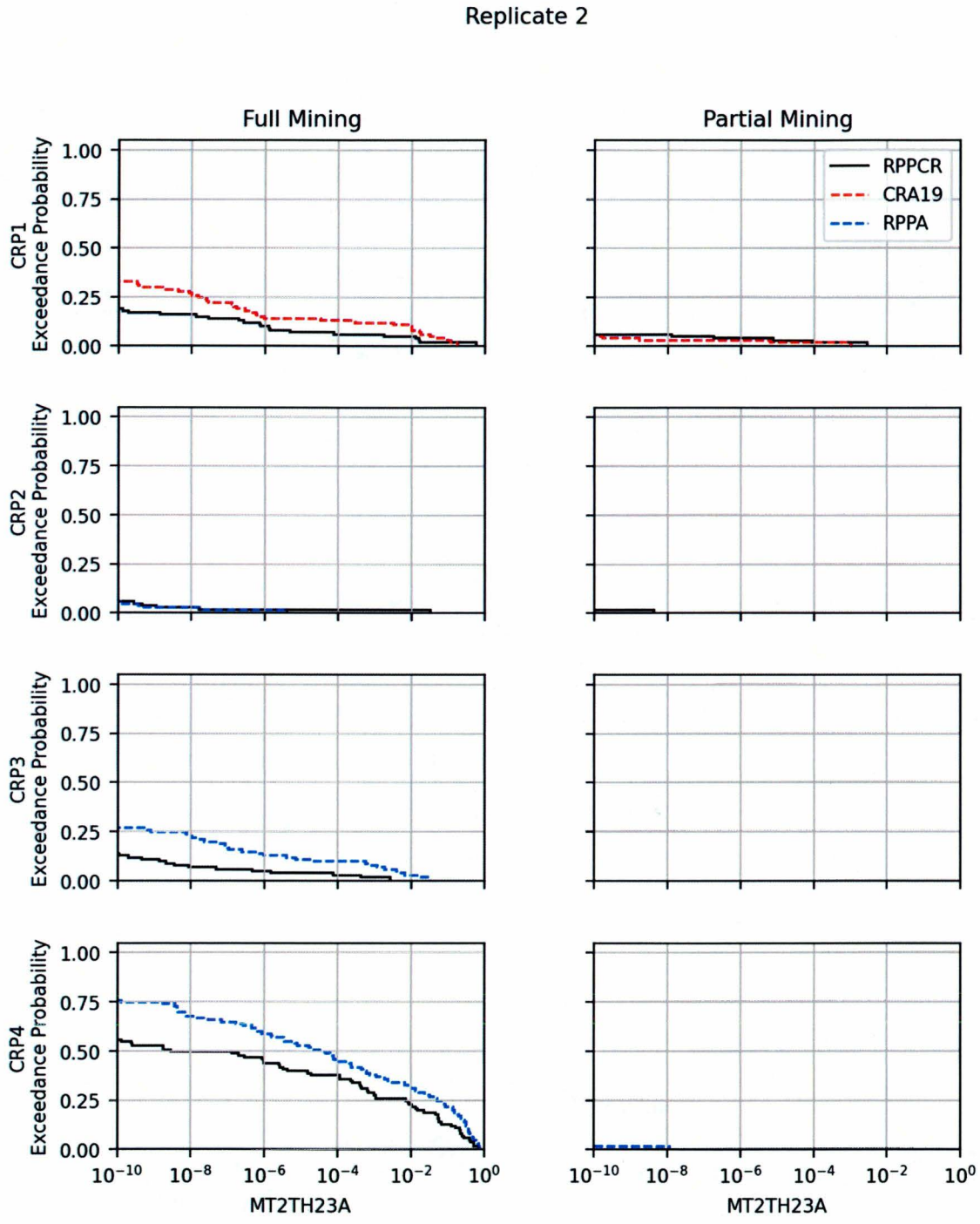


Figure 30 – Exceedance probability of Th-23A mass to LWB in 10,000 years, Replicate 2

Information Only

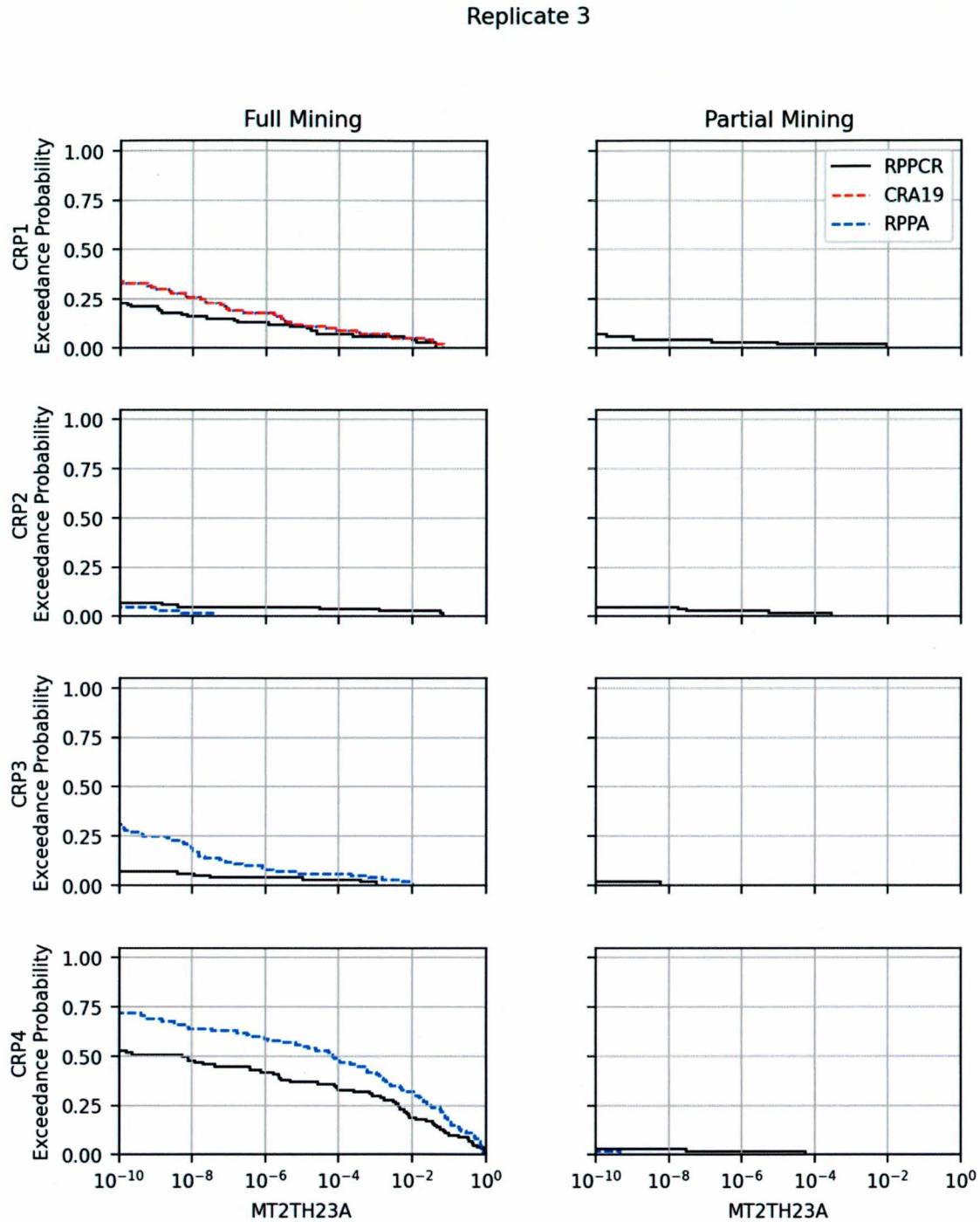


Figure 31 – Exceedance probability of Th-23A mass to LWB in 10,000 years, Replicate 3

Information Only

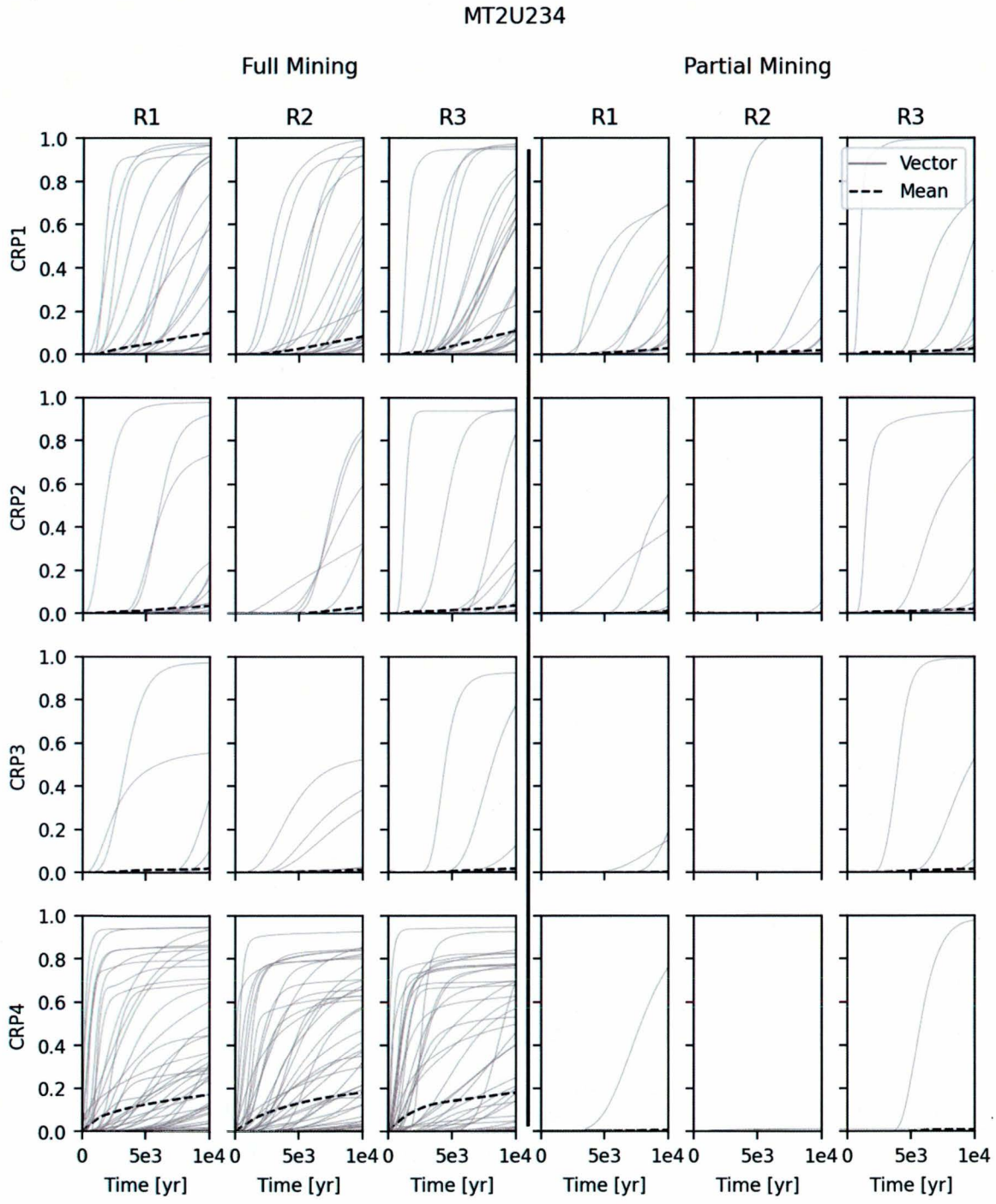


Figure 32 – Mass breakthrough of U-234

Information Only

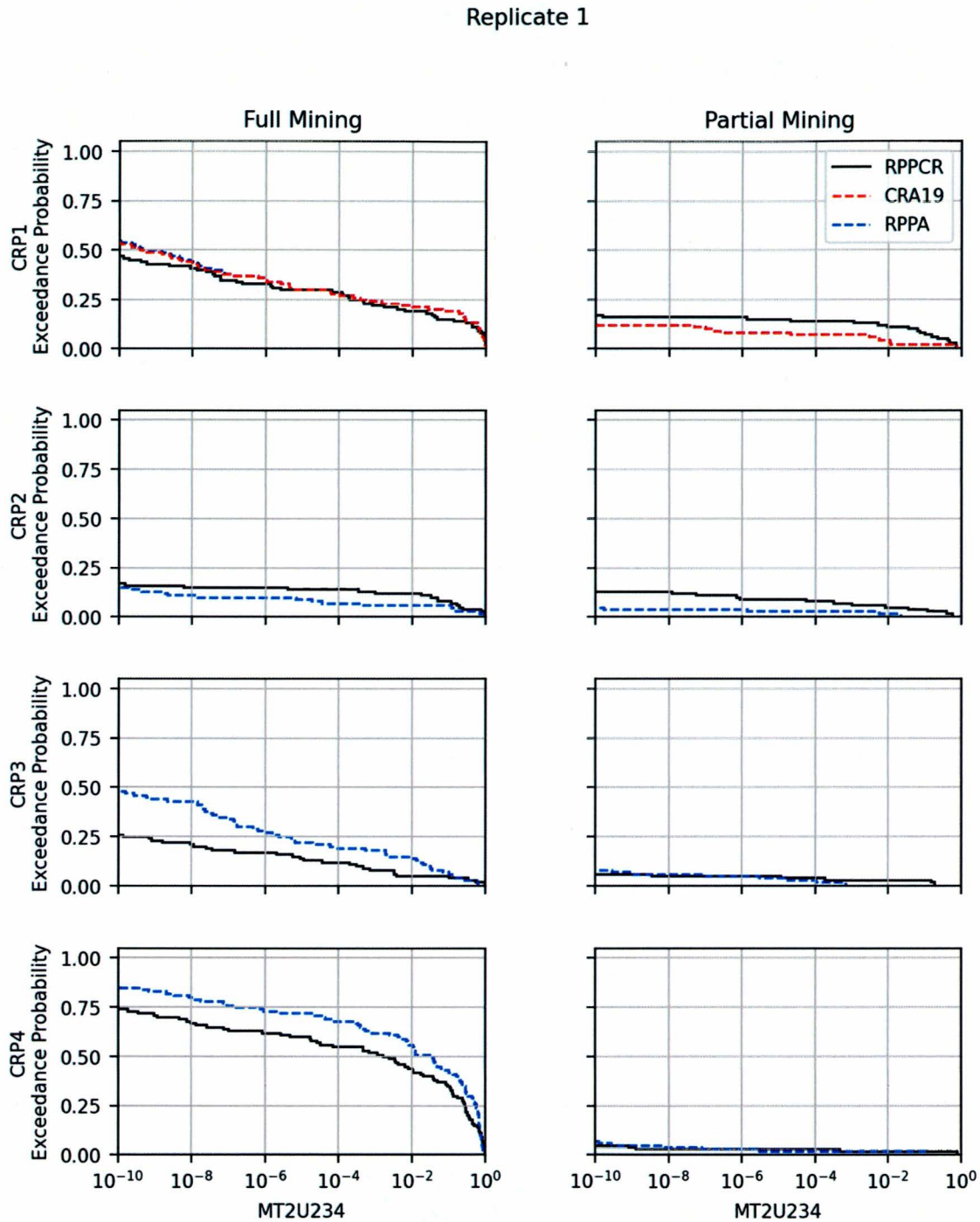


Figure 33 – Exceedance probability of U-234 mass to LWB in 10,000 years, Replicate 1

Information Only

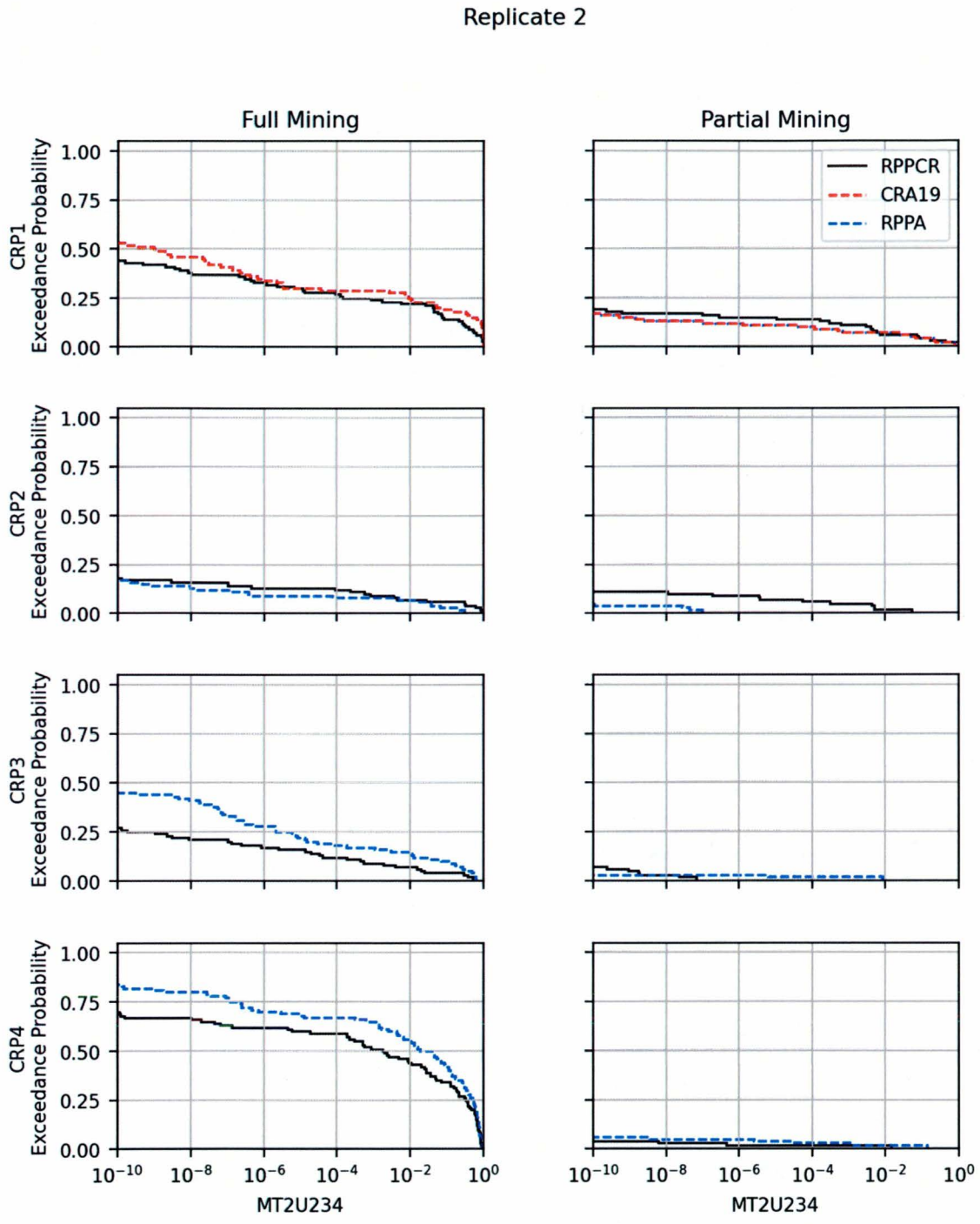


Figure 34 – Exceedance probability of U-234 mass to LWB in 10,000 years, Replicate 2

Information Only

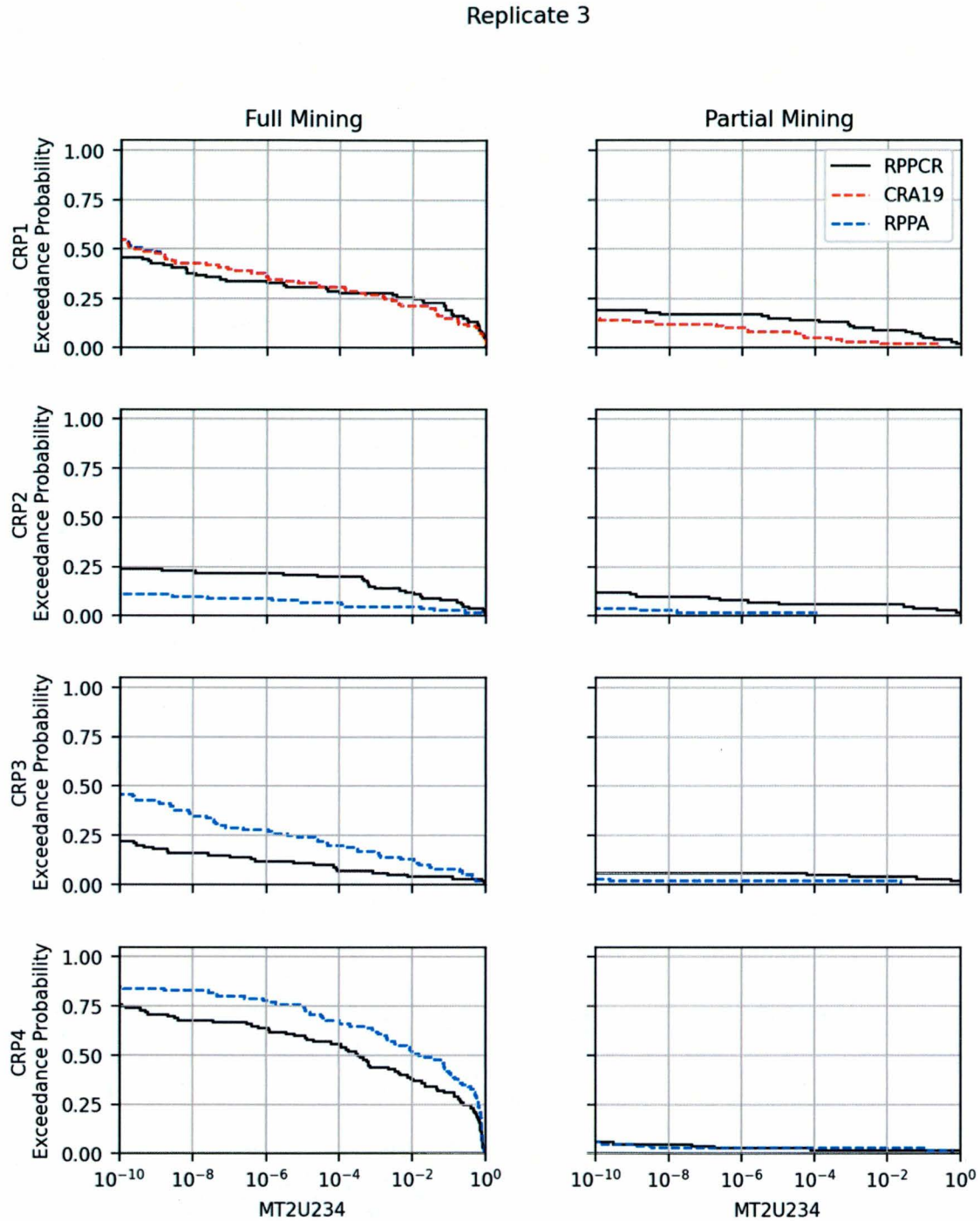


Figure 35 – Exceedance probability of U-234 mass to LWB in 10,000 years, Replicate 3

Information Only

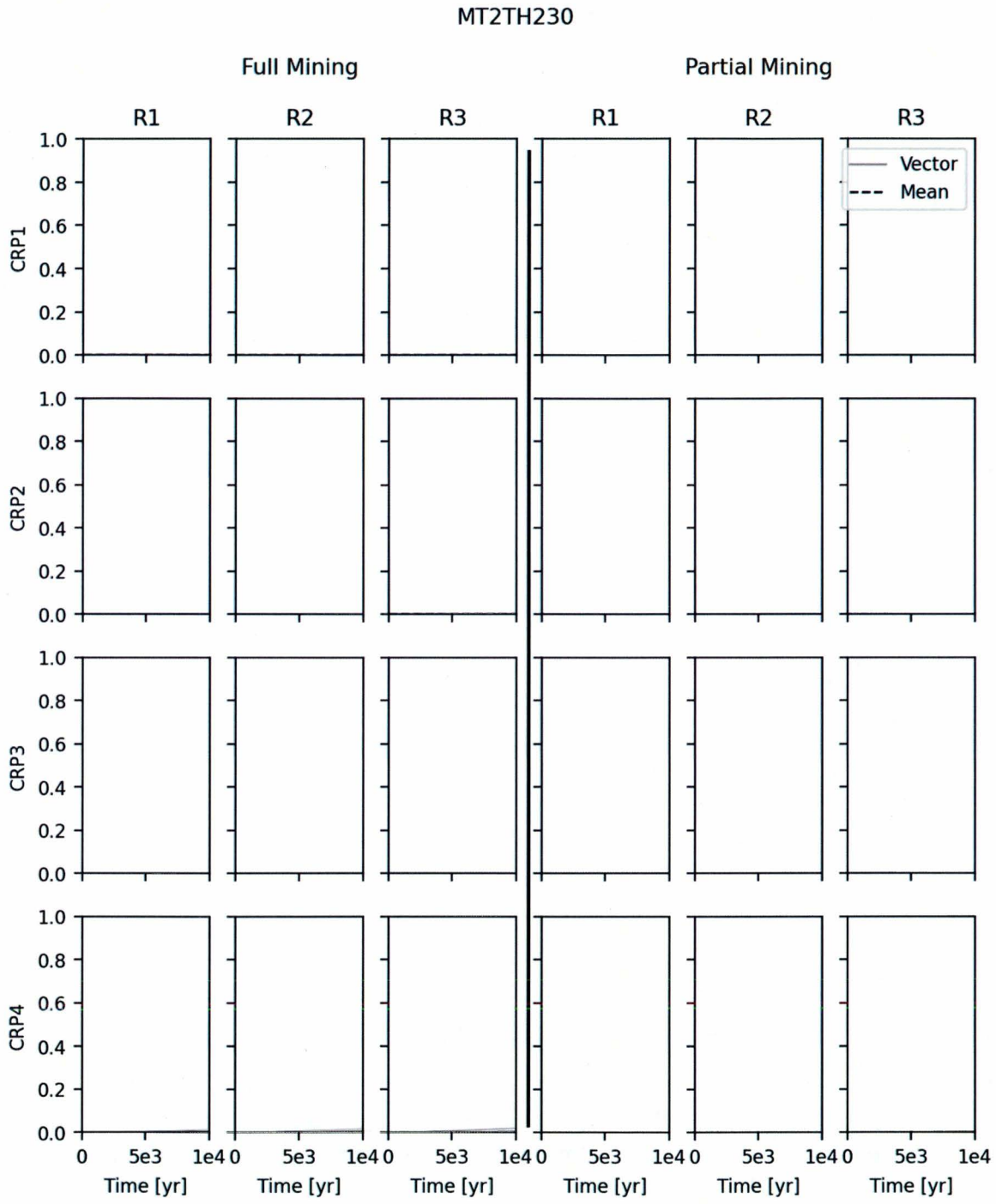


Figure 36 – Mass breakthrough of Th-230

Information Only

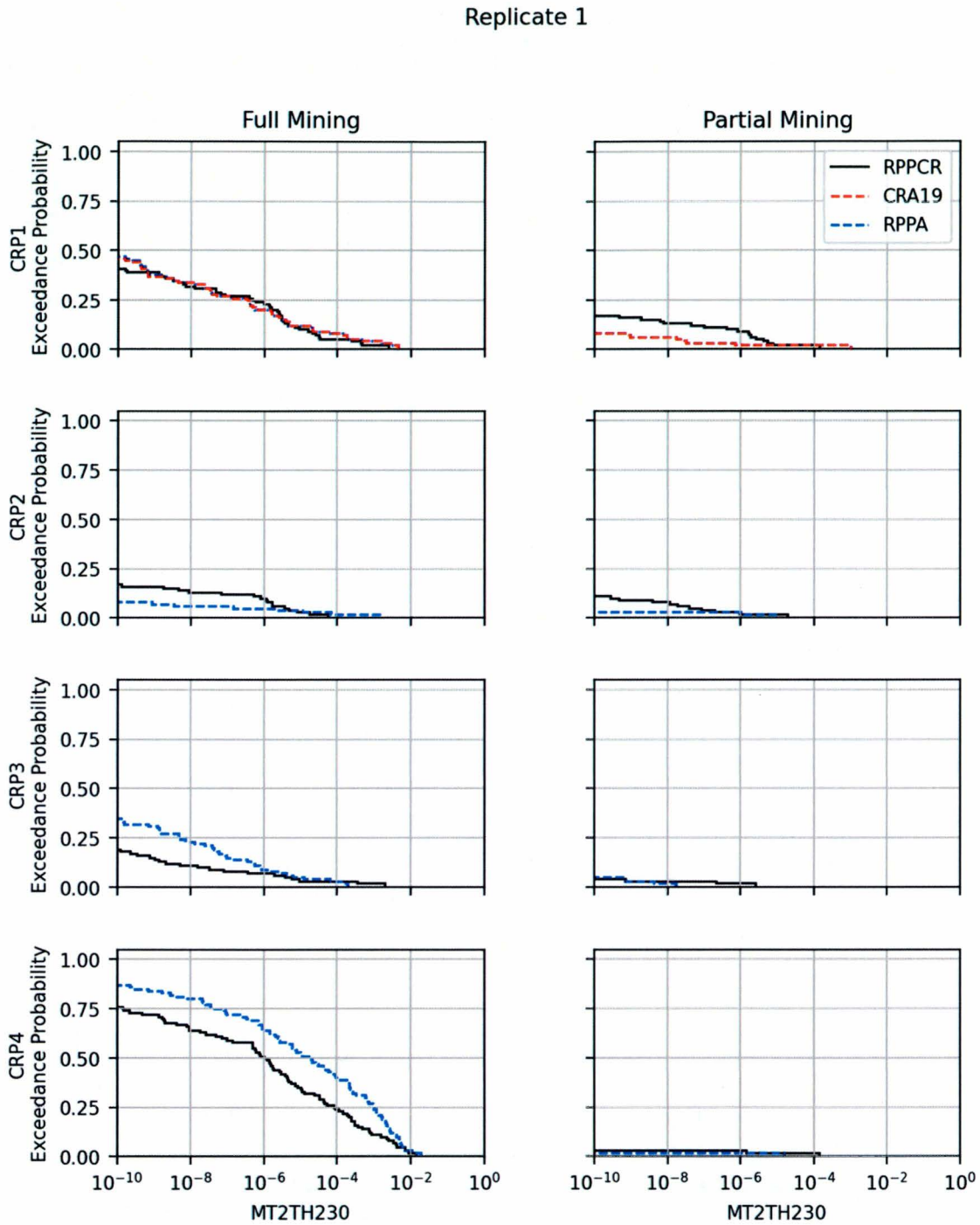


Figure 37 – Exceedance probability of Th-230 mass to LWB in 10,000 years, Replicate 1

Information Only

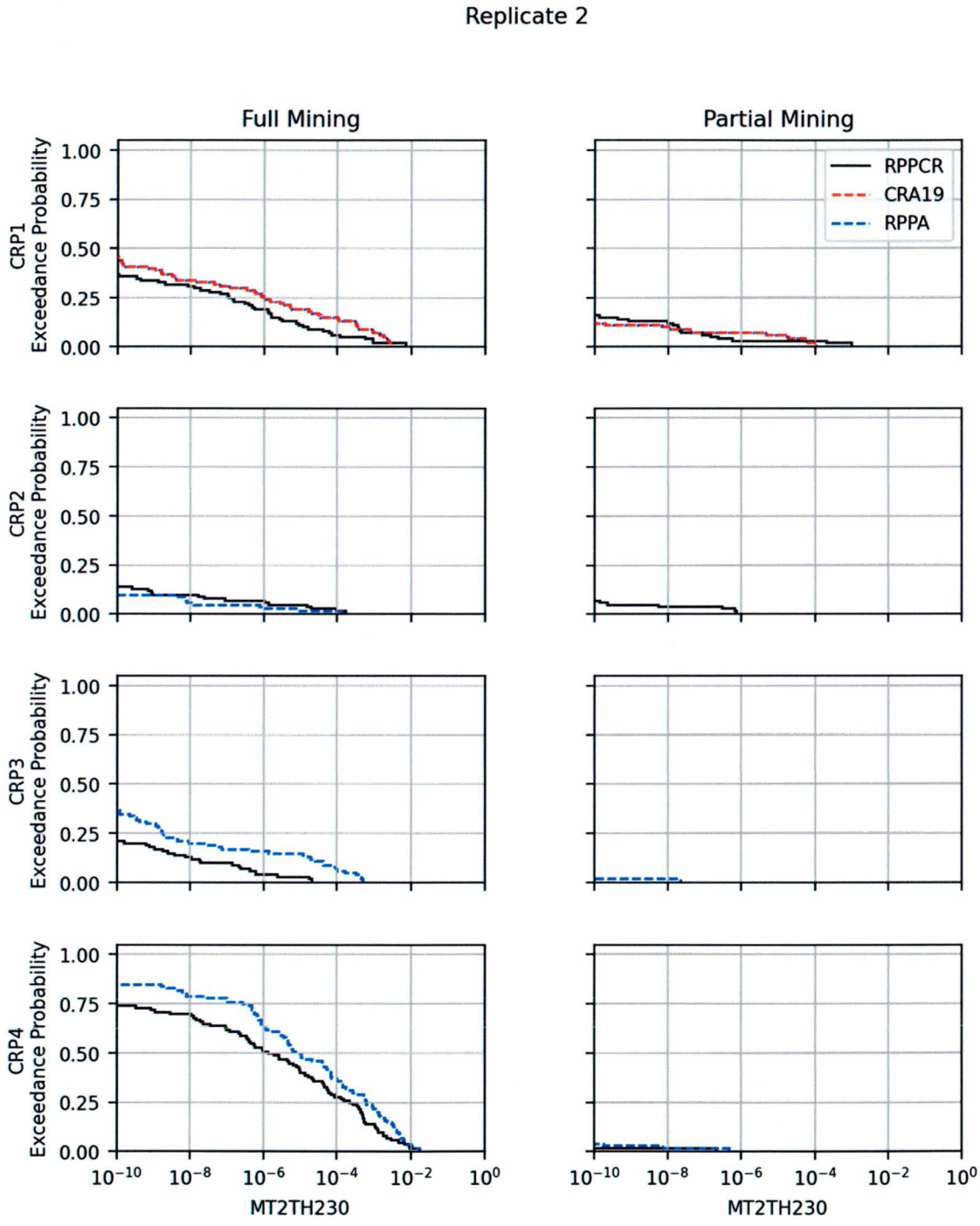


Figure 38 – Exceedance probability of Th-230 mass to LWB in 10,000 years, Replicate 2

Information Only

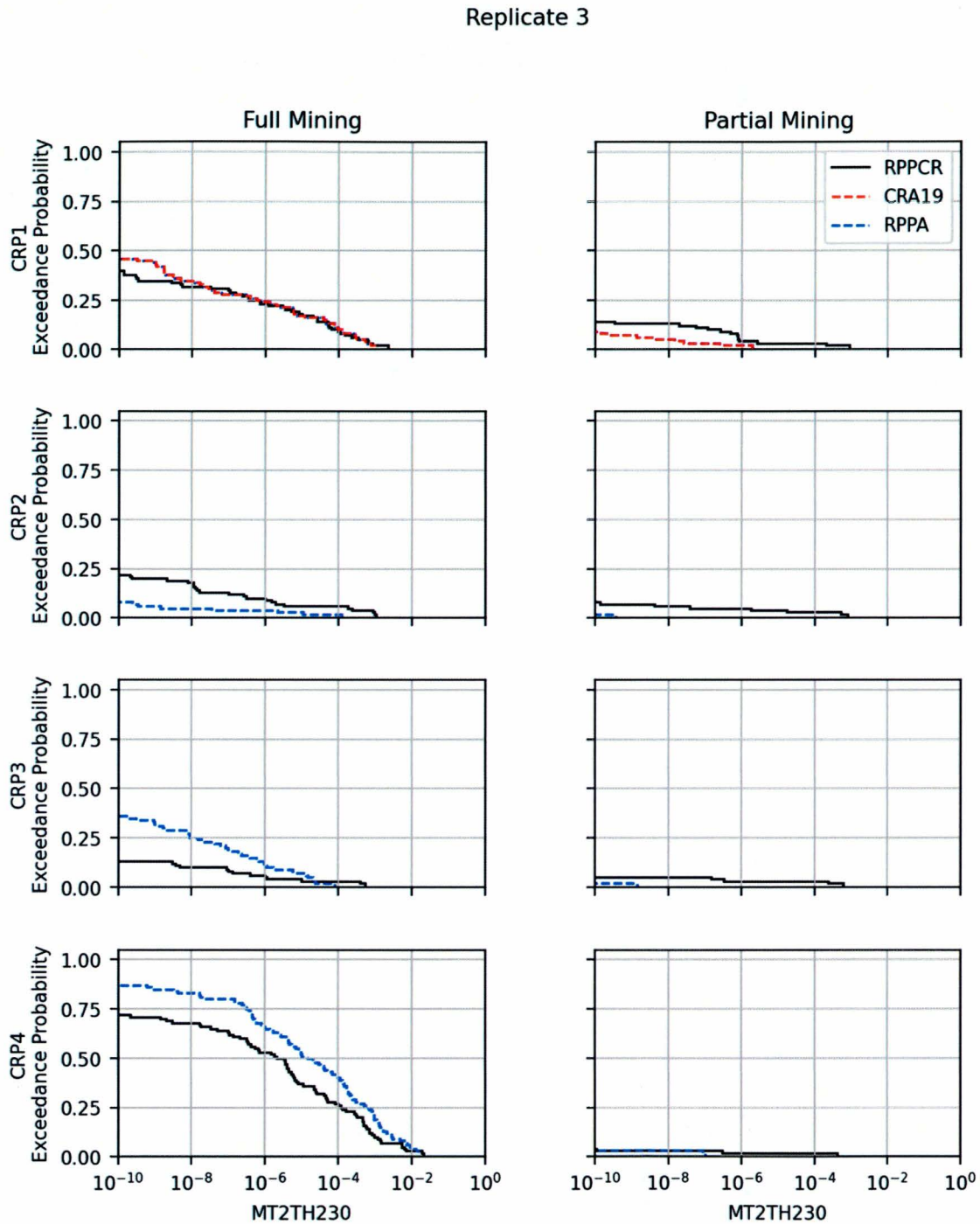


Figure 39 – Exceedance probability of Th-230 mass to LWB in 10,000 years, Replicate 3

Information Only

Table 12 – Mean cumulative mass [kg] to LWB over 10,000 years

Am-241										
	Full Mining					Partial Mining				
	CRA19	CRP1	CRP2	CRP3	CRP4	CRA19	CRP1	CRP2	CRP3	CRP4
R1	5.97E-10	1.40E-10	4.02E-10	3.33E-08	1.05E-03	0.00E+00	1.78E-23	1.27E-22	5.42E-22	7.43E-09
R2	7.85E-08	1.07E-10	1.74E-12	2.66E-06	3.78E-03	1.18E-23	3.99E-21	0.00E+00	7.21E-18	2.72E-08
R3	4.68E-11	1.74E-10	1.02E-13	2.37E-08	9.60E-04	0.00E+00	0.00E+00	0.00E+00	1.04E-23	1.52E-15
GLOBAL	0.00E+00	1.40E-10	1.35E-10	9.04E-07	1.93E-03	3.94E-24	1.34E-21	4.24E-23	2.40E-18	1.15E-08
Pu-239										
	Full Mining					Partial Mining				
	CRA19	CRP1	CRP2	CRP3	CRP4	CRA19	CRP1	CRP2	CRP3	CRP4
R1	6.45E-04	7.51E-03	2.44E-06	9.57E-04	5.06E-02	5.56E-10	1.15E-05	8.49E-12	4.79E-20	1.46E-04
R2	3.98E-03	1.11E-04	8.44E-06	5.54E-06	3.45E-02	3.30E-07	6.89E-08	2.46E-09	1.65E-15	1.05E-10
R3	1.63E-03	7.71E-03	8.19E-03	5.53E-05	5.89E-02	5.70E-09	8.00E-03	5.77E-03	4.24E-05	3.02E-09
GLOBAL	2.08E-03	5.11E-03	2.74E-03	3.39E-04	4.80E-02	1.12E-07	2.67E-03	1.92E-03	1.41E-05	4.88E-05
Th-23A										
	Full Mining					Partial Mining				
	CRA19	CRP1	CRP2	CRP3	CRP4	CRA19	CRP1	CRP2	CRP3	CRP4
R1	4.53E-03	2.19E-03	2.63E-07	1.48E-03	4.89E-02	8.56E-08	1.50E-05	2.17E-08	6.66E-19	9.16E-05
R2	5.14E-03	6.17E-03	3.25E-04	3.05E-05	4.46E-02	9.55E-06	2.89E-05	4.10E-11	7.40E-15	7.67E-11
R3	1.65E-03	1.11E-03	1.24E-03	1.44E-05	5.38E-02	4.01E-14	8.71E-05	2.74E-06	5.67E-11	5.30E-07
GLOBAL	3.78E-03	3.16E-03	5.23E-04	5.10E-04	4.91E-02	3.21E-06	4.37E-05	9.21E-07	1.89E-11	3.07E-05
U-234										
	Full Mining					Partial Mining				
	CRA19	CRP1	CRP2	CRP3	CRP4	CRA19	CRP1	CRP2	CRP3	CRP4
R1	1.08E-01	9.93E-02	3.48E-02	1.98E-02	1.71E-01	7.43E-03	2.92E-02	1.10E-02	3.38E-03	7.62E-03
R2	1.41E-01	8.32E-02	2.94E-02	1.27E-02	1.81E-01	1.32E-02	1.81E-02	6.67E-04	9.62E-10	1.45E-04
R3	8.97E-02	1.10E-01	3.78E-02	1.83E-02	1.80E-01	2.51E-03	2.67E-02	1.96E-02	1.58E-02	9.78E-03
GLOBAL	1.13E-01	9.74E-02	3.40E-02	1.69E-02	1.77E-01	7.72E-03	2.47E-02	1.04E-02	6.39E-03	5.85E-03
Th-230										
	Full Mining					Partial Mining				
	CRA19	CRP1	CRP2	CRP3	CRP4	CRA19	CRP1	CRP2	CRP3	CRP4
R1	9.98E-05	3.69E-05	9.51E-07	2.36E-05	5.87E-04	9.94E-06	1.66E-06	2.00E-07	2.81E-08	1.39E-06
R2	1.55E-04	9.67E-05	2.96E-06	4.24E-07	6.53E-04	2.53E-06	1.16E-05	1.66E-08	2.40E-15	2.08E-09
R3	4.12E-05	5.36E-05	3.23E-05	9.32E-06	7.45E-04	2.16E-08	1.10E-05	1.32E-05	8.42E-06	4.20E-06
GLOBAL	9.88E-05	6.24E-05	1.21E-05	1.11E-05	6.62E-04	4.16E-06	8.08E-06	4.46E-06	2.82E-06	1.86E-06

Information Only

Table 13 – Median cumulative mass [kg] to LWB over 10,000 years

Am-241										
	Full Mining					Partial Mining				
	CRA19	CRP1	CRP2	CRP3	CRP4	CRA19	CRP1	CRP2	CRP3	CRP4
R1	7.42E-19	1.29E-24	0.00E+00	0.00E+00	7.66E-17	0.00E+00	0.00E+00	0.00E+00	0.00E+00	0.00E+00
R2	1.26E-19	6.51E-23	0.00E+00	0.00E+00	5.18E-16	0.00E+00	0.00E+00	0.00E+00	0.00E+00	0.00E+00
R3	1.17E-19	4.41E-23	0.00E+00	0.00E+00	8.42E-16	0.00E+00	0.00E+00	0.00E+00	0.00E+00	0.00E+00
GLOBAL	2.32E-19	2.58E-23	0.00E+00	0.00E+00	3.50E-16	0.00E+00	0.00E+00	0.00E+00	0.00E+00	0.00E+00
Pu-239										
	Full Mining					Partial Mining				
	CRA19	CRP1	CRP2	CRP3	CRP4	CRA19	CRP1	CRP2	CRP3	CRP4
R1	3.24E-14	2.59E-18	0.00E+00	0.00E+00	4.82E-10	0.00E+00	0.00E+00	0.00E+00	0.00E+00	0.00E+00
R2	9.22E-16	6.85E-18	0.00E+00	0.00E+00	1.36E-07	0.00E+00	0.00E+00	0.00E+00	0.00E+00	0.00E+00
R3	1.24E-14	2.36E-18	0.00E+00	0.00E+00	2.47E-11	0.00E+00	0.00E+00	0.00E+00	0.00E+00	0.00E+00
GLOBAL	8.21E-15	3.20E-18	0.00E+00	0.00E+00	1.19E-09	0.00E+00	0.00E+00	0.00E+00	0.00E+00	0.00E+00
Th-23A										
	Full Mining					Partial Mining				
	CRA19	CRP1	CRP2	CRP3	CRP4	CRA19	CRP1	CRP2	CRP3	CRP4
R1	3.98E-14	7.69E-18	0.00E+00	0.00E+00	1.17E-09	0.00E+00	0.00E+00	0.00E+00	0.00E+00	0.00E+00
R2	2.51E-16	3.87E-18	0.00E+00	0.00E+00	2.28E-09	0.00E+00	0.00E+00	0.00E+00	0.00E+00	0.00E+00
R3	1.36E-15	2.02E-19	0.00E+00	0.00E+00	2.74E-09	0.00E+00	0.00E+00	0.00E+00	0.00E+00	0.00E+00
GLOBAL	2.94E-15	6.87E-19	0.00E+00	0.00E+00	1.76E-09	0.00E+00	0.00E+00	0.00E+00	0.00E+00	0.00E+00
U-234										
	Full Mining					Partial Mining				
	CRA19	CRP1	CRP2	CRP3	CRP4	CRA19	CRP1	CRP2	CRP3	CRP4
R1	3.18E-10	1.18E-11	0.00E+00	2.76E-24	1.37E-03	0.00E+00	0.00E+00	0.00E+00	0.00E+00	0.00E+00
R2	6.15E-10	2.84E-12	0.00E+00	4.96E-23	1.29E-03	0.00E+00	0.00E+00	0.00E+00	0.00E+00	0.00E+00
R3	1.96E-10	3.99E-12	0.00E+00	1.86E-23	2.93E-04	0.00E+00	0.00E+00	0.00E+00	0.00E+00	0.00E+00
GLOBAL	2.87E-10	3.57E-12	0.00E+00	1.86E-23	5.55E-04	0.00E+00	0.00E+00	0.00E+00	0.00E+00	0.00E+00
Th-230										
	Full Mining					Partial Mining				
	CRA19	CRP1	CRP2	CRP3	CRP4	CRA19	CRP1	CRP2	CRP3	CRP4
R1	1.29E-11	5.09E-13	0.00E+00	1.45E-23	8.90E-07	0.00E+00	0.00E+00	0.00E+00	0.00E+00	0.00E+00
R2	3.49E-12	1.22E-13	0.00E+00	5.08E-24	1.13E-06	0.00E+00	0.00E+00	0.00E+00	0.00E+00	0.00E+00
R3	8.18E-13	5.97E-15	0.00E+00	1.10E-24	1.95E-06	0.00E+00	0.00E+00	0.00E+00	0.00E+00	0.00E+00
GLOBAL	3.91E-12	1.61E-13	0.00E+00	5.08E-24	1.23E-06	0.00E+00	0.00E+00	0.00E+00	0.00E+00	0.00E+00

Information Only

Table 14 – Maximum cumulative mass [kg] to LWB over 10,000 years

Am-241										
	Full Mining					Partial Mining				
	CRA19	CRP1	CRP2	CRP3	CRP4	CRA19	CRP1	CRP2	CRP3	CRP4
R1	4.70E-08	1.39E-08	4.02E-08	3.31E-06	8.71E-02	0.00E+00	1.78E-21	1.27E-20	3.67E-20	7.43E-07
R2	3.41E-07	8.04E-09	1.57E-10	2.66E-04	2.43E-01	1.13E-21	3.99E-19	3.70E-23	7.07E-16	2.72E-06
R3	4.16E-10	2.29E-08	8.43E-12	2.37E-06	6.74E-02	0.00E+00	0.00E+00	0.00E+00	4.59E-22	1.52E-13
GLOBAL	3.41E-07	2.29E-08	4.02E-08	2.66E-04	2.43E-01	1.13E-21	3.99E-19	1.27E-20	7.07E-16	2.72E-06
Pu-239										
	Full Mining					Partial Mining				
	CRA19	CRP1	CRP2	CRP3	CRP4	CRA19	CRP1	CRP2	CRP3	CRP4
R1	3.30E-02	6.83E-01	2.29E-04	9.56E-02	7.36E-01	3.84E-08	1.04E-03	8.49E-10	2.84E-18	1.46E-02
R2	2.48E-01	6.53E-03	6.58E-04	4.36E-04	6.41E-01	3.30E-05	6.88E-06	2.45E-07	9.20E-16	1.05E-08
R3	1.08E-01	6.72E-01	7.34E-01	2.35E-03	7.19E-01	5.70E-07	8.00E-01	5.77E-01	4.24E-03	2.27E-07
GLOBAL	2.48E-01	6.83E-01	7.34E-01	9.56E-02	7.36E-01	3.30E-05	8.00E-01	5.77E-01	4.24E-03	1.46E-02
Th-23A										
	Full Mining					Partial Mining				
	CRA19	CRP1	CRP2	CRP3	CRP4	CRA19	CRP1	CRP2	CRP3	CRP4
R1	2.06E-01	1.24E-01	1.71E-05	1.28E-01	6.81E-01	8.55E-06	8.94E-04	2.15E-06	6.56E-17	9.16E-03
R2	1.75E-01	5.72E-01	3.25E-02	2.58E-03	7.13E-01	9.49E-04	2.80E-03	4.08E-09	7.45E-13	4.62E-13
R3	6.63E-02	4.22E-02	6.52E-02	1.04E-03	8.69E-01	2.57E-12	8.70E-03	2.69E-04	5.67E-09	5.29E-05
GLOBAL	2.06E-01	5.72E-01	6.52E-02	1.28E-01	8.69E-01	9.49E-04	8.70E-03	2.69E-04	5.67E-09	9.16E-03
U-234										
	Full Mining					Partial Mining				
	CRA19	CRP1	CRP2	CRP3	CRP4	CRA19	CRP1	CRP2	CRP3	CRP4
R1	9.85E-01	9.79E-01	9.77E-01	9.71E-01	9.48E-01	7.10E-01	6.97E-01	5.51E-01	1.88E-01	7.62E-01
R2	9.86E-01	9.91E-01	8.51E-01	5.23E-01	9.26E-01	7.50E-01	1.04E+00	5.21E-02	6.88E-08	1.45E-02
R3	1.02E+00	9.74E-01	9.46E-01	9.24E-01	9.46E-01	2.44E-01	9.97E-01	9.40E-01	9.91E-01	9.78E-01
GLOBAL	1.02E+00	9.91E-01	9.77E-01	9.71E-01	9.48E-01	7.50E-01	1.04E+00	9.40E-01	9.91E-01	9.78E-01
Th-230										
	Full Mining					Partial Mining				
	CRA19	CRP1	CRP2	CRP3	CRP4	CRA19	CRP1	CRP2	CRP3	CRP4
R1	4.24E-03	2.39E-03	5.41E-05	1.99E-03	1.39E-02	9.93E-04	1.40E-04	1.87E-05	2.60E-06	1.37E-04
R2	2.64E-03	6.97E-03	1.67E-04	2.03E-05	1.73E-02	1.03E-04	9.63E-04	7.26E-07	1.15E-13	2.08E-07
R3	9.17E-04	2.14E-03	1.03E-03	5.26E-04	2.07E-02	1.88E-06	8.92E-04	7.81E-04	6.10E-04	4.20E-04
GLOBAL	4.24E-03	6.97E-03	1.03E-03	1.99E-03	2.07E-02	9.93E-04	9.63E-04	7.81E-04	6.10E-04	4.20E-04

Information Only

Table 15 – Cumulative 10,000-yr mass to LWB [count > 10^{-9} kg]

Am-241										
	Full Mining					Partial Mining				
	CRA19	CRP1	CRP2	CRP3	CRP4	CRA19	CRP1	CRP2	CRP3	CRP4
R1	5	3	1	3	29	0	0	0	0	1
R2	6	3	0	1	30	0	0	0	0	1
R3	0	1	0	1	22	0	0	0	0	0
GLOBAL	11	7	1	5	81	0	0	0	0	2
Pu-239										
	Full Mining					Partial Mining				
	CRA19	CRP1	CRP2	CRP3	CRP4	CRA19	CRP1	CRP2	CRP3	CRP4
R1	20	24	5	6	49	3	4	0	0	1
R2	25	14	5	6	55	1	2	1	0	1
R3	21	17	5	12	46	1	4	3	2	3
GLOBAL	66	55	15	24	150	5	10	4	2	5
Th-23A										
	Full Mining					Partial Mining				
	CRA19	CRP1	CRP2	CRP3	CRP4	CRA19	CRP1	CRP2	CRP3	CRP4
R1	20	20	4	9	50	2	5	3	0	1
R2	29	16	3	10	52	3	5	1	0	0
R3	29	20	6	6	50	0	4	4	1	2
GLOBAL	78	56	13	25	152	5	14	8	1	3
U-234										
	Full Mining					Partial Mining				
	CRA19	CRP1	CRP2	CRP3	CRP4	CRA19	CRP1	CRP2	CRP3	CRP4
R1	48	42	15	22	70	11	15	12	5	3
R2	48	41	16	24	66	14	16	10	4	3
R3	47	42	23	17	70	12	18	10	5	4
GLOBAL	143	125	54	63	206	37	49	32	14	10
Th-230										
	Full Mining					Partial Mining				
	CRA19	CRP1	CRP2	CRP3	CRP4	CRA19	CRP1	CRP2	CRP3	CRP4
R1	36	38	15	14	71	5	15	8	2	2
R2	39	33	9	17	71	10	12	4	0	1
R3	42	34	19	12	70	6	12	6	4	2
GLOBAL	117	105	43	43	212	21	39	18	6	5

Information Only

4.4 Sensitivity Analysis

The WIPP sensitivity analysis software STEPWISE was used to perform ranked regression correlation to determine the input variables most strongly associated with uncertainty in cumulative mass transport results of Am-241, Pu-239, U-234, and Th-23A in the CRP1 and CRP4 full mining simulations. Sensitivity analysis for the partial mining scenario, and the CRP2 and CRP3 results from the full mining scenarios is not presented due to the low masses transported in these scenarios.

STEPWISE incremental R-squared values are summarized by parameter in Figure 40 and Figure 41 for the CRP1 and CRP4 results, respectively. Cumulative correlation R-squared values and correlation coefficients are presented by actinide in Table 16 through Table 19.

In CRP1, the matrix distribution coefficient is the input variable with the strongest association with the variability of releases of each actinide. The correlation is negative, indicating that lower matrix distribution coefficients are associated with larger releases, as expected. Other independent variables captured by the analysis include the DTRKMF travel times, climate index, half-matrix block length, and fracture porosity, though only the matrix distribution coefficient exceeds an R-square of 0.20. The extremely low mass transport results from Am-241 appear to be challenging the ability of STEPWISE to identify the impactful variables.

In CPR4, the matrix distribution coefficient is also the input variable with the strongest association with the variability of releases; however, in CRP4, the particle travel time to the LWB emerges as a strong secondary control. The regression coefficient is negative, indicating that shorter travel times are associated with larger releases. The stronger correlations in the CRP4 simulations indicate that the flow field selection exerts more control on the output with releases out to the west. Other independent variables captured by the analysis again include the climate index, half-matrix block length, and fracture porosity, again all with relatively low correlations.

Matrix half-block length is the dual porosity transport parameter most strongly associated with mass releases. Rank correlations with the HMBKLT parameter are consistent across CRP1 and CRP4. The correlation is positive, indicating that larger matrix half-block length values are associated with larger releases. The half-block length is used to calculate the fracture aperture in the mass-transfer equation. A higher half-block length results in a higher fracture aperture, lower specific surface area for mass transfer, and thereby lower rate of mass transfer between the advective and diffusive domains.

Because of the potential for cross-correlations with the DTRKMF particle travel times, the mining factor could not be included as an independent variable in the STEPWISE analysis. To assess the effect the mining factor has on the results, the DTRKMF travel times to the LWB were rank correlated against the mining factor parameter (MINP_FAC). The results show that particle travel time and the mining factor are weakly to moderately correlated for both the partial and full mining scenarios (Figure 42). The mining factor is negatively correlated with particle travel times from CRP4 in the full mining scenario, but positively correlated with particle travel times in all other scenarios.

Information Only

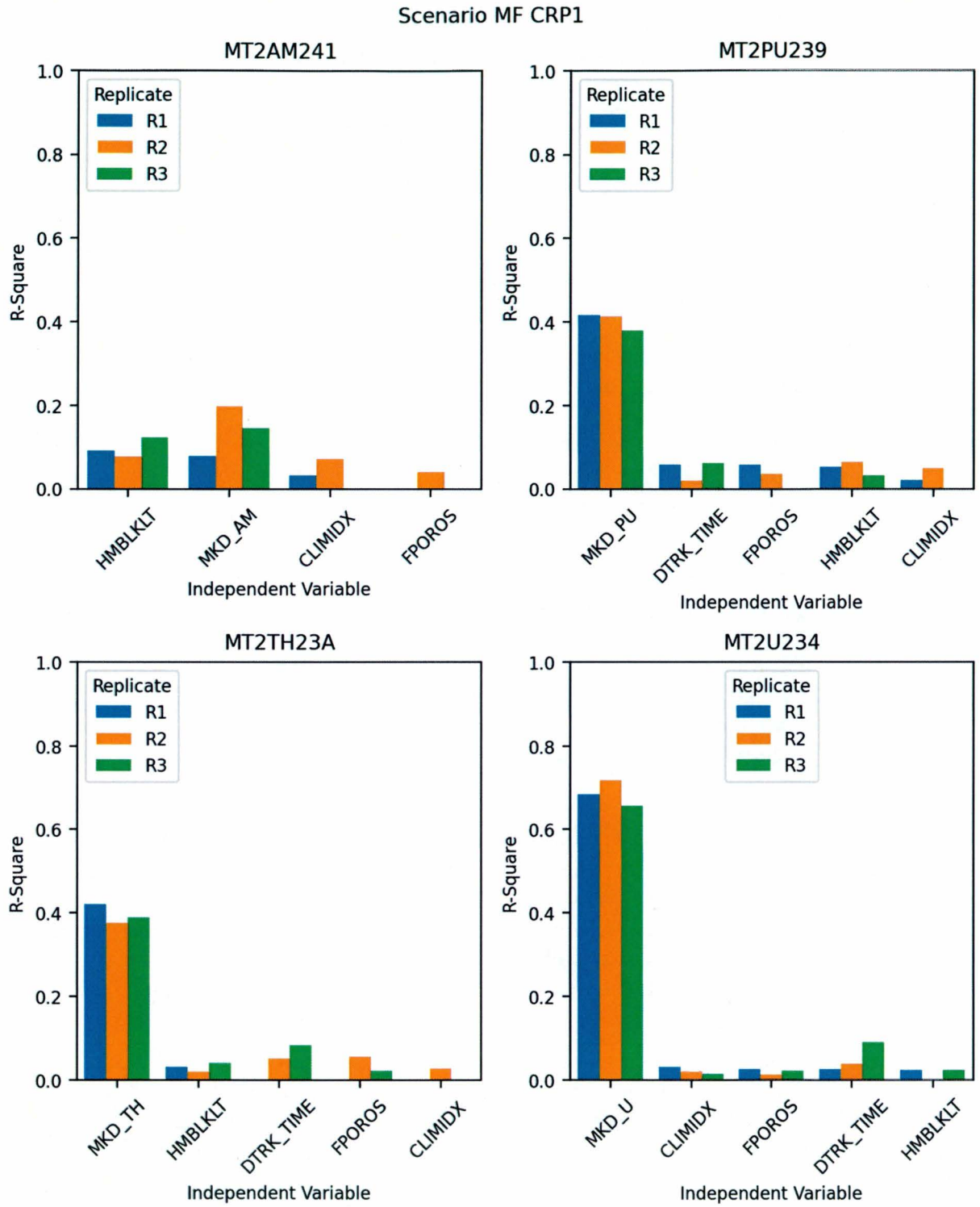


Figure 40 – Transport results sensitivity, full mining, CRP1

Information Only

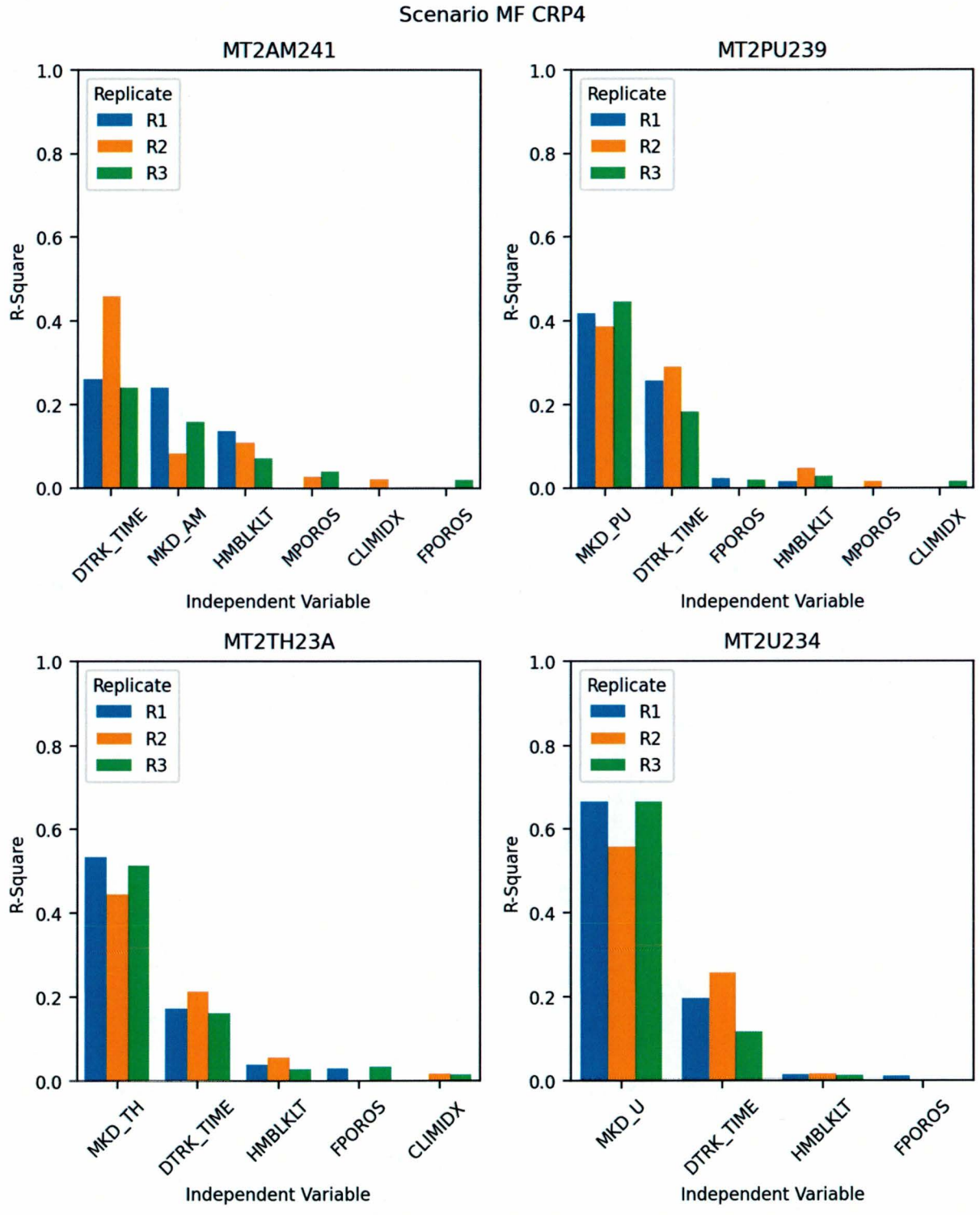


Figure 41 – Transport results sensitivity, full mining, CRP4

Information Only

Table 16 – Rank correlation Am-241

CRP1				CRP4			
Replicate	Variable	R-Square	Regression Coefficient	Replicate	Variable	R-Square	Regression Coefficient
R1	HMBLKLT	0.09	0.30	R1	DTRK_TIME	0.26	-0.54
	MKD_AM	0.17	-0.27		MKD_AM	0.50	-0.48
	CLIMIDX	0.20	0.18		HMBLKLT	0.64	0.37
R2	MKD_AM	0.20	-0.45	R2	DTRK_TIME	0.46	-0.63
	HMBLKLT	0.28	0.28		HMBLKLT	0.57	0.35
	CLIMIDX	0.35	0.27		MKD_AM	0.65	-0.28
R3	MKD_AM	0.15	-0.37	R3	DTRK_TIME	0.24	-0.50
	HMBLKLT	0.27	0.35		MKD_AM	0.40	-0.40
	--	--	--		HMBLKLT	0.47	0.27

Table 17 – Rank correlation Pu-239

CRP1				CRP4			
Replicate	Variable	R-Square	Regression Coefficient	Replicate	Variable	R-Square	Regression Coefficient
R1	MKD_PU	0.42	-0.62	R1	MKD_PU	0.42	-0.63
	DTRK_TIME	0.48	-0.31		DTRK_TIME	0.68	-0.53
	FPOROS	0.53	-0.23		FPOROS	0.70	-0.15
R2	MKD_PU	0.41	-0.67	R2	MKD_PU	0.39	-0.67
	HMBLKLT	0.48	0.25		DTRK_TIME	0.68	-0.52
	CLIMIDX	0.53	0.21		HMBLKLT	0.73	0.22
R3	MKD_PU	0.38	-0.64	R3	MKD_PU	0.45	-0.71
	DTRK_TIME	0.44	-0.25		DTRK_TIME	0.63	-0.44
	HMBLKLT	0.48	0.18		HMBLKLT	0.66	0.18

Information Only

Table 18 – Rank correlation Th-23A

CRP1				CRP4			
Replicate	Variable	R-Square	Regression Coefficient	Replicate	Variable	R-Square	Regression Coefficient
R1	MKD_TH	0.42	-0.65	R1	MKD_TH	0.53	-0.80
	HMBLKLT	0.45	0.18		DTRK_TIME	0.70	-0.45
	--	--	--		HMBLKLT	0.74	0.19
R2	MKD_TH	0.38	-0.65	R2	MKD_TH	0.45	-0.75
	DTRK_TIME	0.43	-0.23		DTRK_TIME	0.66	-0.44
	FPOROS	0.48	-0.23		HMBLKLT	0.71	0.24
R3	MKD_TH	0.39	-0.63	R3	MKD_TH	0.51	-0.79
	DTRK_TIME	0.47	-0.26		DTRK_TIME	0.67	-0.41
	HMBLKLT	0.51	0.21		FPOROS	0.71	-0.19

Table 19 – Rank correlation U-234

CRP1				CRP4			
Replicate	Variable	R-Square	Regression Coefficient	Replicate	Variable	R-Square	Regression Coefficient
R1	MKD_U	0.69	-0.78	R1	MKD_U	0.67	-0.82
	CLIMIDX	0.72	0.17		DTRK_TIME	0.86	-0.46
	FPOROS	0.74	-0.19		HMBLKLT	0.88	0.12
R2	MKD_U	0.72	-0.89	R2	MKD_U	0.56	-0.70
	DTRK_TIME	0.76	-0.19		DTRK_TIME	0.82	-0.50
	CLIMIDX	0.78	0.14		HMBLKLT	0.83	0.13
R3	MKD_U	0.66	-0.75	R3	MKD_U	0.66	-0.81
	DTRK_TIME	0.75	-0.27		DTRK_TIME	0.78	-0.34
	FPOROS	0.77	-0.16		HMBLKLT	0.79	0.11

Information Only

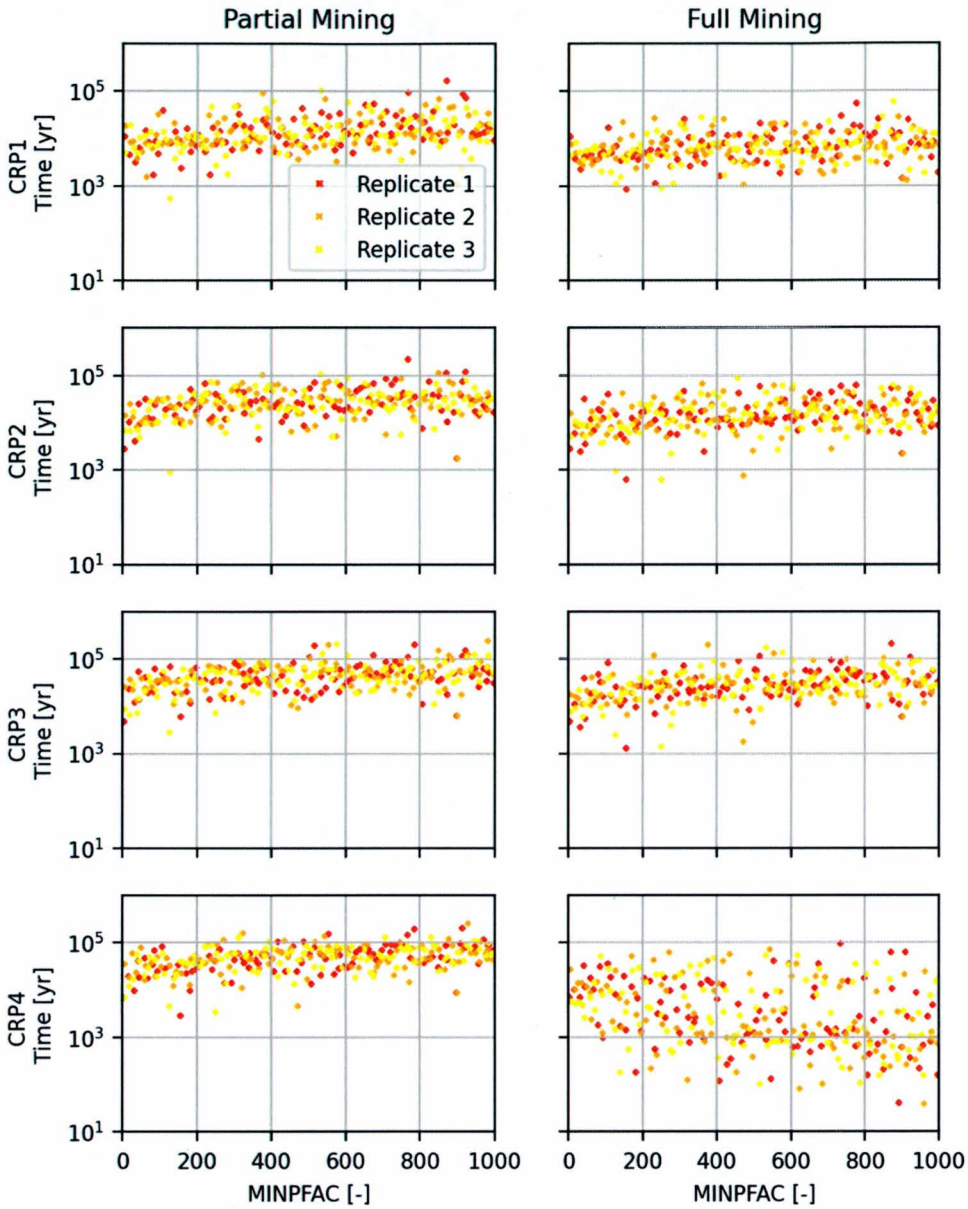


Figure 42 – DTRKMF particle travel time to LWB [years] versus mining factor [MINPFAC]

Information Only

5.0 SUMMARY

The RPPCR Culebra flow transport calculations are presented for 4 isotopes Am-241, Pu-239, Th-23A, U-234, and the decay product of U-234, Th-230, for two mining scenarios and four mass release points. The release points include the centroid of the 10 waste panels used in the CRA19 calculations (CRP1), and three new release points (CRP2 through CRP4) over the proposed additional and replacement waste panel region. Results are compared to the CRA19, which used Culebra flow and transport output from the PABC09. Results from an additional analysis, the RPPA, are presented to isolate the impact of the additional release locations. The RPPA did not include the new T-field calibrations or the updated oxidation state model.

The results indicate mass transport from CRP4 in full mining conditions results in earlier, more complete, and more frequent breakthrough for all isotopes than for any other combination of mining scenario and release point. Mass discharge of U-234 and Pu-239 occurs more frequently, for which approximately 40% and 20% of simulations, respectively, show discharge of at least 0.01 kg across the LWB by 10,000 years. Less total mass is transported from CRP2 and CRP3 to the LWB than from CRP1. Particles released at CRP4 travel relatively quickly to the western edge of the WIPP LWB in full-mining simulations, reaching the LWB with a minimum travel time of 40 years and a 3-replicate median travel time of 2.43E+03 years. Mass transported to the LWB in the partial mining scenario is low on average from all release points and for all isotopes, though a few vectors show mass above 0.1 kg in the Pu-239 and U-234 10,000-yr discharge horsetails.

The impact of the new T-field calibrations has been to reduce the uncertainty in the western region of the controlled area, as visualized by the lower ensemble standard deviations of the flow fields in this area. Particle travel times are higher and mass transport values are lower in the RPPCR CRP4 and CRP3 when compared with the RPPA, indicating that the primary cause for these changes is the new T-fields. Mass release values in the CRP1 simulations are more similar between the RPPCR and RPPA analyses.

The new oxidation state model affects the Pu-239 mass transport results by shifting 25% of simulations from low oxidation Pu(III) to high oxidation Pu(IV)in the RPPCR. However, the uncertainty distribution of the matrix distribution coefficient values of Pu(IV) is broader than that of Pu(III), lower at the low end and higher at the high end, and therefore appears to have a low aggregate affect.

Uncertain quantities that are most strongly associated with uncertainty in mass discharge are the matrix distribution coefficient in both CRP1 and CRP4 simulations and the DTRKMF travel time to the LWB in the CRP4 simulations. The DTKRMF travel times were more impactful for the releases from CRP4 than CRP1, indicating greater sensitivity to the flow fields of releases from the western edge of the additional panels area.

Information Only

This page intentionally left blank.

Information Only

6.0 REFERENCES

Bethune, J. 2022. Impact analysis for the software problem report SPR 21-002 for PRESECOTP2D. ERMS 576691. Carlsbad, NM: Sandia National Laboratories.

Bethune, J. and S. Brunell. 2022. Determination of Culebra Release Points Number and Locations in a Repository with New Panels. ERMS 576493. Carlsbad, NM: Sandia National Laboratories.

Bowman, D. 2022. Analysis Plan for Evaluation and Recalibration of Culebra Transmissivity Fields. AP-203. ERMS 578663. Carlsbad, NM: Sandia National Laboratories.

Bowman, D., R. Kushnereit, M. Pedrazas, P. Johnson, N. Deeds, and J. Pinkard. 2023. Analysis Report Documenting the Data, Generation, and Calibration of T-fields for CRA-2024. ERMS 579507. Carlsbad, NM: Sandia National Laboratories.

Brunell, S. and T. Zeitler. 2023. Analysis Report for Normalized Releases in the Replacement Panels Planned Change Request Performance Assessment. ERMS 579727. Carlsbad, NM: Sandia National Laboratories.

Clayton, D.J. 2009. Update to the Kd values for the PABC-2009. ERMS 552395. Carlsbad, NM: Sandia National Laboratories.

Corbet, T. 1995. Record of FEP Screening Work FEP 10# NS-9 Justification of SEC02D Approximation for PA Transport Calculation. ERMS 230802. Carlsbad, NM: Sandia National Laboratories.

Corbet, T. and P. Swift. 1996. Parameters required for SECOFL2D: Climate Index. ERMS 237465. Carlsbad, NM: Sandia National Laboratories.

Cranston, C.C. 2009. Minable Potash Ore. ERMS 551120. Carlsbad, NM: Bureau of Land Management.

Gilkey, A. 2013. Addendum to Requirements Document (ERMS #245957) Verification and Validation Plan (ERMS #245957) and User's Manual (ERMS #245963) for PRESECOTP2D Version 1.23. ERMS 559778. Carlsbad, NM: Sandia National Laboratories.

Hansen, C.W. 2021. Review of Conceptual Models for the Additional Panels Performance Assessment. ERMS 575523. Carlsbad, NM. Sandia National Laboratories.

Hansen, C. 2022. Analysis Plan for the Replacement Panels Performance Assessment. AP-193. ERMS 576579. Sandia National Laboratories. Carlsbad, NM.

Hansen, C., S. King, J. Bethune, and S. Brunell. 2023. Analysis Plan for the Performance Assessment for Replacement Panels Planned Change Request. AP-204. Carlsbad, NM: Sandia National Laboratories.

Hart, D. B., R.L. Beauheim, and S.A. McKenna. 2009. Analysis Report for Task 7 of AP-114: Calibration of Culebra Transmissivity Fields. Carlsbad, NM: Sandia National laboratories.

Hart, D.B., R.M. Holt, and S.A. McKenna. 2008. Analysis Report for Task 5 of AP-114: Generation of Revised Base Transmissivity Fields. ERMS 552391. Carlsbad, NM: Sandia National laboratories.

Holt, R.M. 1997. Conceptual Model for Transport Processes in the Culebra Dolomite Member of the Rustler Formation. Carlsbad, NM: Sandia National laboratories. SAND 97-0194.

Information Only

Kuhlman, K. 2010. Analysis Report for the CRA-2009 PABC Culebra Flow and Transport Calculations. ERMS 552951. Sandia National Laboratories, Carlsbad, NM.

Langevin, C.D., J.D. Hughes, E.R. Banta, R.G. Niswonger, S. Panday, and A.M. Provost. 2017. Documentation for the MODFLOW 6 Groundwater Flow Model. U.S. Geological Survey Techniques and Methods, Book 6, A55. https://doi.org/10.3133/tm6A55.

Long, J. 2019. Computational Code Execution and File Management for the 2019 Compliance Recertification Application Performance Assessment (CRA-2019 PA). ERMS 571375. Carlsbad, NM: Sandia National Laboratories.

Long, J. 2020. Nuclear Waste Management Procedure NP 19-1 SOFTWARE REQUIREMENTS, Revision 19. Carlsbad, NM: Sandia National Laboratories.

Long, J., S. King. 2022. Summary Report on the Migration of the WIPP PA Codes from Solaris to Linux. ERMS 577606. Carlsbad, NM: Sandia National Laboratories.

Long, J. 2023. Computational Code Execution and File Management for the Replacement Panels Planned Change Request (RPPCR). ERMS 579728. Sandia National Laboratories. Carlsbad, NM.

Loukota, J.J. 1997. Software Problem Report 97-017 for SECOTP2D Versions 1.21Z0, 1.30, 1.31, and 1.41. ERMS 247875. Sandia National Laboratories, Carlsbad, NM.

Lucchini, J., and J. Swanson, J. 2023. LANL ACRSP Parameter Recommendations for CRA-2024 Performance Assessment. Carlsbad, NM: Los Alamos National Laboratory. LCO-ACP-34 Rev. 0.

MacKinnon, R.J. and G. Freeze. 1997a. Summary of EPA-Mandated Performance Assessment Verification Test (Replicate 1) and Comparison With the Compliance Certification Application Calculations, Revision 1. ERMS 422595. Carlsbad, NM: Sandia National Laboratories.

MacKinnon, R.J. and G. Freeze. 1997b. Summary of Uncertainty and Sensitivity Analysis Results for the EPA-Mandated Performance Assessment Verification Test, Rev 1. ERMS 420669. Carlsbad, NM: Sandia National Laboratories.

MacKinnon, R.J. and G. Freeze. 1997c. Supplemental Summary of EPA-Mandated Performance Assessment Verification Tests (All Replicates) and Comparison With the Compliance Certification Application Calculations, Revision 1. ERMS 414880. Carlsbad, NM: Sandia National Laboratories.

Meigs, L.C., Beauheim, R.L. and Jones, T.L., eds., 2000. Interpretation of Tracer Tests Performed in the Culebra Dolomite at the Waste Isolation Pilot Plant Site. SAND 97-3109. Carlsbad, NM: Sandia National Laboratories.

Nielsen, S.R. 2020. Nuclear Waste Management Procedure NP 9-1 Analyses, Revision 11. Carlsbad, NM: Sandia National Laboratories.

Sjomeling, D. 2019. "2:30 Meeting Information," an email to Paul Shoemaker with the attachment "West Mains and Panels peer review info Final 091219.pdf." ERMS 572682. Carlsbad, NM: Nuclear Waste Partnership LLC. October 17, 2019.

U.S. Environmental Protection Agency (EPA). 1998. 40 CFR 194, Criteria for the Certification and Recertification of the Waste Isolation Pilot Plant's Compliance with the Disposal Regulations: Certification Decision: Final Rule, Federal Register. Vol. 63, 27354-27406.

Information Only

U.S. Environmental Protection Agency (EPA). 2022. Overview of EPA Review of U.S. Department of Energy 2019 WIPP Compliance Recertification Application Performance Assessment. EPA-HQ-OAR-2019-0534. Washington, D.C.: U.S. Environmental Protection Agency, Office of Radiation, and Indoor Air.

WIPP Performance Assessment. 2021. User's Manual for LHS, Version 3.00. ERMS 574194. Carlsbad, NM: Sandia National Laboratories.

WIPP Performance Assessment. 2023. User's Manual for PRESECOTP2D, Version 1.24. ERMS 573861. Carlsbad, NM: Sandia National Laboratories.

WIPP Performance Assessment. 2023. Software Problem Report SPR 23-001 DTRKMF Version 1.02. ERMS 579912. Carlsbad, NM: Sandia National Laboratories.

Zeitler, T.R., J. Bethune, S. Brunell, B. Day, D. Kicker, J. Long, and R. Sarathi. 2019. Summary Report for the 2019 Compliance Recertification Application Performance Assessment (CRA-2019 PA). ERMS 571376. Carlsbad, NM: Sandia National Laboratories.

Zeitler, T.R. 2023. Analysis Report for Parameter Sampling in the Replacement Panels Planned Change Request (RPPCR). ERMS 579721. Carlsbad, NM: Sandia National Laboratories.

Information Only

This page intentionally left blank.

Information Only

7.0 APPENDIX A MININGMOD

This appendix describes the use, execution, validation under NP 9-1, and RPPCR implementation of Culebra flow analysis scripts and utilities. Utility scripts described in this section include:

Source/enlarge_mining_areas.py
Source/mining_mod.py
Source/100x100_to_50x50.py

These scripts are used by to define the mining impacted areas, multiply the calibrated arrays of Culebra transmissivity by the mining factor LHS sampled parameter, and resize the flow grid from 100-m to 50-m cells.

Files are archived in the CVS repository:

/data/cvs/CVSLIB/WIPP_CODES/PA_CODES/MININGMOD/

The validation tests described in this appendix are run with the shell script *Test/RunTest.sh,* which prepares input and output directories, checks out the appropriate input files, and executes the scripts on the validation tests. All Python scripts are tested and executed on the WIPP computing cluster FWM with the system install of Python version 2.7.5.

7.1 Utility enlarge_mining_areas.py

The Python script *enlarge_mining_areas.py* enlarges the mining regions to account for the angle of draw and distinguishes the mining impacted cells within the LWB. It is unchanged from the version that was documented in the PABC-2009 Culebra flow and transport analysis report (Kuhlman, 2010). It is documented here for completeness because it is used with the other Culebra flow scripts. All model coordinates are given in UTM Zone 13N NAD27 meters, unless otherwise noted.

The mining impacted areas are expanded in 5×5-cell stencil with 1 additional cell along the 4 compass directions (see shaded cells in Figure 43). Cells within the stencil are assessed to be mining impacted.

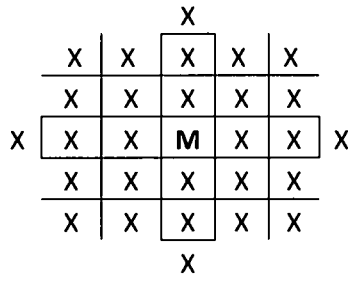


Figure 43 – Mining impacts stencil

7.1.1 Execution and Syntax

The script *enlarge_mining_areas.py* is executed with the following command:

```
$python enlarge_mining_areas.py
```


Information Only

The script reads key inputs from the file *enlarge_mining_areas.in,* which must be present in the execution directory. The inputs in *enlarge_mining_areas.in* are defined in the following order:

Line 1: x0, y0 [float, float]
MODFLOW grid origin coordinates

Line 2: nx, ny [integer, integer]
Number of MODFLOW cells in the x and y directions

Line 3: dx, dy [float, float]
MODFLOW cell size [m] in the x and y directions

Line 4: x1, x2, x3, x4 [float, float, float, float]
X coordinates of the LWB corners

Line 5: y1, y2, y3, y4 [float, float, float, float]
Y coordinates of LWB corners

Line 6: fnminin [string]
Input mining data filename

Line 7: fnminfactout [string]
Output mining data filename with matrix form of input mining areas for debugging

Line 8: fnfullminout [string]
Output full mining array filename

Line 9: fnpartminout [string]
Output partial mining array filename

Line 10: verbose [True or False]
If 'True', additional output is printed to the screen during execution

7.1.2 Input and Output Files

fnminin

Input file containing a listing of MODFLOW cells with UTM coordinates and indicator values of 1 for minable potash and 0 for no minable potash.

fnminfactout

Output file with matrix form of input minable potash areas for debugging and plotting. This file uses indicator values with the following values:

Non-mining outside of the LWB: 0
Mining outside of the mining area: 1
Non-mining inside the LWB: 10
Mining within the LWB: 11

fnminfactoutx

Output file with the x coordinates of the index values in matrix form for plotting.

fnminfactouty

Output file with the y coordinates of the index values in matrix form for plotting.

Information Only

fnfullminout

Output full mining array file, with values of 1 for mining conditions and 0 for no mining conditions.

fnpartminout

Output partial mining array file, with values of 1 for mining conditions and 0 for no mining conditions.

7.1.3 Validation Test 0

Test 0 was developed to validate the functionality of *enlarge_mining_areas.py*. All input files are taken from the CVS repository MiningMod, including *Inputs/mining_areas_xyz.dat* and *Inputs/enlarge_mining_areas.in*, such that the output mining scenario impacts should be the same as the impacts assessed in the PABC09.

The contents of *enlarge_mining_areas.in* are shown in Figure 44.

```
601700.0 3566500.0
284 307
100.0 100.0
616941.0 610495.0 610567.0 617015.0 616941.0
3585109.0 3585068.0 3578623.0 3578681.0 3585109.0
mining_areas_xyz.dat
mining_factor.dat
New_Full_09.dat
New_Part_09.dat
True
```

Figure 44 – enlarge_mining_areas.in contents

After checking in the Inputs to the Test/Input/Test0/ directory, the script is executed with the following command:

```
$python enlarge_mining_areas.py
```

The output files are saved to Output/Test0/. The output files *New_Full_09.dat* and *New_Part_09.dat* are compared to the versions in to the MiningMod repository using the Unix 'diff' command, creating the files `test0_full.diff` and `test0_part.diff`.

Inspection of the diff output files indicates that the script executed successfully and that the output files are the same as the previously validated enlarge mining output files, indicating that the script *enlarge_mining_areas.py* is validated.

7.1.4 RPPCR Execution

The script *enlarge_mining_areas.py* is executed by the MODFLOW6.py WIPP run control script from within the Culebra flow model run directory (Long, 2023). Input files are checked out from the CVS repository MiningMod, including:

Inputs/mining_areas_xyz.dat
Inputs/enlarge_mining_areas.in

Information Only

The output mining scenario impacts are the same as the impacts assessed in the PABC09 and validation Test 0. The utility is executed with the following command:

```
$python enlarge_mining_areas.py
```

Outputs

MININGMOD/Output/New_Full_09.dat
MININGMOD/Output/New_Part_09.dat

7.2 Utility mining_mod.py

The *mining_mod.py* Python script modifies the Culebra flow model input files to account for the impacts of potash mining on transmissivity. The script identifies MODFLOW 6 grid cells in mining impacted areas and multiplies their Culebra transmissivity values by a user-specified factor. More information about the MODFLOW 6 input file format and requirements are described in the U.S. Geological Survey documentation for MODFLOW 6 (Langevin, 2017).

The script also modifies the boundary conditions in certain mined areas consistent with the CRA19 analysis (Kuhlman, 2010). Model interior cells that are both specified head and mining-impacted are changed to normal cells by removing them from the CHD input heads file. Applying the mining factor to these areas without changing the cell from constant head to active would greatly increase the water flowing into the domain, since the constant-head boundary conditions are a potentially infinite source of water. Since these cells are not believed to be a large source of water, constant-head cells that are interior to the model domain and affected by mining modifications are converted to active cells. The cells in the outermost row and columns of the domain (aside from those cells in the inactive or no-flow region) are maintained as constant head, even if they correspond to mined regions. Only constant-head cells in the interior of the model domain corresponding to the halite-sandwiched region of the Culebra are changed to active cells.

Finally, the script also makes minor adjustments to the CHD MODFLOW 6 package files to reference the mining modified input files.

7.2.1 Execution and Syntax

The script *mining_mod.py* is executed with the following command and syntax.

```
$python mining_mod.py Scenario MINPFAC
```

Scenario ("Full" or "Part")
: Indicates mining impacts will be applied in either full or partial mining scenario distributions.

MINPFAC (numeric)
: Mining factor multiplier for the transmissivity field.

The script reads key inputs from the file *mining_mod.in,* which must be present in the execution directory. The inputs are defined in the following order:

Line 1: mining_area_tmp (str)
: Input mining scenario filename template.

Information Only

Line 2: k_field_fn (str)
Input filename with MODFLOW 6 NPF package hydraulic conductivity data array.

Line 3: k_field_fo (str)
Output filename for MODFLOW 6 NPF package mining modified hydraulic conductivity data array.

Line 4: bcs_fn (str)
Input filename with MODFLOW 6 CHD package boundary condition data array.

Line 5: bcs_fo (str)
Output filename for the MODFLOW 6 CHD package with mining modified boundary condition data array.

Line 6: chd_fn (str)
Input MODFLOW 6 CHD package filename with boundary condition array dimensions.

Line 7: chd_fo (str)
Output MODFLOW6 CHD package filename with mining modified boundary condition array dimensions.

Line 8: fmt (str)
Output value format code

7.2.2 Input and Output Files

Four file types are read or written by the mining_mod.py utility, listed below.

Mining impacted array file
Input mining impacts array file generated by *enlarge_mining_areas.py*.

NPF Package hydraulic conductivity data array file
Input filename with MODFLOW 6 NPF package hydraulic conductivity data array.

CHD Package data array file
Output file with the mining modified boundary condition values array in the 4-column (x | y | z | value) format expected by the MODFLOW 6 CHD package.

CHD Package file
Output MODFLOW6 CHD package file with mining modified boundary condition array size.

7.2.3 Validation Test 1

Test 1 validates the functionality of *mining_mod.py* to multiply the MODFLOW hydraulic conductivity data array by the mining multiplier in the regions of mining impact and the functionality to remove boundary conditions that fall within the mining impacted region. The contents of the input file *mining_mod.in* are shown in Figure 45. The test case inputs are saved to Test/Input/Test1/. The output files are saved to Test/Output/Test1/.

Test 1 is executed with the below command.

```
$python mining_mod.py Full 100
```


Information Only

The resulting output values in in *mf6_head.npf_k.mining.txt* should have values equal to MINPFAC (100) times the original values in *mf6_head.npf_k.tx*t in the mining impacted regions.

```
New_{s}_09.txt
mf6_head.npf_k.txt
mf6_head.npf_k.mining.txt
mf6_head.chd_stress_period_data_1.txt
mf6_head.chd.mining.txt
mf6_head.chd
mf6_head.chd.mining
%.11e
```

Figure 45 – Test 1 mining_mod.in contents

The hydraulic conductivity output array is validated visually by plotting both the input and output and the ratio of the output to the input values. Boundary conditions are overlain on the mining hydraulic conductivity array in black. The results show the ratio output to input values is 100 in mining impacted areas, and 1 everywhere else, as expected (Figure 46). Further, the boundary conditions array indicates that the mining impacted cells in the constant head region of the northeast corner of the domain have been converted to active.

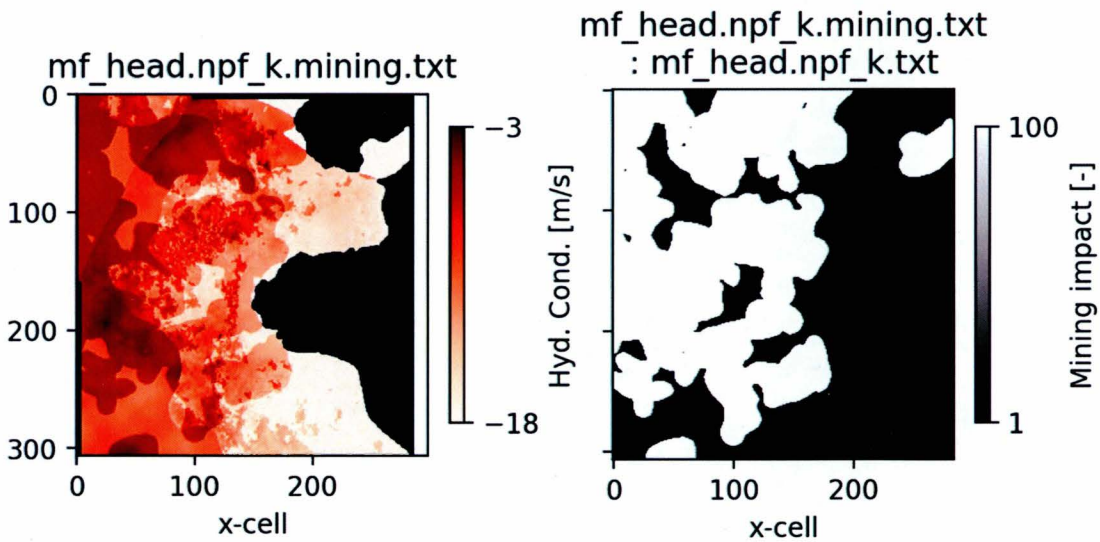


Figure 46 – Calibrated and mining modified T-fields

To validate the revisions to the CHD package input file with the updated number of boundary condition cells, the MAXBOUND value in the output file *mf6_head.chd.mining* is compared to the number of boundary conditions cells in the CHD data package (*mf6_head.chd.mining.txt*). The MAXBOUND value is "19274", consistent with the number of data rows in the file *mf6_head.npf.mining.txt*, as expected.

These results show that the script executed successfully with the correct output values.

Information Only

7.2.4 RPPCR Execution

The *mining_mod.py* script is executed with Slurm scripts that are generated with the MODFLOW6.py WIPP run control script (Long, 2023). Calculations are executed within subdirectories of the Culebra flow model run directory, of the form

MININGMOD/Output/R{r}/{s}/v{vvv}/

in which {r}, {s}, and {vvv} represent the replicate number, scenario, and vector number, respectively.

For each replicate and mining scenario, the Slurm script *run_miningmods_R{r}_{s}.sh* is generated to loops through the LHS vectors, changing to the execution directory, linking to the input T-field realization and mining areas file and passing the MINP_FAC value to *mining_mod.py* as command line input. The run scripts read in the SUMMARIZE output tables of LHS sampled parameters CULEBRA:TRANSIDX and CULEBRA:MINP_FAC (*sum_mf6_rppcr_r{r}.tbl*). The calibrated T-fields are indexed alphabetically by their realization identifier, r000 through r999, in the file *keepers*. The CULEBRA:TRANSIDX parameter is converted to an integer index from 1 to 100 and then used as an index to associate a realization from the *keepers* file with an LHS vector.

$python mining_mod.py {s} {MINP_FAC}

The input file mining_mod.in is the same as in Test 1 (Figure 45). Linked output and calculation are saved in individual subdirectories for each LHS vector.

Outputs:
MININGMOD/Output/R{r}/{s}/v{vvv}/mf6_head.chd.mining
MININGMOD/Output/R{r}/{s}/v{vvv}/mf6_head.chd.mining.txt
MININGMOD/Output/R{r}/{s}/v{vvv}/mf6_head.npf_k.mining.txt

in which {r}, {s}, and {vvv} represent the replicate number, scenario, and vector number, respectively.

7.3 Utility 100x100_to_50x50.py

The SECOTP2D transport mesh is comprised of 50-meter square elements, while the MODFLOW mesh used for calibration is made up of 100-meter square elements. The Python script *100x100m_to_50x50m.py* subdivides each 100-m grid cell into four equal-sized elements, with the properties of the larger cells copied directly into the smaller cells. More information about the MODFLOW 6 input file format and requirements are described in the U.S. Geological Survey documentation for MODFLOW 6 (Langevin, 2017).

The script reads in the MODFLOW grid properties from the boundary files, the top and bottom elevation arrays, the starting head array, and the parameter fields anisotropy, hydraulic conductivity, recharge, and storage. The boundary condition head values are additionally smoothed along the exterior two rows and columns of the domain by first copying the data into the finer mesh without averaging, then applying a smoothing stencil to the head data. If cell h is a boundary condition cell on the model periphery, the smoothing factor is calculated as follows:

$$fact = (h_{\pm 1} - h) * 0.25$$

Information Only

Where ¼ is the distance between the centers of the 50-m cells. If the value of fact is less than 20, then it is added to the cell value.

$$h = h + fact$$

All output filenames for the subdivided grid are given the affix "*.50*".

7.3.1 Execution and Syntax

The script *100x100_50x50.py* is executed with the following command and syntax.

```
$python 100x100_to_50x50.py
```

The file *100x100_50x50.in* must be present in the execution directory. This file defines key inputs in the following order:

Line 1: disbtm_fn

Input filename with MODFLOW 6 DIS package cell bottom elevation data array.

Line 2: distop_fn

Input filename with MODFLOW 6 DIS package cell top elevation data array.

Line 3: disidom_fn

Input filename with MODFLOW 6 DIS package active domain data array.

Line 4: npfk22_fn

Input filename with MODFLOW 6 NPF package anisotropy data array.

Line 5: npfk_fn

Input filename with MODFLOW 6 NPF package hydraulic conductivity data array.

Line 6: npfitype_fn

Input filename with MODFLOW 6 NPF package cell type data array.

Line 7: stosy_fn

Input filename with MODFLOW 6 STO package specific yield data array.

Line 8: stoss_fn

Input filename with MODFLOW 6 STO package specific storage data array.

Line 9: stoicon_fn

Input filename with MODFLOW 6 STO package cell type data array.

Line 10: rcha_fn

Input filename with MODFLOW 6 RCH package data array.

Line 11: init_head_fn

Input filename with MODFLOW 6 initial head array.

Line 12: bcs_file_fn

Information Only

Input filename with MODFLOW 6 boundary condition array.

7.3.2 Input and Output Files

The *100x100_to_50x50.py* script reads and writes files compatible with MODFLOW 6. Refer to the MODFLOW 6 documentation for the formatting and syntax of these files (Langevin, 2017).

7.3.3 Validation Test 2

Test 2 validates the functionality of *100x100_to_50x50.py* to resize the MODFLOW 6 mining modified grid using a sample set of input files from the RPPCR. The test case inputs are saved to Test/Input/Test2/. The input file *100x100_to_50x50.in* is shown in Figure 47. The results are saved to Test/Output/Test2/.

```
mf6_head.dis_botm.txt
mf6_head.dis_top.txt
mf6_head.dis_idomain.txt
mf6_head.npf_k22.txt
mf6_head.npf_k.mining.txt
mf6_head.npf_icelltype.txt
mf6_head.sto_sy.txt
mf6_head.sto_ss.txt
mf6_head.sto_iconvert.txt
mf6_head.rcha_recharge_1.txt
mf6_head.init_head.mod
mf6_head.chd.mining.txt
```

Figure 47 – Test 2 *100x100_to_50x50.in* contents

The test is executed with the following command:

```
$python 100x100_to_50x50.py
```

To validate the output, confirm that the transmissivity values are mapped directly from the coarser grid (*mf6_head.npf_k.txt*) to the finer grid (*mf6_head.npf_k.mining.txt.50*) and that the peripheral boundary condition cells are smoothed in the finer mesh (*mf6_head.chd.mining.txt.50*).

The hydraulic conductivity values depicted in Figure 48 show that the input and output transmissivity field retain the same values and distribution stretched over a grid with twice as many cells in the x and y directions, as expected. The boundary conditions values presented Figure 49 show that the output boundary condition values are being smoothed, as expected. These results validate the functionality of the *100x100_to_50x50.py* script.

Information Only

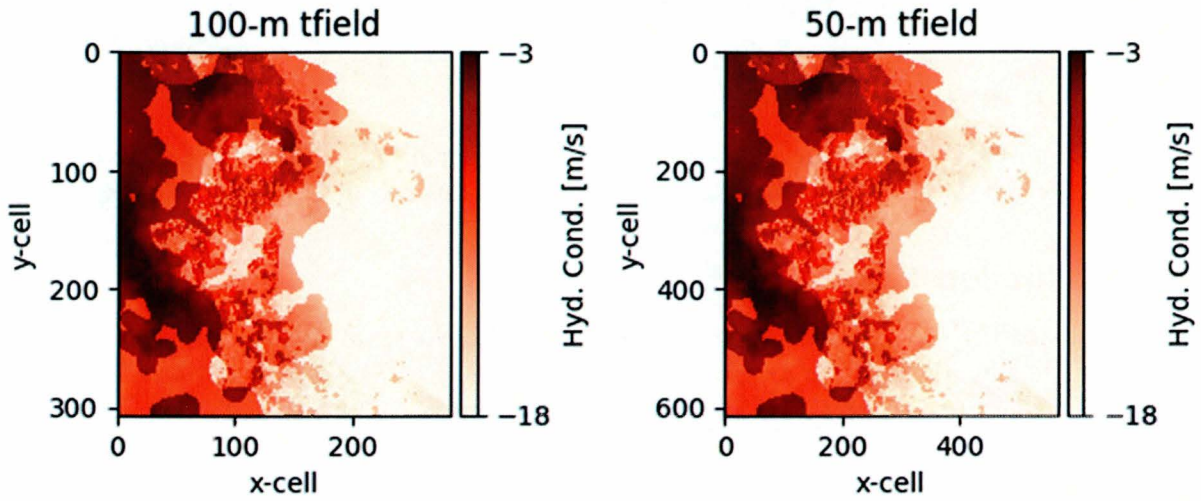


Figure 48 - 100-m input and 50-m output T-field array

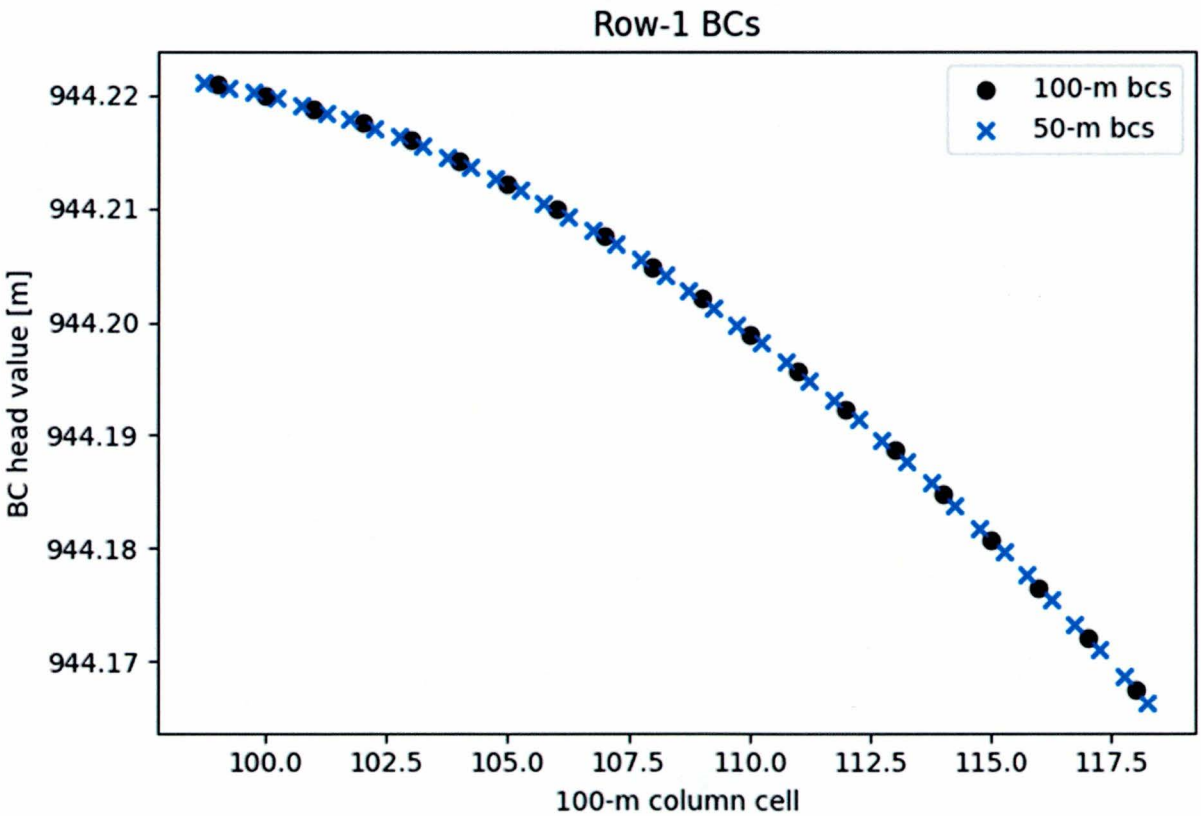


Figure 49. Subset 100-m input and 50-m output boundary conditions

Information Only

7.3.4 RPPCR Execution

The *100x100_to_50x50.py* script is executed with Slurm scripts that are generated with the MODFLOW6.py WIPP run control script (Long, 2023). Calculations are executed within subdirectories of the Culebra flow model:

RESIZE/Output/R{r}/{s}/v{vvv}/

in which {r}, {s}, and {vvv} represent the replicate number, scenario, and vector number, respectively.

The run scripts loop through the LHS vectors, changing to the execution directory, linking to the T-field realization and other inputs, and running the *100x100_to_50x50.py* utility. The input file *100x100_to_50x50.in* is the same as in Test 2 (Figure 45). The utility is run with the following command.

$python 100x100_to_50x50.py

Outputs:

RESIZE/Output/R{r}/{s}/v{vvv}/mf6_head.chd.mining.txt.50
RESIZE/Output/R{r}/{s}/v{vvv}/mf6_head.dis_botm.txt.50
RESIZE/Output/R{r}/{s}/v{vvv}/mf6_head.dis_idomain.50
RESIZE/Output/R{r}/{s}/v{vvv}/mf6_head.dis_top.txt.50
RESIZE/Output/R{r}/{s}/v{vvv}/mf6_head.init_head.mod.50
RESIZE/Output/R{r}/{s}/v{vvv}/mf6_head.npf_icelltype.txt.50
RESIZE/Output/R{r}/{s}/v{vvv}/mf6_head.npf_k22.txt.50
RESIZE/Output/R{r}/{s}/v{vvv}/mf6_head.npf_k.mining.txt.50
RESIZE/Output/R{r}/{s}/v{vvv}/mf6_head.rcha_recharge_1.txt.50
RESIZE/Output/R{r}/{s}/v{vvv}/mf6_head.sto_iconvert.txt.50
RESIZE/Output/R{r}/{s}/v{vvv}/mf6_head.sto_ss.txt.50
RESIZE/Output/R{r}/{s}/v{vvv}/mf6_head.sto_sy.txt.50

7.4 References

Kuhlman, K. 2010. Analysis Report for the CRA-2009 PABC Culebra Flow and Transport Calculations. ERMS 552951. Sandia National Laboratories, Carlsbad, NM.

Langevin, C.D., J.D. Hughes, E.R. Banta, R.G. Niswonger, S. Panday, and A.M. Provost. 2017. Documentation for the MODFLOW 6 Groundwater Flow Model. U.S. Geological Survey Techniques and Methods, Book 6, A55. https://doi.org/10.3133/tm6A55.

Long, J. 2023. Computational Code Execution and File Management for the Replacement Panels Planned Change Request (RPPCR). ERMS 579728. Sandia National Laboratories. Carlsbad, NM.

Information Only

8.0 APPENDIX B SUMMARIZE DTRKMF

This appendix describes the use, execution, NP 9-1 validation, and RPPCR implementation of the script *summarize_dtrkmf.py*. Files are archived in the CVS repository:

/data/cvs/CVSLIB/WIPP_CODES/PA_CODES/SUMMARIZE_DTRKMF/

The *summarize_dtrkmf.py* utility summarizes the breakthrough times of DTRKMF particle track output into tables by vector. The script assumes all input files are in the directory DTRKMF/Output, and it writes its output to the same directory. Consistent with CRA19 analysis, the travel times are converted from 7.75-m thickness of the Culebra flow model to the 4-m thickness of the Culebra transport model by multiplying the time by 4/7.75. The x and y coordinates are transformed from cell indices (i,j) to UTM Zone 13N [m] coordinates assuming the (x, y) origin of the MODFLOW grid is 601700.0 m, 3597100.0 m, and the grid cell size is 100 m.

UTM X = CELL_i [cells] * 100 [m/cell] + 601700 [m]

UTM Y = 3597100 [m] – CELL_j [cells] * 100 [m/cell]

8.1 Execution

The script *summarize_dtrkmf.py* is executed with the following command and syntax.

```
$python summarize_dtrkmf.py a r s c
```

a (str)

Analysis name

r ("r1", "r2", or "r3")

Replicate number

s ("mf" or "mp")

Full ("mf") or partial ("mp") mining scenario

c ("c1", "c2", "c3", or "c4")

Culebra release point identifier

8.2 Input and Output Files

The execution directory must contain DTRKMF output files in the following subdirectory and filename format:

DTRKMF/Output/dtrk_mf6_{a}_{r}_{s}_{c}_v{vvv}.out

In which {vvv} indicates the three-digit LHS vector index and the other variables are as listed above. The DTRKMF particle track output files are described in the DTRKMF User Manual (WIPP PA, 2020). Particle travel time are provided in column 1. Particle X and Y position in model cell coordinates are provided in columns 2 and 3. The final row in the DTRKMF output file corresponds to the time and location when the particle crosses the LWB.

The output is written to the same subdirectory as the input files, with the filename format:

Information Only

DTRKMF/Output/dtrk_mf6_{a}_{r}_{s}_{c}_v{vvv}.out

The output is written into a text file with four columns

vector | dtrktime | x | y

In which dtrktime is the thickness adjusted travel time to the LWB and x and y are the UTM coordinates where the particle exits the LWB, summarized by LHS vector.

8.3 Validation Test

The validation test described in this appendix is run with the shell script *Test/RunTest.sh,* which prepares input and output directories, checks out the appropriate input files, and executes the scripts on the validation tests. All Python scripts are tested and executed on the WIPP computing cluster FWM with the system install of Python version 2.7.5.

The following test case was developed to validate the functionality of *summarize_dtrkmf.py* to correctly compile the DTRKMF output. The test case inputs are saved to Test/Input/Test1/. Prior to test execution, the inputs are linked to the directory DTRKMF/Output. The script output are saved to DTRKMF/Output/.

Test 3 is executed with the below command.

```
$python summarize_dtrkmf.py pRPPCR2 r1 mf c1
```

The execution directory contains the directory DTRKMF/Output/ with DTRKMF output file from a test analysis pRPPCR2. Upon execution, the file *sum_mf6_pRPPCR2_r1_mf_c1.tbl* is written. The output is validated through manual inspection of vector 1 input.

The vector 1 DTRKMF output file (*dtrk_mf6_pRPPCR2_r1_mf_c1_v001.out*) shows a travel time of to the LWB of 1.72775619E+04 in column 1 of the last row of data (line 161). Multiplied by the thickness correction factor:

1.72775619E+04 * (4/7.75) = 8.91745E+03

The x-coordinate and y-coordinates in model space (111.00, 184.57) are equivalent to the UTM coordinates, as shown below:

X: 601700.0 [m] + 100[m/cell]*111.00[cells] = 612800.0 m

Y: 3597100.0 [m] - 100[m/cell]*184.57 [cells] = 3578643.0 m

The vector 1 dtrktime result in the *summarize_dtrkmf.py* script is 8.91745130E+03 as expected. The x and y coordinates are 612800.0 and 3578643.0, as expected. All validation criteria are met, and the script is validated.

8.4 RPPCR Implementation

The script *summarize_dtrkmf.py* is executed by the MODFLOW6.py WIPP run control script from within the Culebra flow model run directory (Long, 2023). As described above, the script is hardcoded to read and write data from the DTRKMF/Outputs subdirectory.

Outputs

DTRKMF/Output/sum_mf6_RPPCR_r{r}_{mf}_c{c}.tbl

Information Only

in which {r}, {s}, and {vvv} represent the replicate number, scenario, and Culebra release point number, respectively.

8.5 References

Kuhlman, K. 2010. Analysis Report for the CRA-2009 PABC Culebra Flow and Transport Calculations. ERMS 552951. Sandia National Laboratories, Carlsbad, NM.

Long, J. 2023. Computational Code Execution and File Management for the Replacement Panels Planned Change Request (RPPCR). ERMS 579728. Sandia National Laboratories. Carlsbad, NM.

WIPP Performance Assessment. 2020. Design Document and User's Manual for DTRKMF, Version 1.02. ERMS 574327. Carlsbad, NM: Sandia National Laboratories.

Information Only

9.0 APPENDIX C CBC2BUD

The Fortran utility *cbc2bud* extracts cell-by-cell flow output from the MODFLOW 6 binary .cbc file and saves it in the MODFLOW-2000 budget format. For a complete description of the MODFLOW 6 binary file format and contents, see the document MODFLOW6 Description of Input and Document (https://water.usgs.gov/ogw/modflow/mf6io_6.0.3.pdf)

9.1 Build Information

Code Name:	CBC2BUD
Version:	1.00
CVS Repository:	/data/cvs/CVSLIB/WIPP_CODES/PA_CODES/CBC2BUD/
Executable:	Build/Linux/cbc2bud
Build Date/Time:	Jun 5 2023 09:36:27
Build Size:	21968 B
Total Size:	22709 B
Executable Tags:	CBC2BUD_100
Platform:	CentOS 7/Dell PowerEdge C6420
Host:	fwm.sandia.gov
Compiler:	gfortran/GCC 8.2.0

The *cbc2bud* executable was generated using the WIPP run control system on the Linux cluster. The core of this system is the software configuration management system CVS and the Python module *rc.py*. A Python program *cbc2bud_Build.py* calls the appropriate *rc.py* routines to check out all needed files (source files, object libraries, and *Makefile*) from CVS, perform the build using *Makefile*, and store the executable and log files in CVS. The build process is run from the script *RunBuild.sh* that checks out the Python module from CVS and executes the Python interpreter to perform the build.

The log files *cbc2bud_100_Build.rtf* and *cbc2bud_100_Build.log* contain tables of files used, a listing of Python program *cbc2bud_Build.py*, and a listing of the compile and link.

RunBuild.sh, *cbc2bud_Build.py*, *rc.py*, *Makefile*, and the log files are stored in CVS Repository /data/cvs/CVSLIB/WIPP_CODES/PA_CODES/CBC2BUD directory RunControl/Linux.

9.2 Execution and Syntax

The *cbc2bud* utility is executed with the following command

```
$cbc2bud cbc_fn grb_fn bud_fn
```

cbc_fn (str)

Input MODFLOW 6 binary cell-by-cell output filename

grb_fn (str)

Information Only

Input MODFLOW 6 binary grid output filename

bud_fn (str)

Output MODFLOW-2000 budget format filename

See the MODFLOW-2000 and MODFLOW 6 documentation for additional information about the formats and requirements of these files.

9.3 Functionality

The CBC2BUD utility has the sole functionality of converting the MODFLOW 6 cell-by-cell flows to MODFLOW-2000 budget format. MODFLOW-2000 writes intercell flow records of FLOW RIGHT FACE, FLOW FRONT FACE, and FLOW LOWER FACE into the binary budget file, with one value for each model grid cell in each record. MODFLOW 6 writes intercell flows to a single 1-D record, with the text identifier FLOW-JA-FACE, record that sequentially stores all flows associated with each cell. For each cell, the number of connections is equal to the number of connections to adjacent cells plus one, to represent the cell itself. For this record, the total number of connections is given as to NJA. Grid connectivity is saved in a binary grid file (grb).

CBC2BUD extracts the right and front face flow values from the FLOW-JA-FACE and converts them into the matrix format used by MODFLOW-2000.

9.4 Validation

CBC2BUD Version 1.00 was tested on the WIPP Linux cluster on Jul 27, 2023, at 16:06:47.

All CBC2BUD test cases are run using the WIPP run control system on Linux. The core of this system is the software configuration management system CVS (Concurrent Versions System) and the Python run control module *rc.py*. The main test script is the Python script *cbc2bud_Test.py* that imports and calls the appropriate *rc.py* routines to check out all test inputs from CVS, runs all the test cases, and stores all test outputs into CVS. The test process is run from a shell script *RunTest.sh* that checks out the Python script from CVS and executes it to perform all tests. The log file for the testing is *cbc2bud_Test.rtf*. All files related to validation testing are stored in CVS Repository /data/cvs/CVSLIB/WIPP_CODES/PA_CODES/CBC2BUD under the following test directories.

- Python scripts *cbc2bud_Test.py* and *rc.py* and the shell script *RunTest.sh* are in directory Test/RunControl/Linux.
- Log file *cbc2bud_100_Test.rtf* is in directory Test/RunControl/Linux.
- All test input files are in directory Test/Input.
- All test output files are in directories Test/Output/Linux_100.
- All auxiliary test files (i.e., Python scripts) are in directory Test/Auxiliary/

The test set for CBC2BUD consists of 1 test case. The purpose of this test case is to verify that CBC2BUD correctly converts MODFLOW 6 cell-by-cell information to MODFLOW-2000 format. This test case uses CBC2BUD to convert a sample MODFLOW 6 output file to MODFLOW-2000 budget format, then two auxiliary Python test scripts convert the input binary file and output binary file to text format for manual inspection.

The test is executed with the following command:

Information Only

```
$./cbc2bud mf6_head.cbc mf6_head.dis.grb cbc2bud_100_t1.bud
```

In which *mf6_head.cbc* and *mf6_head.dis.grb* are the input MODFLOW 6 binary files and *cbc2bud_100_t1.bud* is the output file with the flow data in the MODFLOW-2000 format.

The auxiliary scripts are run with the following commands:

```
$python cbc2txt.py mf6_head.cbc Input/mf6_head.dis.grb

$python bud2txt.py
```

The Python script *cbc2txt.py* is run with the same inputs as the cbc2bud utility. It extracts, reformats, and writes out the flow right face and flow front face arrays to text files *right_face.txt* and *front_face.txt*. The script *bud2txt.py* reads MODFLOW-2000 budget file input and writes output flow values to text files (Appendix D). In the validation test case, *bud2txt.py* writes to the file *cbc2bud_100_t1.asciibud*.

The Python script *compare_txt.py* compares the contents of the files *cbc2bud_100_t1.asciibud* against the output in *right_face.txt* and *front_face.txt* at select cells. It is run with the command:

```
$ python compare_txt.py > compare_txt.diff
```

The first 21 lines of compare_txt.diff are shown below:

```
bud2txt flow right face
val at 40,100 is: -0.000149532463891
cbc2txt flow right face
val at 40,100 is: -0.000149532463891
bud2txt flow front face
val at 347,100 is: 0.000800139709529
cbc2txt flow front face
val at 40,100 is: 0.000800139709529
cbc2txt flow lower face
val at 40,100 is: 6.33337078528e-12
=====
bud2txt flow right face
val at 50,100 is: -0.000278990388826
cbc2txt flow right face
val at 50,100 is: -0.000278990388826
bud2txt flow front face
val at 357,100 is: 0.000567381432756
cbc2txt flow front face
val at 50,100 is: 0.000567381432756
cbc2txt flow lower face
val at 50,100 is: 3.58878807748e-11
```

The values at each displayed cell index and face are identical, indicating that the alternative transformation achieved the same values, as expected. The functionality of CBC2BUD to convert MODFLOW 6 flows to MODFLOW-2000 format is validated.

Information Only

```
import os
import numpy as np


# print values from matrices at given indices

def print_vals(m, r, c):

    print("val at "+str(r) +","+str(c) +" is: "+ str(m[r][c]))
    #print("cbc2txt val at "+str(r) +","+str(c) +" is: "+ str(m2[r][c]))

m1 = np.loadtxt(os.path.join("CBC2BUD", "Auxiliary",
"cbc2bud_100_t1.asciibud"))
m2 = np.loadtxt(os.path.join("CBC2BUD", "Auxiliary", "right_face.txt"))
m3 = np.loadtxt(os.path.join("CBC2BUD", "Auxiliary", "front_face.txt"))
m4 = np.loadtxt(os.path.join("CBC2BUD", "Auxiliary", "lower_face.txt"))

r = [40, 50, 60, 70]
c = [100, 100, 100, 100]

for r,c in zip(r,c):

    print("bud2txt flow right face")
    print_vals(m1, r, c)

    print("cbc2txt flow right face")
    print_vals(m2, r, c)

    print("bud2txt flow front face")
    print_vals(m1, r+307, c)

    print("cbc2txt flow front face")
    print_vals(m3, r, c)

    print("cbc2txt flow lower face")
    print_vals(m4, r, c)

    print("=====")
```

Figure 50. Python script *compare_txt.py*

9.5 RPPCR Implementation

The *cbc2bud* utility is executed with Slurm scripts that are generated with the MODFLOW6.py WIPP run control script (Long, 2023). Calculations are executed from the top directory of the Culebra flow model with the following command

./cbc2bud
./MODFLOW100m/Output/R{r}/{s}/v{vvv}/mf6_head.cbc
./MODFLOW100m/Output/R{r}/{s}/v{vvv}/mf6_head.dis.grb
./CBC2BUD/Output/cbc2bud_RPPATFLD_r{r}_{s}_v{vvv}.bud

Information Only

in which {r}, {s}, and {vvv} represent the replicate number, scenario, and LHS vector, respectively.

9.6 References

Long, J. 2023. Computational Code Execution and File Management for the Replacement Panels Planned Change Request (RPPCR). ERMS 579728. Sandia National Laboratories. Carlsbad, NM.

MODFLOW6 Description of Input and Document, available online at: https://water.usgs.gov/ogw/modflow/mf6io_6.0.3.pdf.

Information Only

This page intentionally left blank.

Information Only

10.0 APPENDIX D BUD2TXT

The Python script *bud2txt.py* converts MODFLOW-2000 format flow budget files into ASCII text files for postprocessing. The source for this script is given below.

```
# JCB June 6, 2023
# -added datablock header/footer precision parameter
# -revised data precision to be user input variables
# -fixed tab-related file corruption

# this script reads in the binary MODFLOW budget files, saved in
# the compact format.  ASCII arrays (with one blank line between them)
# for "FLOW RIGHT FACE" and "FLOW FRONT FACE" (qx and qy) are saved to file
#
# INPUT:  MODFLOW binary budget file
# OUTPUT: ASCII file with qx and qy matricies
#
# NB: this script assumes one layer in binary file, if there is more than one
# the last layer present will overwrite the previous layers in the ASCII file

import struct
from itertools import izip
from sys import exit,argv

if __name__ == "__main__":
    ################################################
    # read input data
    try:
        # input name has same name as script ending with ".in"
        # "instead of ".py"
        scrfname = argv[0]
        inpfname = scrfname.replace('.py','.in')
        fin = open(inpfname,'r')
    except IOError:
        print 'ERROR: %s input file "%s" not found.' %(scrfname,inpfname)
        exit(1)

    global ifmt
    global dfmt
    global hfmt

    fnbinaryin = fin.readline().strip()  # MODFLOW binary budget file
    outfmt = fin.readline().strip()      # desired ASCII format
    fnasciiout = fin.readline().strip()  # ASCII output file
    verbose = fin.readline().strip()
    # data formats
    ifmt, dfmt, hfmt = [int(a) for a in fin.readline().strip().split(' ')]
    fin.close()

    verbose = verbose[0] == 'T' or verbose[0] == 't'

    if verbose:
        print 'echo input'
        print '=================='
        print 'fnbinaryin',fnbinaryin
        print 'outfmt',outfmt
```


Information Only

```
        print 'fnasciiout',fnasciiout
        print 'int format', ifmt
        print 'double format', dfmt
        print 'header/footer format', hfmt
        print '==================='

################################################
# define class and functions needed below

class FortranFile(file):
    """ modified from May 2007 Enthought-dev mailing list post
    by Neil Martinsen-Burrell
    """

    def __init__(self, fname, mode='r', buf=0):
        file.__init__(self, fname, mode, buf)
        self.ENDIAN = '<'  # little endian
        self.di = ifmt  # integer bytes
        self.dr = dfmt  # real bytes
        self.dh = hfmt  # jcb added data block header/footer bytes

    def readReals(self):
        """Read in an array of reals (default precision) with error checking
        prec=d is 'double precision' or 64-bit reals,
        prec=f is 'single-precision' with 32-bit reals
        """
        if self.dr == 8:
            prec='d'  # double
        elif self.dr == 4:
            prec='f'  # float
        else:
            print 'incorrectly specified default real'
            exit(1)
        #read header
        h = struct.unpack(self.ENDIAN+'i',self.read(self.dh))[0]
        data_str = self.read(h)
        if h % self.dr != 0:
            raise IOError('Error reading array of reals from data file')
        num = h/self.dr
        reals = struct.unpack(self.ENDIAN+str(num)+prec,data_str)
        # check against footer
        if struct.unpack(self.ENDIAN+'i',self.read(self.dh))[0] != h:
            raise IOError('Error reading array of reals from data file')
        return list(reals)

    def readInts(self):
        """Read in an array of integers with error checking
        """
        # read header
        h = struct.unpack('i',self.read(self.di))[0]
        data_str = self.read(h)
        len_int = struct.calcsize('i')
        if h % len_int != 0:
            raise IOError('Error reading array of integers from data file')
        num = h/len_int
        ints = struct.unpack(str(num)+'i',data_str)
        # check against footer
```


Information Only

```
        if struct.unpack(self.ENDIAN+'i',self.read(self.di))[0] != h:
            raise IOError('Error reading array of integers from data file')
        return list(ints)

    def readRecord(self):
        """Read a single fortran record, potentially mixed reals, ints,
        and characters
        """
        # read header
        dat = self.read(self.dh)
        if len(dat) == 0:
            raise IOError('Empy record header')
        h = struct.unpack(self.ENDIAN+'i',dat)[0]
        data_str = self.read(h)
        if len(data_str) != h:
            raise IOError('Didn''t read enough data')
        check = self.read(self.dh)
        if len(check) != self.dh:
            raise IOError('Didn''t read enough data')
        # check against footer
        if struct.unpack(self.ENDIAN+'i',check)[0] != h:
            raise IOError('Error reading record from data file')
        return data_str

def reshapev2m(v,nx,ny):
    """Reshape a vector that was previously reshaped in C-major order
    from a matrix back into a C-major order matrix (here a list of lists).
    """
    m = [None]*ny
    n = nx*ny
    iz = izip(xrange(0, n-nx+1, nx), xrange(nx, n+1, nx))
    for i,(lo,hi) in enumerate(iz):
        m[i] = v[lo:hi]
    return m

def floatmatsave(filehandle,m):
    """Writes array to open filehandle.
    Outer list is rows, inner lists are columns.
    """
    for row in m:
        f.write(''.join([outfmt % col for col in row]) + '\n')

################################################

if __name__ == "__main__":

    # open binary file
    ff = FortranFile(fnbinaryin)

    # format of MODFLOW header in binary budget file
    # little endian, 2 integers, 16-character string, 3 integers
    # jcb changed to allow for 4-byte ints (i) and 8-byte ints (q)
    i_dict = {4:'i', 8:'q'}
    fmt = '<2{i}16s3{i}'.format(i=i_dict[ifmt])

    errmsg = "{q} is not expected size; check binary format"
    while True:
```


Information Only

```
        try:
            # read in header
            h = ff.readRecord()

        except IOError:
            # exit while loop
            break

        else:
            # unpack header
            kstp,kper,text,ncol,nrow,nlay = struct.unpack(fmt,h)
            if verbose:
                print kstp,kper,text,ncol,nrow,nlay

            # second header read but not needed
            throw_away = ff.readRecord()

            if text.strip() == 'FLOW RIGHT FACE':
                qx = ff.readReals()
                assert len(qx) == nrow*ncol, errmsg.format(q="qx")

            elif text.strip() == 'FLOW FRONT FACE':
                qy = ff.readReals()
                assert len(qy) == nrow*ncol, errmsg.format(q="qy")

            # text.strip() == 'CONSTANT HEAD' (and potentially other cases)
            else:
                # 'num' number of constant head records (3 int 1 real)
                num = ff.readInts()[0]
                # seek (1) incates a seek relative to current position
                jump = num*(3*ff.di + ff.dr)
                if verbose:
                    print 'num:',num,'jump:',jump
                ff.seek(jump,1)

    ff.close()

    # save ASCII file
    f = open(fnasciiout,'w')
    floatmatsave(f,reshapev2m(qx,ncol,nrow))
    f.write('\n')
    floatmatsave(f,reshapev2m(qy,ncol,nrow))
    f.close()
```


Information Only